UNIVERSITY OF CALIFORNIA,
IRVINE

The composition of fire emissions from ecosystems vulnerable to global change

DISSERTATION

submitted in partial satisfaction of the requirements
for the degree of

DOCTOR OF PHILOSOPHY

in Earth System Science

by

Elizabeth Brooke Wiggins

Dissertation Committee:
Professor James T. Randerson, Chair
Professor Claudia I. Czimczik
Professor Mike L. Goulden
Professor Mike Pritchard

2018

DEDICATION

To my family and friends

TABLE OF CONTENTS

LIST OF FIGURES

LIST OF TABLES

ACKNOWLEDGMENTS

Funding for this research was provided in part by a graduate research fellowship from the National Science Foundation (NSF#2013172241). This fellowship has allowed me the freedom to pursue and conduct the research that I was most interested in, and I am extremely thankful.

I would like to express the deepest appreciation to my committee chair, Professor James Randerson, who has an outstanding and diverse perspective on Earth System Science. Jim has been and is a scientific role model for me. His compassionate and respectful approach to collaborators along with his incredible breadth of knowledge is remarkable. Without his guidance and persistent help this dissertation would not have been possible.

I would like to thank my committee members, Professor Claudia Czimczik, Professor Mike Pritchard, and Professor Mike Goulden, whose feedback and research guidance has been invaluable over the duration of my PhD. Coming from a diverse set of research backgrounds and experience, Claudia, Mike P., and Mike G. have provided crucial insight that has shaped the direction and content of my thesis. Many others have contributed to this dissertation work, including Guaciara Dos Santos and Xiaomei Xu who taught me how to analyze samples for their radiocarbon content.

During the highest highs and lowest lows of graduate school, my family, friends, and fellow ESS graduate students have been an incredible source of encouragement. My wife and best friend, Mary Brill, has been and is my biggest fan. Words cannot express how thankful I am for her unending love and support that has carried me and steadied me over the last couple years. My parents, Mindy Johnson and Paul Johnson, and my siblings, Jessica Wiggins, Matthew Wiggins, and Ethan Johnson shaped me into the person I am today. I will forever be thankful for their constant encouragement, support, and love. Without my family none of this would have been possible.

CURRICULUM VITAE

Elizabeth B. Wiggins

Department of Earth System Science, University of California Irvine
3200 Croul Hall, Irvine, CA 92697
◆ wigginse@uci.edu ◆ (229) 402-0339 ◆ sites.uci.edu/lizwiggins

EDUCATION

Ph.D. **Earth System Science, University of California Irvine** Sept 2013 – August 2018
Thesis advisor: James Randerson

M.S. **Earth System Science, University of California Irvine** May 2015

B.S. **Earth and Atmospheric Science, Georgia Institute of Technology** May 2013
High Honors

PROFESSIONAL EXPERIENCE

NASA ABoVE Science Team Member Jan 2016 – August 2018

National Aeronautics and Space Administration (NASA)
Arctic and Boreal Vulnerability Experiment (ABoVE)
Project Title: Developing a spatially-explicit understanding of fire-climate forcings and their management implications across the ABoVE domain.

Graduate student science team member of the NASA ABoVE campaign. Our specific project contributes to the campaign through an investigation of greenhouse gas and particulate emissions from boreal forest fires and climate interactions. We collect in-situ data from under-sampled fires in Central Canada and add constraints to a statistical combustion model.

University of California Irvine Teaching Assistant Sept 2014 – August 2018

Classes: Modeling the Earth System, Land Surface Processes, Atmospheric Chemistry, Climate Change, Catastrophes

Teaching assistant for Earth System Science undergraduate courses. Responsibilities include: conducting recitations, substituting for lectures, grading, and holding office hours.

NASA CARVE Science Team Member July 2013 – Dec 2014

National Aeronautics and Space Administration (NASA)
Carbon in Arctic Reservoirs Vulnerability Experiment (CARVE)
Project Title: Quantifying the influence of boreal forest fires on regional trace gas variability.

Graduate student science team member of the NASA CARVE campaign. Our particular project adds to the campaign through an investigation of greenhouse gas concentrations measured at a tower located in central Alaska that is equipped with a cavity ring-down spectrometer. We model fire contributions to regional CO, CO_2, and CH_4 using in-situ measurements from the tower, a statistical combustion model, and an inverse atmospheric transport model. Emission factors from boreal forest fires are quantified using tower observations.

RELEVANT SKILLS

- Insight into translating data acquired by NASA satellite-based measurement platforms including, but not limited to, Moderate Resolution Imaging Spectroradiometer (MODIS), Multi-angle Imaging SpectroRadiometer (MISR) and Soil Moisture Active Passive (SMAP).

- Extensive experience using MATLAB programming to interpret remotely sensed and in-situ data to be applied to wildfire emission and atmospheric transport models.
- Proficiency in collecting and measuring carbonaceous aerosol concentrations and isotopic signatures using thermo-optical methods (Sunset OC-EC aerosol analyzer), accelerator mass spectrometry (AMS) and stable isotope ratio mass spectrometry (IRMS).

PUBLICATIONS

- E.B. Wiggins, S. Veraverbeke, J. Henderson, C. Sweeney, C. Miller, J.T. Randerson (2018), Evidence for a larger contribution of smoldering combustion to boreal forest fire emission factors from tower observations in Alaska, *Journal of Geophysical Research: Atmospheres*, in-prep.

- E.B. Wiggins, C. Czimczik, G. dos Santos, X. Xiu, C.F. Harvey, S. Holden, Y. Chen, F. Kai, Y. Liya, and J.T Randerson (2018), Smoke radiocarbon measurements from Indonesian fires provide evidence for burning of millennia-aged peat. *Proceedings of the National Academy of Science*, in review.

- S. Veraverbeke, B.M. Rogers, M.L. Goulden, R.R. Jandt, C.E. Miller, E.B. Wiggins, J. T. Randerson, (2017). Lightning as a major driver of recent large fire years in North American boreal forests. *Nature Climate Change*, *7*(7), 529-534.

- E.B. Wiggins, S. Veraverbeke, J. Henderson, A. Karion, J. Miller, J. Lindaas, R. Commane, C. Sweeney, K. Luus, M. Tosca, S. Dinardo, S. Wofsy, C. Miller, J.T. Randerson (2016), The influence of daily meteorology on boreal fire emissions and regional trace gas variability. *Journal of Geophysical Research: Biogeosciences*, *121*(11), 2793-2810.

- G. Mouteva, C. Czimczik, S. Fahrni, E. Wiggins, B. Rogers, S. Veraverbeke, X. Xu, G. Santos, J. Henderson, and C. Miller (2015), Black carbon aerosol dynamics and isotopic composition in Alaska linked with boreal fire emissions and depth of burn in organic soils, *Global Biogeochemical Cycles*, *29*(11), 1977-2000.

PRESENTATIONS

- E.B. Wiggins, C. Czimczik, G. dos Santos, X. Xiu, Y. Chen, F. Kai, Y. Liya, and J.T Randerson (2017), The age and origin of fire aerosols during El Nino-induced haze events in Singapore, poster presentation at 2017 Fall meeting, AGU, New Orleans, LA.

- E.B. Wiggins, C. Czimczik, G. dos Santos, X. Xiu, Y. Chen, F. Kai, Y. Liya, and J.T Randerson (2017), The age and origin of carbon in fire aerosols during El Nino-induced haze events in Singapore, invited oral presentation at 2nd international radiocarbon conference, Debrecen, Hungary.

- E.B. Wiggins, C. Czimczik, G. dos Santos, X. Xiu, Y. Chen, F. Kai, Y. Liya, and J.T Randerson (2017), Utilizing radiocarbon to determine the depth of soils in Indonesia peatlands, oral presentation at 2017 Spring meeting, ACS, San Francisco, CA.

- E.B. Wiggins, J. Henderson, C. Sweeney, C. Miller, and J.T. Randerson (2017), Environmental controls on boreal forest fire emission ratios, poster presentation at Alaska Fire Science Consortium workshop, Fairbanks, AK.

- E.B. Wiggins, J. Henderson, C. Sweeney, C. Miller, and J.T. Randerson (2016), Environmental controls on boreal forest fire emission ratios, oral presentation at 2nd International Smoke Symposium Conference, Long Beach, CA.

- E.B. Wiggins, J. Henderson, C. Sweeney, C. Miller, and J.T. Randerson (2016), Environmental controls on boreal forest fire emission ratios, poster presentation at 2016 Fall Meeting, AGU, San Francisco, CA.

- E.B. Wiggins, S. Veraverbeke, J. Henderson, A. Karion, J. Miller, J. Lindaas, R. Commane, C. Sweeney, K. Luus, M. Tosca, S. Dinardo, S. Wofsy, C. Miller, J.T. Randerson (2014), The influence of daily meteorology on boreal forest fire emissions and regional trace gas variability, oral presentation at 2014 Fall Meeting, AGU, San Francisco, CA.

- E.B. Wiggins, H. Sayani, K. Cobb (2013), The influence of freshwater dissolution on coral morphology and geochemistry, poster presentation at 2012 Fall Meeting, AGU, San Francisco, CA.

HONORS AND AWARDS

National Science Foundation Graduate Research Fellowship	May 2013 – August 2018
Outstanding Student Poster Award *Alaska Fire Science Consortium Workshop*	Apr 2017
NASA Group Achievement Award CARVE Airborne Science Campaign Team *NASA Jet Propulson Laboratory*	Aug 2014
Graduate Dean's Recruitment Fellowship *University of California Irvine*	Sept 2013
Presidents Undergraduate Research Award *Georgia Institute of Technology*	May 2012

PROFESSIONAL AFFILIATIONS

American Chemical Society	Apr 2017 – August 2018
International Association of Wildland Fire	Nov 2016 – August 2018
NASA ABoVE Science Team	Jan 2016 – August 2018
Alaska Fire Science Consortium	Apr 2017 – August 2018
American Geophysical Union	Dec 2012 – August 2018
NASA CARVE Science Team	Jun 2013 – Dec 2014

ABSTRACT OF THE DISSERTATION

The composition of fire emissions from ecosystems vulnerable to global change

By

Elizabeth Brooke Wiggins

Doctor of Philosophy in Earth System Science

University of California, Irvine, 2018

Professor James T. Randerson Irvine, Chair

Fire impacts climate over wide spatial and temporal scales via many complex, interdependent, and often poorly understood processes. For example, fires emit substantial amounts of greenhouse gases and aerosols. Vulnerable regions worldwide are becoming more prone to larger, and more intense wildfires. Global change in the form of climate change and/or land use change is impacting fire regimes across the globe. In the boreal forest, climate change is causing a combination of warmer temperatures, drought, earlier snowmelt, and favorable fire weather that encourages the development of wildfires. In the tropics, specifically Indonesia, extensive land use change involving the degradation of naturally-existing peatlands to support agricultural productivity is also causing a significant increase in wildfires and corresponding emissions. There is a need to quantify and characterize the composition of emissions in wildfire-prone regions to fully understand the climate and human health related impacts of changing fire regimes.

In my first study, I examined the influence of daily meteorology on boreal forest fire emissions and regional trace gas variability. I coupled a statistical fire combustion model with an inverse atmospheric transport model to quantify the influence of fires on trace gas variability

observed at a tower in Alaska equipped with a cavity-ring down spectrometer. I discovered that basic meteorological variables, including temperature and vapor pressure deficit, explained variability in fire activity better than complex fire weather indices. Next, I analyzed environmental controls on boreal forest fire emission factors during an anomalously large fire year in Alaska (2015). I used the same coupled modeling approach to determine times when fires influenced trace gas variability at the tower. Tower observations were used to calculate 23 individual boreal fire emission factors, substantially contributing to the database of emission factors. In my final study, I analyzed wildfire aerosol emissions in Indonesia during the devastating 2015 haze event. Considerable uncertainty exists with regards to whether the particulate emissions originate from deforestation fires, agricultural burning, or peatland fires. To address this, I analyzed aerosol samples collected in Singapore, a major city downwind of Indonesian wildfires, for their radiocarbon content. The radiocarbon content of the fire-emitted aerosol was depleted in ^{14}C, indicating the majority of fire $PM_{2.5}$ emissions originated from the burning of peatlands. The collective results of the studies from this dissertation will vastly improve our characterization of trace gas and particulate emissions from fires in globally important and vulnerable ecosystems.

Chapter 1

1. Introduction

1.1 Global change and fire feedbacks in highly vulnerable biomes

Fire is an important natural disturbance in the Earth system, modifying regional and global climate over a wide range of spatial and temporal scales and through many complex, interdependent, and often poorly understood processes [*Bonan*, 2008; *Li et al.*, 2014]. Active fires can directly impact atmospheric composition and air quality through injection of trace gases and particulate matter into the surrounding atmosphere [*Langmann et al.*, 2009]. After a fire has occurred, surface albedo can be significantly altered, but varies considerably as a function of seasonality and local vegetation dynamics [*Bowman et al.*, 2009]. Post-fire changes in surface albedo can influence climate decades after a fire has ensued [*Randerson et al.*, 2006]. Fire can also initiate successional ecosystem changes, impact species richness and community composition, and redistribute key nutrients [*Turner et al.*, 1998]. Directly following a fire, carbon uptake by local vegetation is reduced or halted depending on the severity of the fire. Loss of vegetation cover causes immediate changes in carbon, energy, and water fluxes locally [*Beringer et al.*, 2003]. Climate, in turn, modulates fires by influencing fuel moisture, fuel structure, and the likelihood of ignition and fire spread [*Moritz et al.*, 2012]. The complex feedback loops between fires, climate, and ecosystems are important to quantify because of the short and long-term influences fire can ultimately have on the Earth system. These relationships vary significantly among different regions because of differences in regional climate, vegetation, atmospheric dynamics, and anthropogenic influence on the landscape [*Moritz et al.*, 2012].

The ultimate impact of fire emissions on climate and human health depends on the amount and chemical composition of active fire emissions coupled with their atmospheric

transport [*Langmann et al.*, 2009]. The composition of primary fire emissions is influenced by a wide variety of environmental factors including fuel conditions (type, structure, quantity, and moisture content) and fire weather (temperature, humidity, wind speed, precipitation), which, in turn, can be rapidly modified by fires as they burn [*Schultz et al.*, 2008]. More complete combustion, commonly known as flaming combustion, emits more highly oxidized gas emissions such as CO_2, H_2O, NO_x, SO_2, and black carbon [*Andreae and Merlet*, 2001; *Akagi et al.*, 2011]. Less complete combustion, or smoldering combustion, produces most of the CO, CH_4, non-methane volatile organic compounds, and primary organic aerosol [*Andreae and Merlet*, 2001; *Akagi et al.*, 2011]. Flaming combustion is more likely to occur under hot and dry oxygen-rich conditions while smoldering combustion is more common in oxygen-depleted, cool and moist environments. Over the life cycle of a fire, varying combinations of flaming and smoldering combustion can result in varying emissions at different times and at different locations within a fire [*Schultz et al.*, 2008].

Fire carbon emissions (C_T) are commonly quantified by multiplying burned area (A), biomass density (B), the fraction of biomass that is carbon (f_c), and fuel consumption (β) (equation 1.1) [*Van der Werf et al.*, 2010].

$$C_T = A * B * f_c * \beta \quad (1.1)$$

Each of these variables is determined through a combination of remote sensing observations and in-situ field measurements and all have considerable uncertainty. Carbon emissions can be converted to specific trace gas or aerosol species using a scalar known as an emission factor (g species per kg biomass combusted) [*Akagi et al.*, 2011]. Although emission factors are almost

always treated as a static scalar that is separately applied for each biome, in reality they are dynamic and highly sensitive to the combustion phase, combustion completeness and related environmental drivers.

Globally, total burned area has experienced a negative trend over the last 18 years as a consequence of expanding agricultural activity and resulting landscape fragmentation in savanna regions that ultimately limits the spread of fire [*Andela et al.*, 2017]. However, over the past two decades there has also been a rise in the number of large, out of control fires, in temperate and boreal ecosystems [*Liu et al.*, 2010]. Anthropogenic climate change and land use change in susceptible ecosystems can significantly modify the amount and composition of fire emissions and thus exacerbate the detrimental impact of fires for human health and climate [*Lavorel et al.*, 2007; *Turetsky et al.*, 2015].

Fires in peatlands are of particular interest, because of their extremely high fuel loads. Peatlands consist of partially decayed organic material in an anoxic, waterlogged environment. These vast stores of carbon in organic rich peatland soil layers can be released to the atmosphere when the water table drops and surface layers are ignited by lightning or humans. Peatlands currently contain the same magnitude of carbon as the present-day atmospheric carbon pool [*Turetsky et al.*, 2015]. Pristine peatlands are naturally resilient to fire, because of the high water table associated with the development of peat. However, climate change in boreal peatlands and land use change in tropical peatlands is ultimately causing these naturally protected landscapes to become more vulnerable to fire [*Van Der Werf et al.*, 2008a; *Turetsky et al.*, 2011; *Miettinen et al.*, 2012].

Smoldering peatland fires emit substantial amounts of greenhouse gasses and fine particulate matter that can influence regional to global climate and human health [*Marlier et al.*,

2013], but have not been systematically measured in situ in many areas. Fires that occur in peatlands are dominated by the smoldering phase of combustion, and once ignited peat fires can continue to burn for weeks or months [*Turetsky et al.*, 2015]. Excessive fire in peatlands can change the ecosystem from a carbon sink to a carbon source that contributes to the buildup of atmospheric greenhouse gasses [*Page et al.*, 2002; *Turetsky et al.*, 2015]. Peatland fires emit the most organic carbon, carbon monoxide, etc., per unit mass combusted of all fires in natural landscapes [*Stockwell et al.*, 2016; *Jayarathne et al.*, 2018; *Wooster et al.*, 2018]. It is imperative to understand how global change is influencing the magnitude and chemical composition of peatland fire emissions to fully capture the impact of fire on climate and human health.

1.2 Boreal forest fire emissions and climate change

The boreal forest covers roughly 17% of the Earth's land surface, but contains more than 30% of all carbon in the terrestrial biome [*Kasischke and Stocks*, 2012], mostly in thick carbon-rich soil layers [*Harden et al.*, 2000; *Turetsky et al.*, 2011]. Fire is a common, natural disturbance in the boreal forest that influences ecosystem dynamics, carbon balance, and climate feedbacks in the high latitudes of the Northern hemisphere [*Johnson*, 1996; *Harden et al.*, 2000; *Turetsky et al.*, 2015]. However, climate change may significantly alter fire feedbacks [*Stocks et al.*, 2000]. A climate driven change in the fire regime can influence radiative forcing by altering surface albedo [*Amiro et al.*, 2006; *Rogers et al.*, 2012] and via substantial emissions of greenhouse gases and climate-warming aerosols [*Martin et al.*, 2006; *Preston and Schmidt*, 2006; *Flanner et al.*, 2007; *Akagi et al.*, 2011].

Climate is changing most rapidly in the high-latitude regions of the northern hemisphere, and this trend is expected to continue (Figure 1.1) [*Jones et al.*, 2012; *Gauthier et al.*, 2015;

Nazarenko et al., 2015]. Warmer temperatures, earlier snowmelt, and a longer growing season are creating more widespread ideal fire weather conditions for boreal forest fires to occur and spread [*Stocks et al.*, 1998; *Young et al.*, 2017]. Favorable fire weather conditions and an increase in lightning are causing an increase in burned area and the number of large fires in the North American boreal forest [*Veraverbeke et al.*, 2017]. A complete understanding of the positive feedback loop between climate and fire activity requires knowledge of the overall radiative forcing caused by boreal fires, including the amount and composition of fire emissions and the role of fire in modifying surface biophysics.

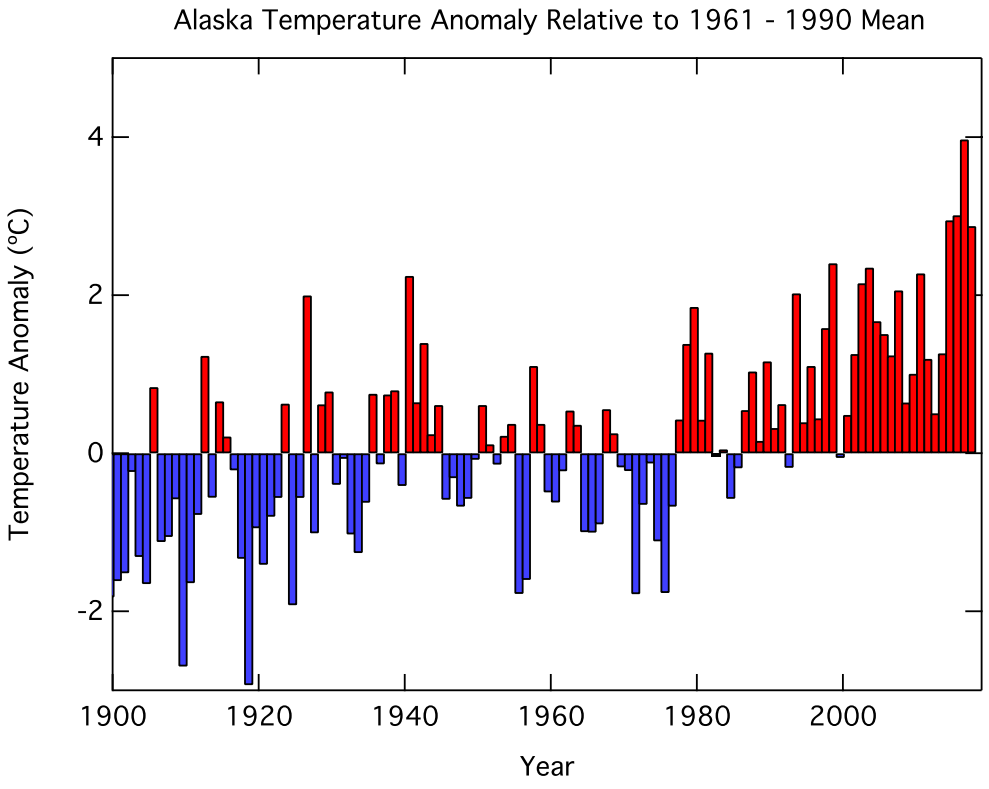

Figure 1.1 Annual mean temperature anomaly time series for Alaska created using the Climate Research Unit (CRU) land station temperature database [*Jones et al.*, 2012]. Temperature anomalies are calculated relative to the mean from 1961 – 1990. Blue bars represent years with means below the average and red bars represent years above the average.

The net radiative effect of boreal forest fires is historically slightly negative, because of the seasonally integrated albedo changes in the landscape over a century or more [*Randerson et*

al., 2006]. However, active fire emissions can directly influence regional to global atmospheric chemistry and albedo immediately following a fire, via emissions of greenhouse gases and climate-warming and/or cooling aerosols. The quantity and chemical composition of fire emissions is highly variable and dependent on current and antecedent environmental conditions [*Bessie and Johnson*, 1995; *Johnson*, 1996]. Although the influence of weather on fire behavior is well established in boreal ecosystems [*Alexander*, 1982; *De Groot*, 1998; *Abatzoglou and Kolden*, 2011; *Sedano and Randerson*, 2014], quantitative models linking weather with emissions are needed to better understand fire impacts at on atmospheric composition at regional and global scales under a changing climate.

Both flaming and smoldering combustion can occur simultaneously during a fire, but in boreal fires a flaming fire front usually moves through the aboveground biomass and is followed by smoldering combustion in the organic soil layers left behind [*French et al.*, 2002]. The majority of emissions from boreal forest fires are believed to originate from the carbon-rich soil [*Harden et al.*, 2000; *Turquety et al.*, 2007; *Boby et al.*, 2010; *Rogers et al.*, 2014; *Walker et al.*, 2018]. Only a relatively small number of previous studies have measured in-situ fire emissions to understand the relative proportions of flaming and smoldering in aboveground and belowground biomass [*Cofer et al.*, 1990; *Radke et al.*, 1991; *Nance et al.*, 1993; *Cofer et al.*, 1998; *Goode et al.*, 2000; *Simpson et al.*, 2011]. The paucity of studies creates a high level of uncertainty in emission factors for boreal forest fires. Almost all previous studies have sampled boreal fire emissions by flying an aircraft near an active fire plume and collecting canisters of air to be analyzed in a laboratory at a later date (Table 1.1).

Table 1.1 Compilation of all previous emission factor studies in the boreal forest. CO and CH_4 emission factors (EF) have units of g per kg biomass combusted. The final column is the modified combustion efficiency (MCE) average for each individual study.

	Location	Sampling Strategy	# Fires	Fire Type	CO EF*	CH_4 EF*	MCE*
Cofer et al. (1990)	Canada	Aircraft Flask	2	Prescribed	101 ± 29	6.12 ± 2.74	0.91
Radke et al. (1991)	Canada	Aircraft Gas Analyzer	1	Prescribed	175 ± 91	5.6 ± 1.7	0.86
Nance et al. (1993)	Alaska	Aircraft Flask	1	Wildfire	82 ± 13	2.7 ± 1.0	0.93
Cofer et al. (1998)	Canada	Aircraft Flask	2	Prescribed	142 ± 59	5.1 ± 3.8	0.88
Goode et al. (2000)	Alaska	Aircraft Gas Analyzer	4	Wildfire	90 ± 7.5	3.0 ± 0.5	0.92
Simpson et al. (2011)	Canada	Aircraft Flasks	5	Wildfire	113 ± 72	4.7 ± 2.9	0.90
Wiggins et al. (2016)	Alaska	Tower-based Ground	3^+	Wildfire	134 ± 25	7.74 ± 1.1	0.89

*CO and CH_4 emission factors and MCE vary as a function of combustion completeness. Higher EFs and lower MCEs are indicative of smoldering combustion and vice versa indicate flaming combustion.

In total, only 18 individual fire plumes have been sampled from active boreal forest fires and all samples were acquired during the day, usually in the afternoon. This approach may create a bias towards sampling active fires burning in the afternoon, when boundary layer dynamics supports more flaming combustion [*Johnson*, 1996], and likely only captures a small fraction of the variability in fire behavior and corresponding emissions that occurs over day-night cycles and synoptic weather timescales. Under the context of a rapidly changing climate, it is essential to improve the accuracy of emission factors in order to understand the feedback loops between climate and boreal fires.

1.3 Anthropogenic land use change and fire in Indonesia

Peatlands began forming in Indonesia between 26,000 and 6,000 years ago, serving as a terrestrial carbon sink for millenia [*Jaenicke et al.*, 2008]. Indonesian peatlands currently store around 55 ± 10 Gt of carbon in organic soil layers that can be up to 20 m thick [*Jaenicke et al.*, 2008]. Before human intervention, most of these peat deposits were covered with pristine swamp forest and were naturally protected from fires by the height of the water table [*Page et al.*, 2004]. Over the last several decades humans have subjected these peatlands to intensive logging,

drainage, and conversion to agricultural plantations [*Anshari et al.*, 2010]. While pristine peatlands are naturally resistant to fire, degraded peatlands have a lower water table and are vulnerable to fire. Fires in tropical peatland release carbon to the atmosphere that has been stored for thousands of years, contributing to the build-up of atmospheric CO_2 concentrations and climate change [*Marlier et al.*, 2015]. Deforestation related fires and burning in deep layers of accumulated peat are important for quantifying greenhouse gas budgets and indicates the peat reservoirs are no longer in steady state with regards to the carbon cycle [*Page et al.*, 2002].

Biomass burning in Sumatra and Borneo is an important contributor to global and regional budgets of atmospheric greenhouse gases and aerosols [*Miettinen et al.*, 2017a]. These fire emissions negatively impact human health [*Koplitz et al.*, 2016], cause interference with cloud processes [*Tosca et al.*, 2011; *Chen et al.*, 2018], influence the radiative balance of the planet [*Podgorny et al.*, 2003], and increase tropospheric ozone [*Sudo and Takahashi*, 2001]. Fire emissions in Indonesia and Malaysia have increased substantially since the 1980s due to an amplification of drought-induced anthropogenic biomass burning including deforestation, slash and burn agriculture, land management fires, agricultural waste burning, and peat fires [*Field et al.*, 2009].

During September - October 2015, Indonesia experienced an exceptionally high fire season caused by El Niño-induced dry season drought [*Field et al.*, 2016]. The resulting haze event caused an estimated 100,000 premature deaths in Indonesia, Malaysia, and Singapore due to illness stemming from exposure to fine particulate matter ($PM_{2.5}$) emitted by the fires [*Koplitz et al.*, 2016]. In addition to hazardous $PM_{2.5}$ emissions, there were considerable CO_2 emissions from fires. Indonesian fires are believed to have contributed to 0.2 ppm or 20% of the 1 ppm increase in global CO_2 concentrations during 2015 [*Betts et al.*, 2016]. Similar events occurred

during the most recent comparable El Niño years in 2006 and 1997 with haze pollution mortality affecting thousands of people across the region [*Marlier et al.*, 2013].

Determining the landscape source of carbonaceous aerosol emissions is important for future mitigation of haze events and understanding carbon cycle dynamics in Indonesia. Knowing the landscape source of fire emissions provides insight on types of land management activities that can potentially be targeted for managing air pollution episodes. The land cover in Sumatra and Borneo, consisting of highly degraded natural forests and a plethora of agricultural activity juxtaposed with natural intact peatlands, creates a challenging problem for source attribution. Previous studies using remote sensing have a limited ability to quantify fire emission contributions from three major fire types in the region: agricultural fires, deforestation related fires, and peat fires [*Marlier et al.*, 2013; *Abood et al.*, 2015; *Marlier et al.*, 2015; *Lohberger et al.*, 2018]. Although it is generally believed a large portion of Indonesian fire emissions are from peat fires, there is considerable uncertainty in the source attribution. There is a need to quantify fire emission contributions from agricultural waste burning, deforestation, and peat fires to inform fire management policy and mitigate future haze events.

1.4 Organization of research

The goal of this thesis is to improve our understanding of the composition of fire emissions in vulnerable fire-prone ecosystems that are influenced by important global change drivers.

In chapter 2 I investigated the influence of environmental conditions on boreal fire emissions and fire contributions to regional trace gas variability. I assessed the relative importance of different climate variables and fire weather indices in explaining the temporal variability of active fires,

fire radiative power, burned area, and emissions. I then combined fire emissions from the Alaska Fire Emissions Database (AKFED) with an atmospheric model to simulate continuous trace gas observations from tower observations in Alaska. In this approach I used the Coupled Polar Weather Research and Forecasting/Stocastic Time-Inverted Lagrangian Transport (PWRF-STILT) model to link emissions with trace gas observations at the tower. The injection height of fire emissions was constrained using the mean injection height derived from an analysis of 2013 fire plumes in Alaska observed by the Multi-angle Imaging Spectroradiometer (MISR).

The following questions were addressed in this research:

1. How much of the variability in fire activity can be explained using meteorological and fire weather indices?
2. Can trace gas variability observed at a tower in interior Alaska be explained using a fire emissions database coupled with an atmospheric transport model?

This chapter was published in the Journal of Geophysical Research – Biogeosciences as: Wiggins, E. B., Veraverbeke, S., Henderson, J. M., Karion, A., Miller, J. B., Lindaas, J., Commane, R., Sweeney, C., Luus, K.A., Tosca, M.G. and Dinardo, S.J. (2016). The influence of daily meteorology on boreal fire emissions and regional trace gas variability. *Journal of Geophysical Research: Biogeosciences*, *121*(11), 2793-2810.

In chapter 3 I used the modeling approach developed in chapter 1 to quantify boreal forest fire emission factors from high-resolution tower-based trace gas observations. I focused on observations from an anomalously high fire year, 2015. During the summer of 2015, Alaska

experienced the second largest fire season since records began in this region in the 1940s. I isolated periods in the observational dataset when fire had a dominant influence on trace gas variability observed at the NOAA/NASA CRV tower. Emission factors for CO and CH_4 along with modified combustion efficiencies (MCE) were calculated using these fire influenced periods. Emission factors were sorted into three categories to represent the dominant phase of combustion: smoldering, mixed, or flaming. I then coupled a fire emissions inventory (AKFED) with an atmospheric transport model (PWRF-STILT) to quantify the spatial and temporal variability of fires and their influence on CO, CH_4, and CO_2 at the CRV tower. This approach allowed us to isolate individual fire contributions to trace gas variability at CRV tower.

The research was motived by the following questions:

1. Can a continuous tower-based approach capture more variability in fire activity and behavior than traditional aircraft techniques?
2. Have the products of smoldering combustion been underestimated in previous boreal fire emission factor studies because of sampling biases?

This chapter is in preparation for submission to Atmospheric Chemistry and Physics as: Wiggins, E.B., Sweeney, C., Miller, J.B., Andrews, A., Miller, C.E., and Randerson, J.T. (2018), Evidence for a greater contribution of smoldering combustion to boreal forest fire emission factors from a tower-based approach . *Journal of Geophysical Research: Atmospheres*. In-prep.

In chapter 4 I investigated the radiocarbon age of carbonaceous aerosols emitted from fires in Indonesia during the catastrophic fire season of 2015. During 2015, El Nino induced drought

exacerbated fire activity in Indonesia, which led to a deadly regional haze event. However, the amount of emissions that originated from agricultural waste burning, deforestation-related fires, or burning in peatlands remains uncertain. I analyzed $PM_{2.5}$ aerosol samples that were collected downwind of major fire activity in Singapore from August 2014 – October 2015. The samples were measured for total carbon concentration and for the radiocarbon content of the total carbon. I used a Keeling plot approach and a box model to determine the radiocarbon signature of carbonaceous aerosols emitted from fires. The radiocarbon signature of the aerosols provides evidence to determine the source of the fire-emitted aerosols. This research was motivated by the following questions:

1. What is the radiocarbon signature and corresponding age of fire-emitted smoke aerosols in Indonesia?
2. Was the deadly haze event in Indonesia during 2015 caused by particulate emissions from agricultural waste burning, deforestation, or peatland fires?

This chapter was submitted to the Proceedings of the National Academy of Sciences and is currently in review as:

Wiggins, E.B., Czimczik, C.I., Santos, G.M., Chen, Y., Xu, X., Holden, S.R., Randerson, J.T., Harvey, C.F., Kai, F., Liya, Y. (2018). Smoke radiocarbon measurements from Indonesian fires provide evidence for burning of millennia-aged peat. *Proceedings of the National Academy of Sciences*. In review.

Chapter 5 summarizes the main findings of my dissertation work. I discuss broader implications of my research and future directions for the science. Chapters 2 and 4 are slightly altered versions of previously published or submitted papers. The chapters were altered for formatting purposes only. The content of each chapter is identical to the original manuscript. Chapter 3 is a version of a manuscript currently being written that will be submitted to *Journal of Geophysical Research: Atmospheres* later this year.

Chapter 2

The influence of daily meteorology on boreal fire emissions and regional trace gas variability

Adapted from:

Wiggins, E.B., Veraverbeke, S., Henderson, J.M., Karion, A., Miller, J.B., Lindaas, J., Commane, R., Sweeney, C., Luus, K.A., Tosca, M.G., Dinardo, S.J., Wofsy, S., Miller, C.E., and Randerson, J.T. (2016), The influence of daily meteorology on boreal fire emissions and regional trace gas variability. *Journal of Geophysical Research: Biogeosciences*, *121*(11), 2793-2810.

2.1 Introduction

Boreal forest fires are an important driver of ecosystem dynamics, carbon balance, and climate feedbacks in the Northern Hemisphere [*Johnson*, 1996; *Turetsky et al.*, 2015]. At a landscape scale, fires influence the age structure of forests, with post-fire succession modifying species composition over a period of many decades [*Viereck*, 1983; *Wirth et al.*, 1999]. Within individual burns, environmental conditions at the time of the fire can modify fire severity, and ultimately the recruitment and composition of vegetation that establishes in early successional stages [*Johnstone et al.*, 2004; *Johnstone and Chapin*, 2006]. Boreal ecosystems are carbon rich, with accumulation rates enhanced by cold temperatures and slow decomposition rates [*Apps et al.*, 1993; *Trumbore and Harden*, 1997; *Harden et al.*, 2000; *Hobbie et al.*, 2000; *McGuire et al.*, 2010]. Much of this carbon is contained in organic soil layers that are vulnerable to fire [*Apps et al.*, 1993; *Rapalee et al.*, 1998] and account for 80-90% of the carbon released during combustion [*Boby et al.*, 2010; *Turetsky et al.*, 2011; *Rogers et al.*, 2015]. A change in fire regime thus has the potential to influence radiative forcing by means of several different

pathways, including modification of surface biophysics [*Amiro et al.*, 2006; *Rogers et al.*, 2013], terrestrial carbon stocks [*Harden et al.*, 2000; *Turetsky et al.*, 2011], and emissions of black carbon [*Martin et al.*, 2006; *Preston and Schmidt*, 2006; *Flanner et al.*, 2007; *Akagi et al.*, 2011]. To reduce uncertainties in fire-climate feedbacks and allow more accurate prediction of future change, more information is needed to understand how meteorological factors influence the amount and composition of pyrogenic emissions.

Weather and climate strongly influence fire dynamics in boreal forests on time scales of hours to decades [*Johnson*, 1996]. Ambient weather conditions control lightning ignition probability [*Latham and Schlieter*, 1989; *Nash and Johnson*, 1996; *Anderson*, 2002] and fire spread rates [*Sedano and Randerson*, 2014] through their influence on convection, fire weather, and fuel moisture. The moisture content of fine surface fuels rapidly responds to variations in vapor pressure deficit over a period of hours or days, whereas the moisture content of deeper soil layers responds to the cumulative effects of precipitation and evapotranspiration over the course of the fire season [*Van Wagner and Pickett*, 1985]. In permafrost areas, soil moisture is also regulated by heat inputs that influence thaw rates of the active layer [*Lawson*, 1986]. The likelihood of deep burning, high levels of fuel consumption, and enhanced carbon emissions are sensitive to the moisture levels of deeper layers [*Kasischke et al.*, 1995; *Turetsky et al.*, 2011; *Veraverbeke et al.*, 2015].

Climate and weather variability influence the energy release during combustion and the depth of burning in organic soils [*Nash and Johnson*, 1996; *Turetsky et al.*, 2011], and as such govern the amount and composition of trace gases emitted from fire. Flaming combustion is responsible for the more highly oxidized gas emissions such as CO_2, H_2O, NO_x, SO_2, and black carbon, whereas smoldering combustion produces most of the CO, CH_4, non-methane volatile

organic compounds, and primary organic aerosol [*Akagi et al.*, 2011]. Smoldering and flaming combustion often occur simultaneously during a fire, and smoldering fires often exist as residual burning after a flaming fire front has moved through a particular area. Flaming combustion likely account for most of the fire spread under hot and dry conditions whereas smoldering fires move more slowly, often in more humid conditions, but may contribute to combustion losses over longer intervals [*Akagi et al.*, 2011; *Turetsky et al.*, 2015]. Variables such as fuel moisture content and wind speed can influence the quantity of biomass consumed during either flaming or smoldering combustion phases [*Akagi et al.*, 2011; *French et al.*, 2014]. *Anderson et al.* [2015], for example, found that integrating fire weather conditions into a carbon emissions model increases the spatial and temporal variability of the emissions time series. Although the influence of weather on fire behavior and spread rate is well established in boreal ecosystems [*Alexander*, 1982; *Van Wagner and Pickett*, 1985; *Abatzoglou and Kolden*, 2011; *Sedano and Randerson*, 2014], quantitative models linking weather with emissions and emission factors are currently lacking. In this context, new modeling approaches and atmospheric trace gas observations are needed to improve our understanding of how the composition of boreal fire emissions may respond to new extremes in fire weather.

Several approaches exist for estimating carbon emissions from fires. One paradigm is the *Seiler and Crutzen* [1980] approach whereby emissions are estimated as the product of area burned, fuel loads, the fraction of fuels combusted, and emission factors for different gas species that relate trace gas production to a fixed amount of consumed biomass. In boreal forests, this approach has been used extensively, along with advances in remote sensing, to estimate emissions [*French et al.*, 2002; *Kasischke et al.*, 2005]. *Veraverbeke et al.* [2015] estimated pyrogenic carbon consumption from relationships between field observations of carbon

consumption and environmental variables, including a remotely sensed indicator of burn severity. They also leveraged the Moderate Resolution Imaging Spectroradiometer (MODIS) active fire/thermal anomaly data to obtain burned area and thus carbon emissions with a daily time step. Major sources of uncertainty with these modeling approaches include uncertainties in the algorithms used to estimate the amount of carbon consumed from above- and belowground carbon pools [*French et al.*, 2004; *Veraverbeke et al.*, 2015]. Errors for trace gases and aerosols are likely amplified by the use of temporally and spatially uniform emission factors.

Remote sensing also allows development of top-down models of emissions from fires using an approach based on fire radiative energy. Previous studies have established a relationship between fire radiative energy and smoke aerosol or trace gas emission rates [*Wooster et al.*, 2005; *van der Werf et al.*, 2006; *Kaiser et al.*, 2009a]. The rate at which a fire releases energy has a direct, linear relationship to its rate of biomass consumption [*Ichoku and Kaufman*, 2005; *Wooster et al.*, 2005]. Multiple satellite observations per day are needed to construct a diurnal cycle of fire radiative power (FRP), and the integral of this diurnal cycle, fire radiative energy, is directly related to total emissions. Remote sensing information on the number of thermal anomaly detections, such as active fire counts and FRP measurements from the MODIS sensors on the Terra and Aqua satellites, have been used to assign spatial and temporal variability in emissions. For example, *Wiedinmyer et al.* [2011] assigned a biome-specific burned area to MODIS active fire detections, enabling the creation of a global daily emissions time series at a 1 km resolution and in near real time. Similarly, *Mu et al.* [2011] used active fires from MODIS and Geostationary Operational Environmental Satellite (GOES) radiometers to redistribute monthly fire emissions from the Global Fire Emissions Database (GFED) to daily and 3-hourly resolutions.

Smoke modeling systems rely on the emissions models described above to simulate fire impacts on regional air quality [*Freitas et al.*, 2007; *Freitas et al.*, 2009]. For this class of model, fire emissions estimates can be combined with an atmospheric transport model to estimate regional concentrations of aerosols or trace gases [*Grell et al.*, 2010]. The BlueSky smoke modeling framework uses a modular assimilation of fire information, fuel loading, fuel consumption informed with meteorology, and aerosol emission factors to ultimately provide information about aerosol concentrations and the dispersion of fire plumes [*Larkin et al.*, 2010]. Environment and Climate Change Canada's North American air quality forecast system, FireWork, uses near real time wildfire emissions estimates and a similar modeling framework that incorporates the BlueSky Fire Emissions Product Simulator (FEPS) module to provide regional forecasts of trace gases and aerosols [*Pavlovic et al.*, 2016].

Here we examined the influence of daily meteorology on fire emissions and trace gas variability in interior Alaska as a part of NASA's Carbon in Arctic Reservoirs Vulnerability Experiment (CARVE). In a first step, we assessed the relative importance of different meteorological variables and fire weather indices in explaining the temporal variability of active fires, fire radiative power, burned area, and emissions within the state of Alaska during the summer of 2013. In a second step we combined estimates from the Alaskan Fire Emissions Database (AKFED) with an atmospheric model to simulate continuous trace gas observations from the CARVE-NOAA Global Monitoring Division tower in Fox, Alaska (hereafter referred to as the CRV tower). We used the AKFED model because it was developed and constrained specifically for our region of study and because of its high spatial and temporal resolution. In our approach we use the Coupled Polar Weather Research and Forecasting/Stochastic Time-Inverted Lagrangian Transport model (PWRF-STILT) to link emissions with trace gas observations at the

CRV tower. This approach also allowed us to isolate contributions from individual fires to observed trace gas time series. To help constrain the transport model, we used CRV tower observations during high fire periods to estimate emission factors for carbon monoxide and methane, and multi-angle remote sensing observations to estimate plume injection heights.

2.2 Methods

2.2.1 Meteorological Data

We used daily meteorological summaries from the National Climatic Data Center (http://www7.ncdc.noaa.gov/CDO/cdopoemain.cmd) for three stations in interior Alaska to assess synoptic-scale variability in fire weather. These stations were the Fairbanks International Airport, Eielson Air Force Base, and Minchumina. The Fairbanks and Eielson stations were selected because of their close proximity to the Stuart Creek II and Mississippi fires that accounted for about 12% of the total burned area in interior Alaska during 2013. Minchumina was selected because of its proximity to a set of fires to the southwest of Fairbanks, near Denali National Park (Figure 2.1). At each station we extracted hourly precipitation, mean surface air temperature, dew point temperature, and wind speed. Hourly relative humidity for each station was calculated using the August-Roche-Magnus approximation with the dew point and air temperature time series [*Lawrence*, 2005]. Hourly saturation vapor pressure was calculated following *Tetens* [1930] as a non-linear function of temperature. Hourly vapor pressure deficit (VPD) was calculated by subtracting the actual vapor pressure from the saturation vapor pressure. We extracted the noon local time data for precipitation, temperature, relative humidity, and wind speed to compare with the fire weather indices described below.

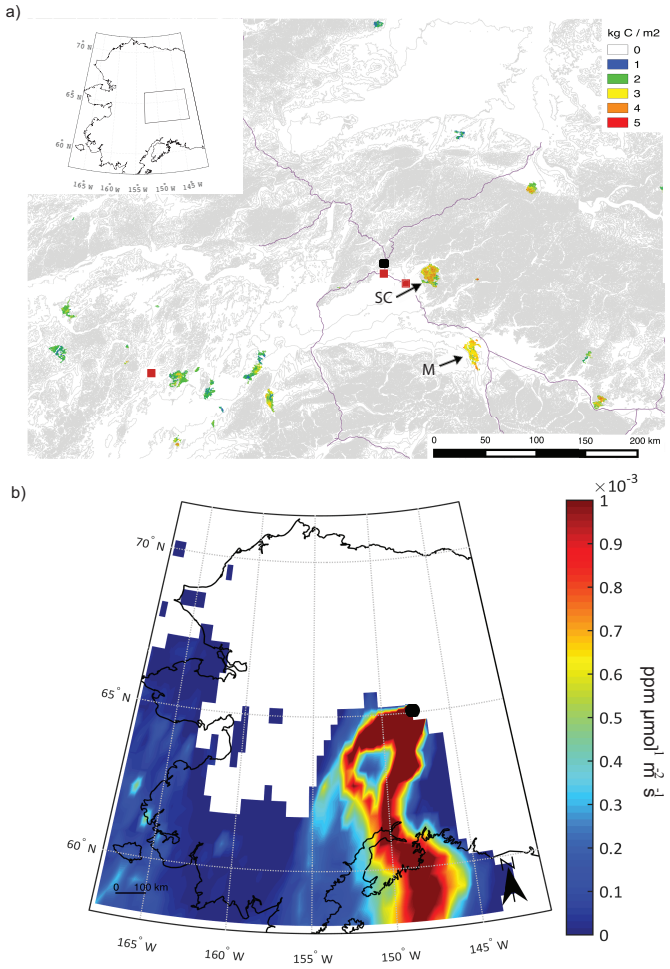

Figure 2.1 (a) Map of fire characteristics in our Alaska study domain during the summer of 2013. Alaska Fire Emissions Database (AKFED) total carbon emissions from fires are shown in kg C per m^2. (b) The daily mean of all PWRF-STILT footprints during a representative high fire period on 5 July 2013. In both panels, the location of CRV tower is denoted with a black circle, and Figure 1a the location of the Minchumina, Fairbanks International Airport, and Eielson Air Force Base weather stations are shown from left to right with red squares. In Figure 2.1a, the locations of the Stuart Creek II fire and the Mississippi fire are denoted by SC and M, respectively, major roads are shown as purple lines, and elevation is shown with gray shading.

We used the noon local standard time observations described above to estimate fire indices from the Canadian Forest Fire Weather Index System [*Van Wagner and Pickett*, 1985]. This system has three codes to characterize the moisture of fuel classes. The fine fuel moisture code (FFMC) is representative of fine fuels such as litter consisting of a dry weight layer approximately 1.2 cm deep. The FFMC attempts to capture the relatively fast drying of fine fuel in response to temperature, relative humidity, wind speed, and rainfall on short time-scales. It has

been used to indicate ease of ignition or ignition probability [*Van Wagner and Pickett*, 1985]. The duff moisture code (DMC) provides a metric for loosely packed decomposing organic material in surface soils 7 cm deep. The drought code (DC) represents deep compact organic material 18 cm deep and is an indicator of potential depth of burn. Each of these codes depends on a combination of temperature, humidity, wind speed, and precipitation. Three additional indices are derived from these codes. The initial spread index (ISI) combines wind and the FFMC to estimate fire weather influence on the spread rate. The build-up index (BUI) combines the duff moisture code and the drought code. The fire weather index (FWI) combines ISI and BUI to represent the energy release by the fire per unit length of fire front. In our analysis, we examined the ability of these indices from the Canadian Forest Fire Weather Index System that are aimed at capturing variability in fire spread rates. The, FFMC, ISI, and FWI indices are widely used by the fire management community to quantify different aspects of fire behavior and risk.

2.2.2 Emission Factors

We used high-resolution measurements from the CRV tower during periods of high fire influence from the summer of 2013 to determine emission factors for our modeling analysis. A CO threshold of 0.7 ppm was applied to isolate periods when fires had significant influence on CO_2 mole fraction. We estimated emission ratios by calculating the slope of CRV tower CO and CH_4 enhancements above background (ΔCO and ΔCH_4) relative to that of CO_2 (ΔCO_2). The Δ refers to CRV tower observations of trace gas mole fractions with background values subtracted. We applied a type II linear regression and then multiplied by a scalar to convert the molar ratio into grams of species emitted per kilogram of biomass burned, assuming 450 g C are emitted per kilogram of biomass burned [*Yokelson et al.*, 1997; *Akagi et al.*, 2011]. We used estimates from

Karion et al. [2016] to remove background levels of CO, CH_4, and CO_2. For CO_2 we also estimated and removed the influence of net ecosystem exchange (NEE) associated with gross primary production and ecosystem respiration fluxes. CO_2 anomalies originating from NEE were estimated by coupling the Polar Vegetation Photosynthesis Respiration Model (PVPRM) [*Luus and Lin*, 2015] fluxes with PWRF-STILT [*Henderson et al.*, 2015] simulations at the CRV tower. PVPRM provided three-hourly estimates of net ecosystem exchange from high latitude ecosystems for regions north of 55°N.

2.2.3 Plume Heights from the Multi-Angle Imaging Spectroradiometer (MISR)

The PWRF-STILT model used to quantify the influence of terrestrial net ecosystem exchange on CO_2 variability at CRV assumes that upwind air parcels that are transported within the bottom half of the planetary boundary layer are subsequently modified by surface exchange. Fire emissions, in contrast, have the potential to be injected in fast rising plumes through the full boundary layer and into the free troposphere [*Duck et al.*, 2007; *Leung et al.*, 2007; *Turquety et al.*, 2007; *Kahn et al.*, 2008]. Here we directly measured fire plume heights to create a better representation of fire injection in PWRF-STILT. The MISR instrument on Terra provides stereographic images of clouds and plumes, enabling the retrieval of height information [*Kahn et al.*, 2008]. We used the MISR Interactive Explorer (MINX) software program [*Nelson et al.*, 2013] to manually digitize the plume perimeters from all available imagery in Alaska during the summer of 2013. Plume heights were then computed by MINX for each 1 km MISR pixel in each perimeter, along with aggregate statistics of the mean, standard deviation, and maximum heights. In parallel we extracted boundary layer heights at the time of the MISR overpass from Modern-Era Retrospective Analysis for Research and Applications (MERRA) [*Reichle et al.*, 2011]. As described below in Section 2.3.3, we found the mean plume heights were

approximately the same as the boundary layer heights. Thus, results below defined the surface influence volume in STILT as extending from the surface to the top of the planetary boundary layer (PBL), with the assumption that the fire emissions were equally distributed within the PBL [*Turquety et al.*, 2007; *Kahn et al.*, 2008].

2.2.4 Active Fires, Fire Radiative Power, and the 2013 Fire Season

The spatial and temporal variability of active fires and fire radiative power was determined using fire detection observations from MODIS on NASA's Terra and Aqua satellites [*Giglio et al.*, 2003]. We specifically used the MCD14ML product and report fire detections for all confidence levels, because commission errors are generally low in boreal forest ecosystems. Observations between 58° to 71.5°N and 141° to 168.5°W were aggregated to create a daily time series with a 0.5° spatial resolution.

The 2013 Alaskan fire season had levels of fire activity, burned area, and emissions that were somewhat below long-term means. Annual burned area from AKFED in 2013, for example, was 533 kha compared with a 2001-2010 mean of 655 kha per year. Similarly, carbon emissions were 12.7 Tg C compared with a decadal average of 18 Tg C [*Veraverbeke et al.*, 2015]. In this context, it is also important to note that the year-to-year variability of wildfire emissions is extremely high in Alaskan forests. During 2001-2010 emissions were at a maximum in 2004 at 69 Tg C, and were at a minimum in 2008 at 1 Tg C.

2.2.5 Emissions Modeling

We compared the ability of three different fire emissions modeling approaches to capture variability in trace gas observations measured at the CRV tower. The three approaches were derived from satellite-derived observations of active fires, satellite-derived estimates of FRP, and daily emissions estimates from AKFED [*Veraverbeke et al.*, 2015]. Each approach provided a

slightly different temporal and spatial distribution of emissions in interior Alaska. AKFED is an empirical model of carbon consumption with a spatial resolution of 450 m and a temporal resolution of one day. Measurements of pre-fire fractional tree cover, difference normalized burned area, elevation, and day of burning determines fuel consumption in aboveground vegetation and soil organic layers. The timing of carbon releases in AKFED is determined by assigning the timing of the closest active fire detection for each burned pixel. The AKFED model estimated an annual total of 12.7 Tg C of emissions within our study domain during 2013 (Figure 2.1).

For the active fire emissions model, MODIS Aqua and Terra observations of active fires were binned each day to the resolution of our atmospheric model (0.5°). We then applied a conversion scalar (S_{FC}) to convert active fires into kg of carbon. S_{FC} was derived as the ratio of the annual sum of total emissions from AKFED and the annual sum of active fires within our domain. With this approach, the annual sum was constrained to yield the same annual integral of emissions; however, the spatial and temporal pattern of emissions was determined solely by the spatial distribution and timing of active fires.

$$E_{FC}\,(x,t) = \frac{S_{FC} \times FC\,(x,t)}{A\,(x)} \qquad (2.1)$$

where E_{FC} is the fire emissions with units of kg C m^{-2} day^{-1} in grid cell x and at day t, S_{FC} is the globally uniform scalar with units of kg C per active fire detection, FC is the sum of active fire detections in the grid cell each day, and A is the land surface area of each grid cell. The FRP model had a similar form:

$$E_{FRP}\,(x,t) = \frac{S_{FRP} \times FRP\,(x,t)}{A\,(x)} \qquad (2.2)$$

where E_{FRP} is the fire emissions with units of kg C m^{-2} day^{-1}, S_{FRP} is the globally uniform scalar with units of kg C per MW, and FRP is the sum of fire radiative power for all of the active fires in the grid cell each day. AKFED provides an output of daily fire emissions with units of kg C m^{-2} day^{-1}, and these emissions were averaged within each 0.5°grid cell of the atmospheric model. The daily time series of the AKFED, active fire, and FRP-derived emissions derived using these approaches are shown in Figure 2.2.

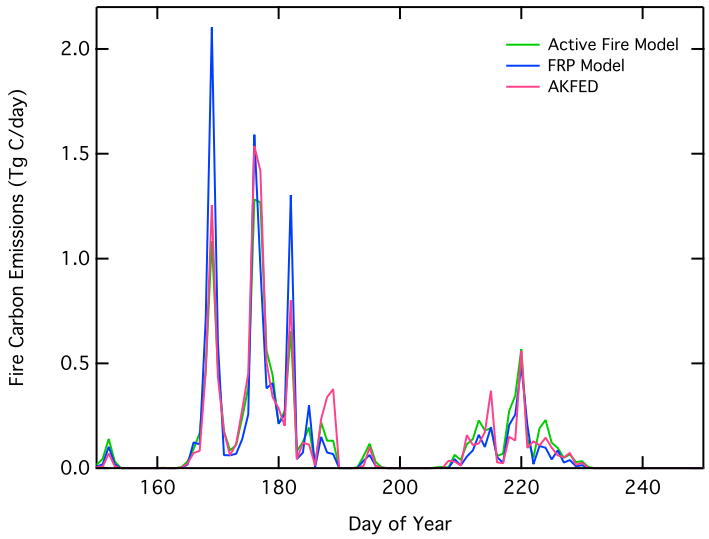

Figure 2.2 Time series of total daily fire carbon emissions (Tg C/d) for the active fire, fire radiative power (FRP), and Alaska Fire Emissions Database (AKFED) modeling approaches.

2.2.6 CRV Tower Observations

Atmospheric CO, CH_4, and CO_2 mole fractions during the summer of 2013 were measured at the CRV tower in Fox, Alaska (Figure 2.1a) using a Cavity Ring-Down Spectrometer (CRDS, Picarro models 2401 and 2401-m) [*Karion et al.*, 2016]. The tower is 32 m in height and is located on a ridge 611 meters above sea level in central Alaska at 64.986°N, 147.598°W. Atmospheric measurements from air drawn from 5 m, 17 m, and 32 m heights from

the base of the tower are averaged in 30-second increments (native measurement frequency for these CRDS units is approximately 0.5 Hz). In this study we used observations only from the 32 m intake because this level had the highest measurement density, with observations for 50 minutes out of every hour, and because this level was likely to have the smallest sensitivity to local ecosystem fluxes near the tower [*Karion et al.*, 2016].

The raw 30-second average measurements were processed by applying a water correction that was empirically determined in the laboratory prior to deployment of each CRDS unit, following procedures similar to those described in previous studies [*Chen et al.*, 2013; *Rella et al.*, 2013]. The CRDS instruments were calibrated using five reference tanks with mole fractions traceable to the WMO standard scales for all three gases, and drift-corrected using the average drift of two tanks (also traceable to WMO standard scales) measured every 8 hours. Total uncertainty (reproducibility and comparability to other NOAA network sites) of hourly mole fraction measurements at the site are generally <0.2 ppm for CO_2, 2 ppb for CH_4, and 5 ppb for CO (1-sigma). The measurement system at the CRV tower is described in more detail by *Karion et al.* [2016].

2.2.7 Atmospheric Modeling

STILT [*Lin et al.*, 2007] is a Lagrangian Particle Dispersion Model (LPDM), coupled offline to the PWRF regional atmospheric numerical weather prediction model [*Skamarock et al.*, 2005; *Chang et al.*, 2014; *Henderson et al.*, 2015], that computes the sensitivity - effectively the adjoint of the transport model - of measured atmospheric trace gas measurements to upwind fluxes in the form of a surface influence function (the "footprint" field; units of mole fraction / (μmol m^{-2} s^{-1})). We note that the spatial resolution of the PWRF model is 3.3 km over interior Alaska, however the PWRF-STILT footprints were evaluated on a 0.5° x 0.5° aggregated grid

[*Chang et al.*, 2014]. Each footprint field is calculated by counting the number of particles released in a reverse-time simulation in a surface-influenced volume and the time spent in that volume [*Lin et al.*, 2007]. In this study, 500 particles were released from the receptor location at each time step for the footprint calculations. To obtain the contribution (units of mole fraction) by the upwind fluxes to the observed concentration, the footprint field is convolved with an estimate of the upwind fluxes. *Nehrkorn et al.* [2013] for instance, studied the transport of CO_2 in Salt Lake City using WRF-STILT footprints in which the depth of the atmospheric layer influenced by surface fluxes was defined as half the depth of the PBL.

We used PWRF-STILT footprints to determine the contribution of fire emissions to CO, CH_4, and CO_2 mole fraction observations at the CRV tower. The footprints for CRV are on a 0.5° latitude-longitude grid with a temporal resolution of 1 hour during the day (hours 0600 to 1800 local time) and 3 hours during the night (hours 1800 to 0600). An example of the spatial distribution for the daily mean of footprints for the study period is shown in Figure 2.1b. The footprints are multiplied by an a *priori* flux field, defined here as the fire emissions ($E_{FC,}$ E_{FRP}), to quantify the mole fraction measured at the CRV tower location. To identify sensitivities to the injection height, the definition of the top of the surface-influenced layer in STILT was varied from the default of half the depth of the PBL to, respectively, 1.0 and 1.5 times the depth of the PBL. For each case, the flux remained the same, but the vertical resolution of the surface influenced volume was modified. For the 1.0 PBL case, which best matched the MISR plume observations, the influence of fire emissions on CRV trace gas mole fractions were reduced by approximately 14% relative to the model default. All other aspects of the modeling system follow directly from *Henderson et al.* [2015].

To impose diurnal variation in the fire emissions we binned daytime (0600 to 1800) and nighttime (1800-0600) FRP each day in each grid cell, and assumed the relative fractions of FRP were proportional to emissions. Emission factors (g trace gas species (kg biomass)$^{-1}$) were used to convert total carbon emissions to CO, CH_4, and CO_2 emissions. We obtained and implemented emission factors from the CRV tower measurements as described below.

2.3 Results

2.3.1 Influence of Variability in Daily Meteorology on Fire Activity and Emissions

Two distinct high fire periods occurred during the summer of 2013 in interior Alaska, as measured using the number of satellite-detected active fires (Figure 2.3a). The first, between day of year (DOY) 168 and 192, was coincident with the highest midday surface air temperatures (Figure 2.3b) and lowest relative humidity levels of the year (Figure 2.3c). Precipitation during this interval was low, with only a single significant event recorded at Fairbanks Airport and Minchumina on DOY 173 and several smaller precipitation days observed between DOY 180 and 185 (Figure 2.3d). A second period of fire activity occurred between DOY 210 and 230. High temperatures, low relative humidity, and an absence of precipitation events also characterized this second period. Wind speeds were variable throughout the season (Figure 2.3e). After DOY 230, a series of precipitation events terminated the 2013 fire season.

To assess the influence of daily meteorology in modulating regional fire activity, burned area, and emissions, we conducted a regression analysis with individual daily meteorological variables and fire weather indices. Among the different variables shown in Figure 2.3, daily temperature was most strongly correlated with the different fire products, followed by relative humidity, precipitation, and wind speed (Table 2.1). VPD, derived from a combination of

temperature and relative humidity, was slightly better than temperature as a predictor for FRP and burned area, but had about the same level of performance for the other fire time series. The relatively high performance of VPD as a predictor for burned area observed here is consistent with earlier work indicating that VPD anomalies in interior Alaska synchronizes spread rates across multiple fires [*Sedano and Randerson*, 2014].

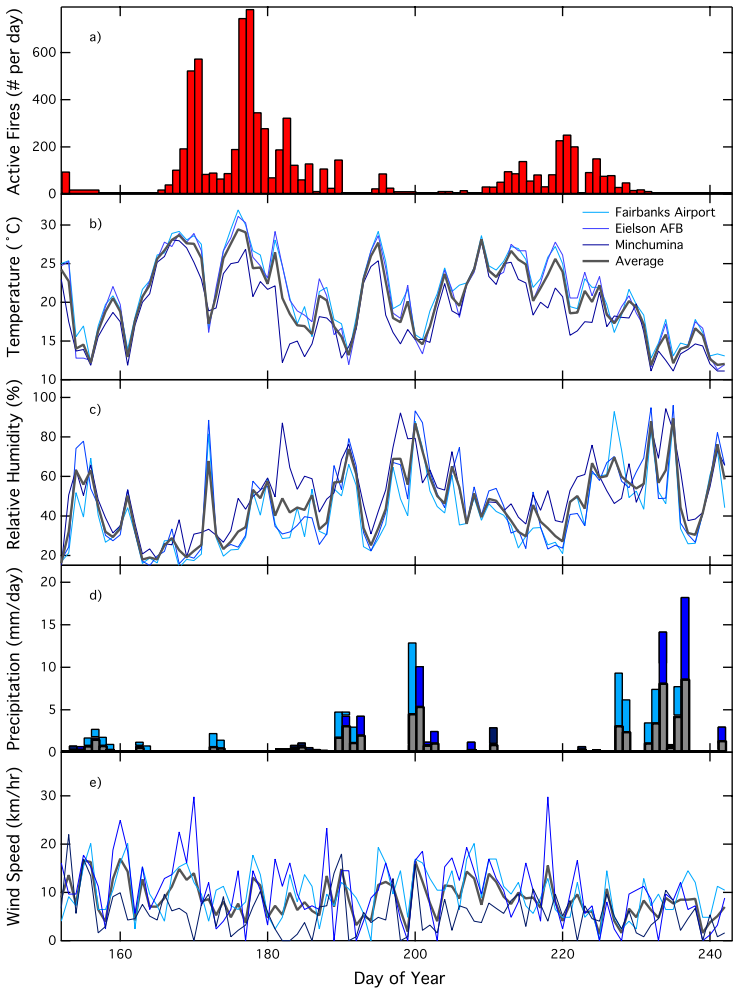

Figure 2.3 Comparison of daily weather variables from three stations in interior Alaska, including Fairbanks International Airport, Eielson Air Force Base, and Minchumina. The different panels show (a) the number of active fires per day, (b) temperature (C°), (c) relative humidity (%), (d) precipitation (mm/d), and (e) wind speed (km/h). All of the variables except precipitation represent the hourly average at noon local standard time. Precipitation is the 24 h sum.

Of the 6 fire weather indices that we analyzed from the Canadian Forest Fire Weather Index System, FFMC, ISI, and FWI indices had the strongest relationships with the daily time

series of fire activity. The FFMC and ISI indices were moderately correlated with daily fire activity, explaining between 14 and 21% of the variance of the different daily fire time series (Table 2.1; Figure 2.4). FWI was the most successful predictor of all of the different fire weather indices examined here, capturing between 24% of the variance for FRP and 29% for burned area. Compared with the meteorological variables, FWI had a similar level of predictive capacity as VPD and temperature.

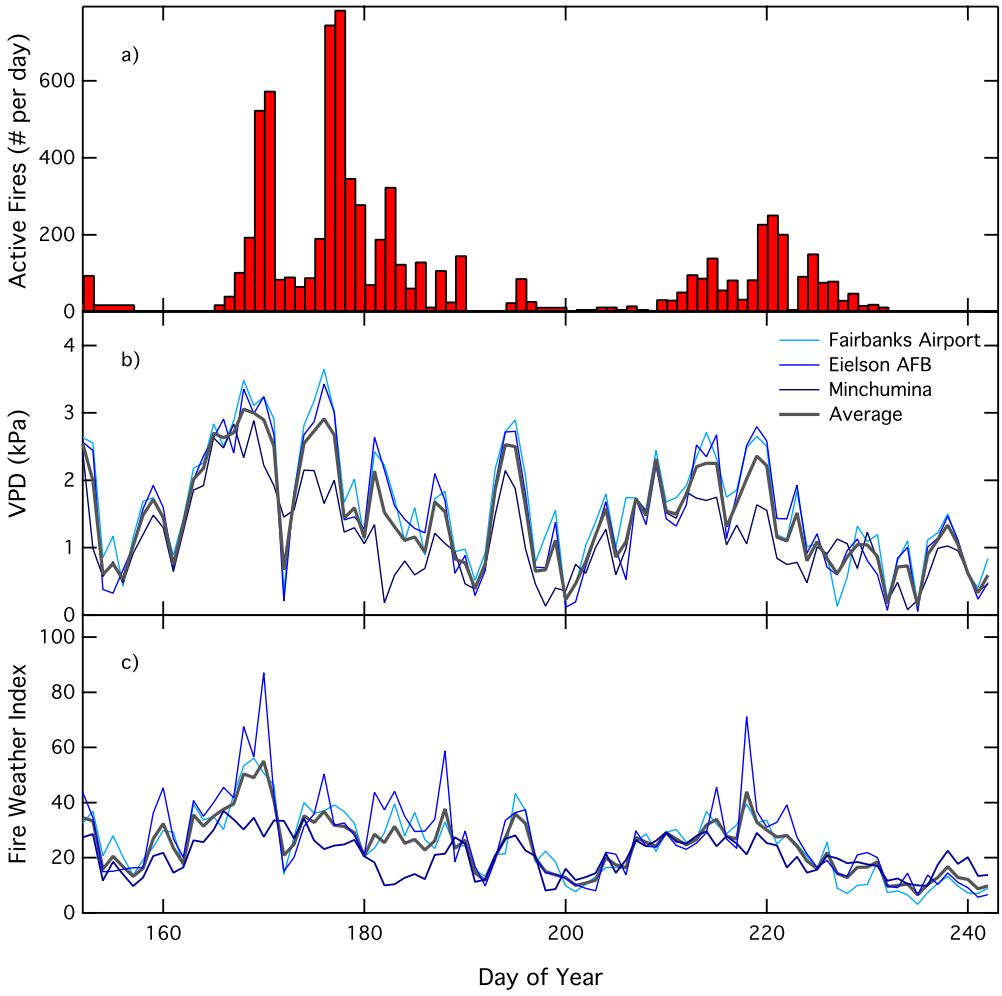

Figure 2.4 Comparison of daily complex weather variables from Fairbanks Airport, Eielson Air Force Base, Minchumina, and the average. (a) The number of active fires per day. (b) Vapor pressure deficit (VPD). (c) The Canadian Forest Fire Weather Index (FWI).

Table 2.1 Pearson's Coefficient of Determination (r^2) Between Daily Weather Variables, Fire Weather Indices, and Time Series Fire Activity[a].

	Meteorological					Fire Weather Indices					
	T	RH	P	WS	VPD	FFMC	DMC	DC	ISI	BUI	FWI
Active Fires	0.32	0.11	0.05	4e-4	0.31	0.20	0.17	0.02	0.18	0.09	0.28
Fire Radiative Power	0.20	0.09	0.03	0.001	0.23	0.15	0.11	0.03	0.18	0.04	0.24
AKFED Burned Area	0.28	0.12	0.04	4e-6	0.31	0.21	0.15	0.04	0.21	0.06	0.29
AKFED Emissions	0.25	0.09	0.04	0.001	0.25	0.17	0.18	0.03	0.14	0.08	0.23

[a]All correlations were significant at $p<0.05$ except for precipitation and the drought code. These daily correlations were computed over the period from day of year 152 to day of year 242. The weather variables we analyzed included temperature (T), relative humidity (RH), precipitation (P), wind speed (WS), and vapor pressure deficit (VPD). The fire weather indices included the fine fuel moisture code (FFMC), duff moisture code (DMC), drought code (DC), initial spread index (ISI), buildup index (BUI), and fire weather index (FWI). The Alaskan Fire Emissions Database is abbreviated as AKFED.

2.3.2 Emission Factors

We identified six periods of significant fire influence when a synchronized enhancement of CO, CH_4, and CO_2 was observed at CRV tower during July and August. We used these intervals to estimate emission factors for CO and CH_4 (Figure 2.5). Emission factors for CO ranged from 104 - 166 g CO kg^{-1} of combusted biomass and emission factors for methane varied between 6.26 – 8.96 g CH_4 kg^{-1} biomass (Table 2.2; Figure 2.6). All six periods had high correlations between ΔCO and ΔCO_2 (r between 0.96 and 0.99) and between ΔCH_4 and ΔCO_2 (r values ranging between 0.96 and 0.99). Averaging across these periods, the mean $\Delta CO/\Delta CO_2$ emission factor was 134±25 g CO kg^{-1} biomass and the mean $\Delta CH_4/\Delta CO_2$ emission factor was 7.74±1.06 g CH_4 kg^{-1} biomass. The errors associated with the final average emission factors were calculated as one standard deviation between the average emission factors for all six of the high fire periods. We used these mean emission factors in our transport model simulations of fire contributions to the CRV tower described below sections 2.3.4.

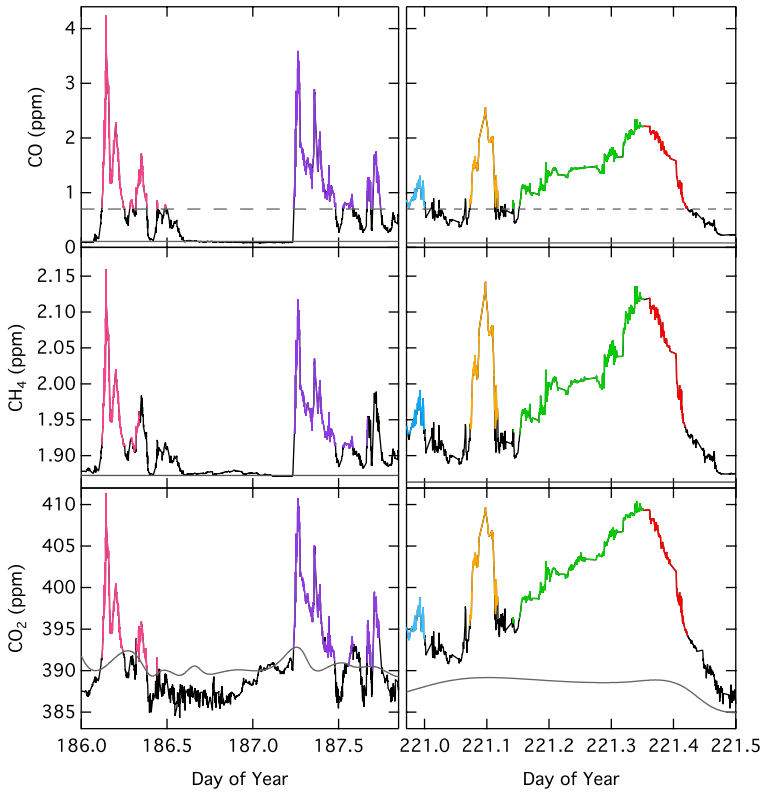

Figure 2.5 The original data from the CRV tower used to calculate emission ratios. (left column) July and (right column) August. (top row) CO (ppm), (middle row) CH_4 (ppm), and (bottom) CO_2 (ppm) are displayed. Background threshold for CO is given by dashed gray line; backgrounds for CH_4 and CO_2 are shown by solid gray lines. The time intervals used in emission ratio calculations are highlighted in color: July period 1 (pink), July period 2 (purple), August period 1 (blue), August period 2 (orange), August period 3 (green), and August period 4 (red).

Table 2.2 Emission ratios and emission factors (g species emitted kg^{-1} biomass burned) from selected observations during high fire periods at CRV tower. Correlations are given as Pearson's correlation coefficient (r).

				$\Delta CO/\Delta CO_2$		**$\Delta CH_4/\Delta CO_2$**	
Date	Time	# Data Points	Correlation CO (CH_4)	Emission Ratio	Emission Factor[1]	Emission Ratio	Emission Factor
July 5 – P1	12am – 12pm	183	0.98 (0.98)	0.158±0.002	166±2.1	0.0110±0.0002	6.62±0.12
July 6 –P2	5am – 7pm	325	0.97 (0.96)	0.152±0.002	160±2.1	0.0104±0.0002	6.26±0.12
August 8 – P1	10:30pm – 12am	74	0.96 (0.96)	0.122±0.004	128±4.2	0.0137±0.0005	8.24±0.30
August 9 – P2	1:30am – 3am	96	0.99 (0.99)	0.127±0.002	133±2.1	0.0149±0.0002	8.96±0.12
August 9 – P3	3:30am – 8:30am	443	0.97 (0.97)	0.099±0.0002	104±0.2	0.0136±0.0002	8.18±0.12
August 9 – P4	8:30am – 10:30am	139	0.99 (0.99)	0.109±0.0008	114±0.8	0.0136±0.0001	8.18±0.06
Mean				0.128±0.023	134±25	0.0139±0.0018	7.74±1.06

1. To estimate emission factors from emission ratios, we assumed that combusted biomass was comprised of 45% carbon [*Yokelson et al.* 1997; *Akagi et al.,* 2011].

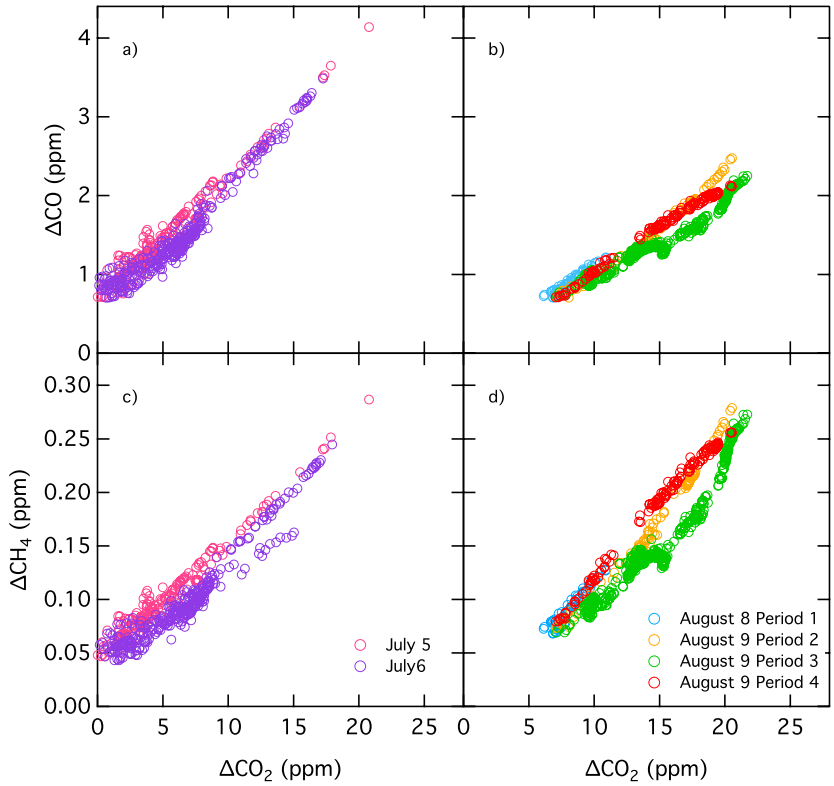

Figure 2.6 Relationship between ΔCO (CO observed - CO background) and ΔCO_2 (CO_2 observed - CO_2 background) for periods of high fire influence at the CRV tower in (a) July and (b) August. (c and d) Relationship between ΔCH_4 (CH_4 observed - CH_4 background) and ΔCO_2 (CO_2 observed - CO_2 background) is shown for the same two periods, respectively.

Table 2.3 Pearson's Correlation Coefficient (r) Between Daily Fire Emissions and Observations From CRV Tower[a]

	Active Fire Model	**FRP Model**	**AKFED**
CO hourly	0.65*	0.63*	0.68*
CH_4 hourly	0.45*	0.51*	0.42*
CO_2 hourly	0.10	0.18	0.04

*Significant correlations with p values <0.01. These correlations were computed using daily data over the period from DOY 152 to DOY 242.
[a]Background concentrations for CO, CH_4, and CO_2 were subtracted from CRV observations for this comparison.

2.3.3 Injection Heights

We digitized a total of 35 individual fire plumes in our study domain during the summer of 2013 to extract injection heights from the MISR imagery. This set represented all of the fire plumes we could visibly identify from the complete set of available MISR imagery, aided by

MODIS active fire detections, between DOY 130 and DOY 270. The plumes had an average mean height and standard deviation of 1250 ± 551 meters above terrain and an average maximum height of 2480 ± 931 meters above terrain (Figure 2.7). We separated the plume and boundary height information into two periods corresponding to the first and second high fire periods visible in Figure 2.3a. The first covered the interval from DOY 168 to 192 and the second from DOY 210 to 230. Maximum plume heights during the first high fire period were significantly higher ($p < 0.02$) than during the second period (2920 ± 636 vs. 2300 ± 980 meters above terrain). Mean plume heights, however, were not significantly different between the two periods.

Planetary boundary layer height estimates from Modern-Era Retrospective Analysis for Research and Applications (MERRA) reanalysis, sampled on the same days and grid cells as the plume observations, had a mean of 1520 ± 450 meters. For 20 out of the 35 plume observations, the MERRA planetary boundary layer was higher than the mean but lower than the maximum reported plume heights from MISR. Considering the relatively high level of agreement between planetary boundary layer and plume heights, and moderate levels of uncertainty in estimating both of these measures, we modified PWRF-STILT for the fire simulations so that the surface influenced volume extended through the full planetary boundary layer height in each grid cell (see section 2.2.7).

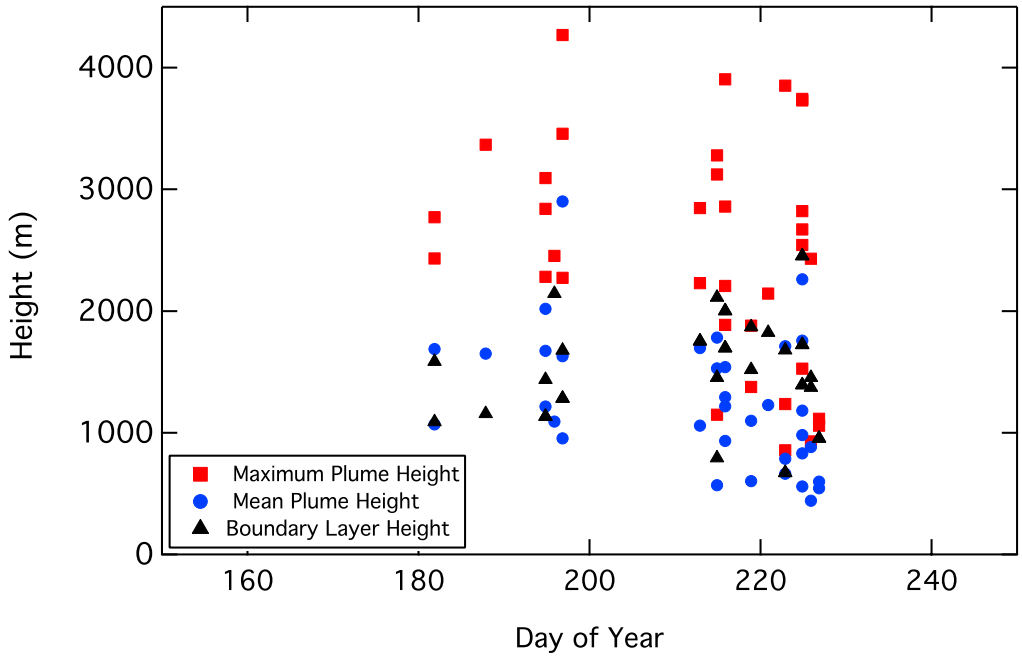

Figure 2.7 Daily Multiangle Imaging SpectroRadiometer (MISR) derived maximum plume heights (red squares) and mean plume heights (blue circles) compared with geographically and temporally matched Modern-Era Retrospective Analysis for Research and Applications (MERRA) boundary layer heights (black triangles).

2.3.4 Modeling Fire Contributions to Trace Gas Variability

During the summer of 2013 there were two periods during which elevated CO and CH_4 were observed at the tower (Figure 2.8). The first period occurred from DOY 186 to 189, and the second period occurred from DOY 221 to 222. During the first period in July maximum trace gas mole fractions were 6.91 ppm for CO, 2.15 ppm for CH_4, and 411 ppm for CO_2. Similarly, during the second period in August maximum observed mole fractions were 2.57 ppm CO, 2.14 ppm CH_4, and 412 ppm CO_2. As described below, the synchronized enhancement of all three trace gas species during these two time periods indicated that fire emissions were a driver of the observed variability.

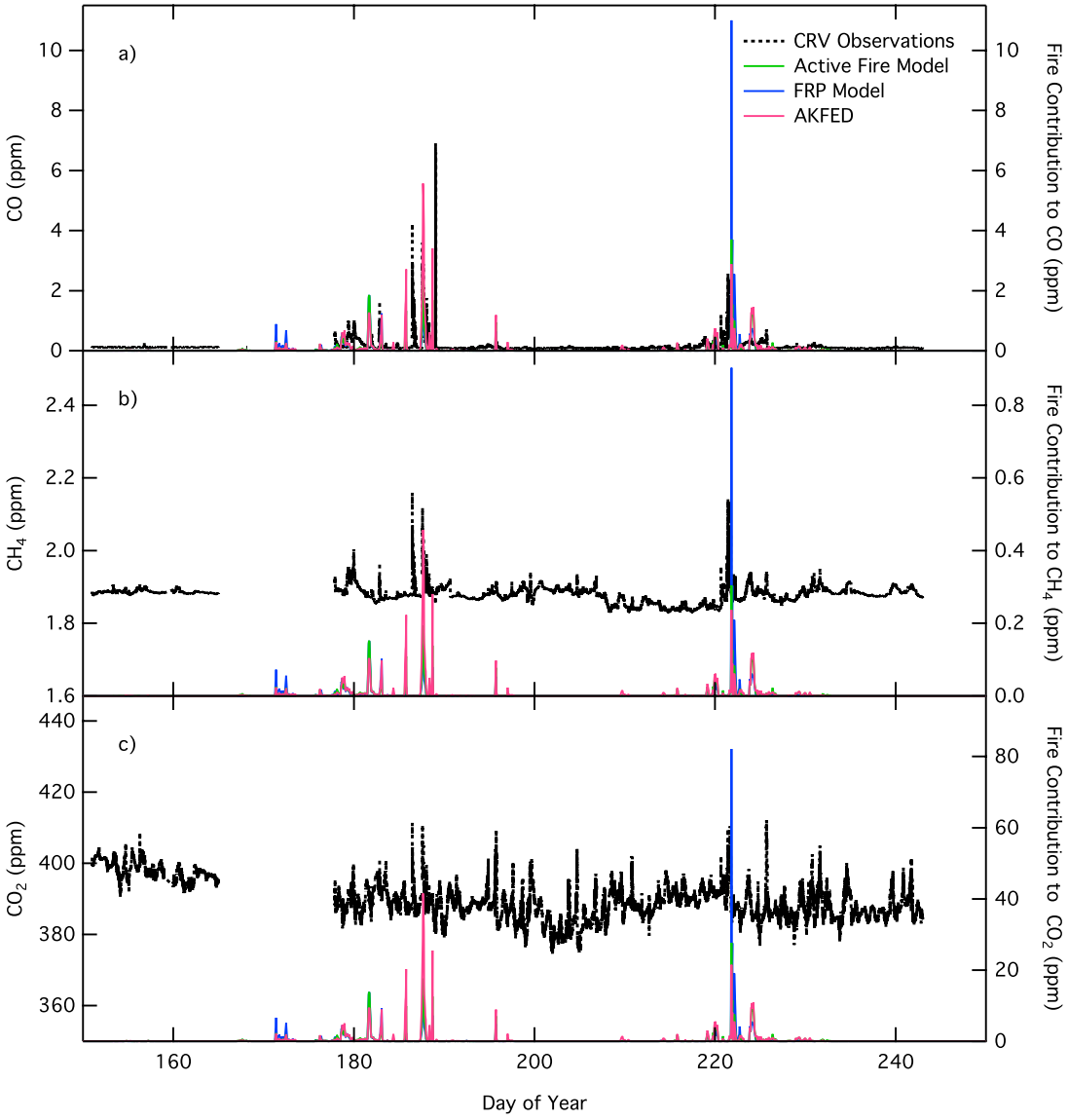

Figure 2.8 Observations from the CRV tower (black dashed line) versus active fire approach (green), FRP approach (blue), and AKFED (pink) for (a) CO (ppm), (b) CH_4 (ppm), and (c) CO_2 (ppm). Left y axis corresponds to CRV tower observations.

The model simulations combining fire emissions with PWRF-STILT provided evidence that the two anomalously high periods of CO and CH_4 at the CRV-NOAA tower were attributable to boreal fire emissions from interior Alaska (Figure 2.8). For AKFED, the model had a correlation coefficient of 0.68 with observed daily mean CO and had a high bias of approximately 60%. CO estimates from the model driven by active fires or FRP had similar

levels of correlation with the observations as AKFED (Table 2.3), although the timing of individual daily peaks varied among the different emissions sources (Figure 2.8a). These results suggest the performance of AKFED, in terms of capturing daily and synoptic variability in trace gas variability, was similar to more established approaches that have relied on active fires to capture fine temporal scale variability in emissions (e.g., *Mu et al.* [2011]). Our model simulations were able to explain a smaller amount of the variability in CH_4 (Figure 2.8b), which is consistent with the response of widespread methane sources in lowland ecosystems of interior Alaska responding in parallel to the synoptic-scale variability shown in Figure 2.3 [*Chang et al.*, 2014]. Fires explained only a very small amount of the variability in atmospheric CO_2 during the growing season period (Figure 2.8c). This finding is consistent with only moderate levels of fire emissions observed during 2013 in Alaska (12.7 Tg C) that are near the decadal annual mean (18 Tg C) [*Veraverbeke et al.*, 2015], and a dominant role of photosynthesis and ecosystem respiration in influencing surface atmospheric CO_2 variability on synoptic and seasonal time scales in high latitude ecosystems [*Luus and Lin*, 2015; *Karion et al.*, 2016].

2.3.5 Individual Fire Contributions to Modeled Trace Gas Mole Fractions

The combined AKFED-PWRF-STILT model allowed us to isolate the daily contribution of individual fires to simulated trace gas simulations at the CRV tower. In our analysis, we separated contributions from the Stuart Creek II fire, which was located approximately 58 km southeast of the tower, and the Mississippi fire, which was located about 144 km southeast of the tower, from all other fires in the state. We identified the grid cells containing the individual fires of interest using burn perimeters from the Alaska Large Fire Database. We then masked all fire emissions in these grid cells to zero in AKFED, and then re-ran the convolution of AKFED and PWRF-STILT. The individual fire contributions were then calculated by subtracting this version

of the combined AKFED-PWRF-STILT model from the original simulation. The Stuart Creek II fire accounted for 75% of the total CO mole fraction signal from fire when integrated over the fire season, whereas the Mississippi fire accounted for 6% of the signal at the CRV tower – with most of its impact occurring during the second high fire period (Figure 2.9). Other more remote fires were responsible for the remaining 19% of the CO mole fractions at the CRV tower. The capability to link individual fires to tower observations is novel, and may allow the exploration of relationships between regionally varying ecosystem processes and trace gas emissions and composition in future work.

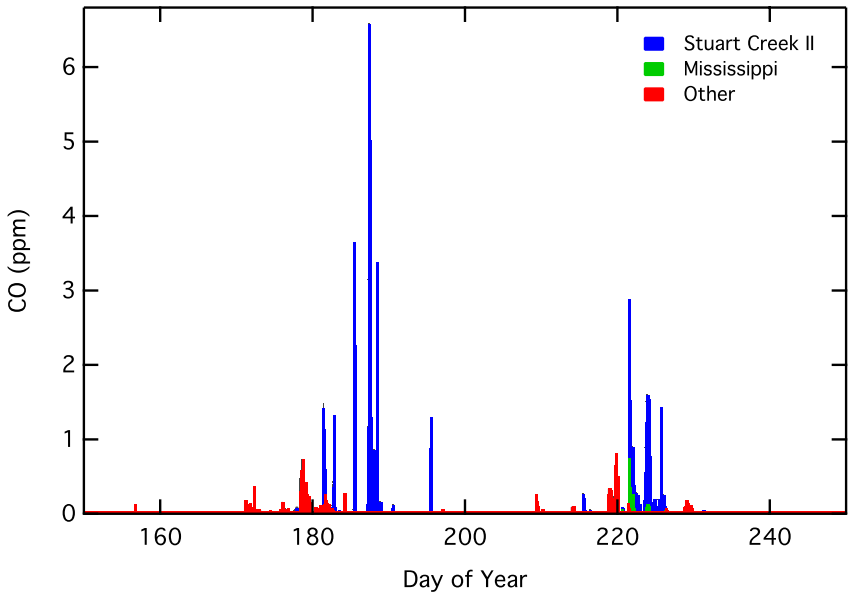

Figure 2.9 Contributions to CO (ppm) observed at the CRV tower from individual fire events. The Stuart Creek II fire is shown in blue, the Mississippi fire in green, and the sum of other fires is shown in red.

2.4 Discussion

2.4.1 The Influence of Daily Variations in Meteorology on Fire Activity

Daily variability in meteorology is well known to influence many aspects of boreal fire behavior [*Johnson*, 1996]. Here we found that temperature and vapor pressure deficit were the most important meteorological fields to explain daily fire activity during the summer of 2013.

The importance of these variables has been noted in past studies at different temporal and spatial scales [*Flannigan and Harrington*, 1988; *Bessie and Johnson*, 1995; *Duffy et al.*, 2005; *Sedano and Randerson*, 2014]. Monthly burned area in different Canadian provinces was shown to vary considerably as a function of extended periods of days with low precipitation or relative humidity [*Flannigan and Harrington*, 1988]. *Duffy et al.* [2005] found that June temperature was an important variable in explaining year-to-year variations in Alaskan burned area. VPD is an indicator of fire spread in boreal forest ecosystems and the sum of positive daily VPD anomalies is correlated with annual burned area [*Sedano and Randerson*, 2014].

The Canadian Forest Fire Weather Index System has been used extensively to quantify past, present, and future patterns in fire behavior [*Stocks et al.*, 1998; *Flannigan et al.*, 2001; *Bergeron et al.*, 2004; *Bedia et al.*, 2015]. For example, *Stocks et al.* [1998] found that under a doubled CO_2 scenario, the fire season started earlier and areas with high to extreme fire danger expanded across Canada and Russia. *Bedia et al.* [2015] found that fire weather in boreal forests will become increasingly sensitive to short-term climate fluctuations in a warming scenario to 2045. We found that temperature and VPD had a similar level of predictive capacity as FWI, and that FWI performed better than all of the other fire weather indices. Although the Canadian Forest Fire Weather Index System is a useful tool for estimating future fire weather conditions, our results suggest other more direct weather variables, like VPD, also have the potential to explain variations in fire dynamics in boreal forest ecosystems. VPD has been used as a driver of a global scale prognostic fire model [*Pechony and Shindell*, 2009], and our results confirm that there is a strong mechanistic relationship between this variable and daily burned area and emissions in boreal North America.

2.4.2 CO and CH_4 Emission Factors

Although recent aircraft and ground observations have reduced uncertainties in wildfire emission factors for individual biomes [*Akagi et al.*, 2011], a lack of long-term time series of atmospheric composition data near large fire complexes limits our ability to dynamically model emission factors as a function of changing environmental conditions. For the boreal forest, relatively few direct measurements of emission factors exist, and this has led to the prescription of biome-invariant values in large-scale fire models, like the Global Fire Emissions Database [*Van der Werf et al.*, 2010], the Fire Inventory from the National Center for Atmospheric Research [*Wiedinmyer et al.*, 2011], and the Wildland Fire Emissions Information System [*French et al.*, 2014]. Previous aircraft and field campaigns have led to the sampling of 23 fresh boreal fire plumes over the last three decades using flasks [*Cofer et al.*, 1990; *Radke et al.*, 1991; *Nance et al.*, 1993; *Cofer et al.*, 1998; *Goode et al.*, 2000] and continuous flow gas analyzers [*Simpson et al.*, 2011]. A synthesis of these data by *Akagi et al.* [2011] yielded a mean CO emission factor of 127 ± 45 g CO kg^{-1} biomass and a mean CH_4 emission factor of 5.96±3.14 g CH_4 kg^{-1} biomass. Here, during two high fire periods, we obtained emission factors that were slightly higher than the mean from *Akagi et al.* [2011]. Our estimates of 134 ± 25 g CO kg^{-1} biomass and 7.74 ± 1.06 g CH_4 kg^{-1} biomass suggests that the 2013 Alaskan fires may have had a somewhat larger relative contribution from a smoldering combustion phase.

Our analysis suggests that continuous, high temporal resolution tower measurements of greenhouse gases in a high fire region can provide new information on emission factors that complements aircraft plume sampling. Even during a moderate fire season, we were able to identify six periods in which trace gas signals from individual fires were large enough to derive emission factors. While background CO and CH_4 concentrations were relatively constant over

time, enabling a relatively clean separation of the anomaly caused by fires, CO_2 was much more variable due to numerous ecosystem sources and sinks that fluctuated on diurnal, synoptic, and seasonal timescales. This variability makes it critical to accurately simulate and remove the CO_2 variability originating from terrestrial net ecosystem exchange using ecosystem models and observations from low fire periods [*Karion et al.*, 2016].

Further work using high temporal resolution tower observations is necessary to understand environmental controls on boreal forest fire emission ratios. More observations may provide a way to relate emission factors to fire type (smoldering vs. flaming), weather variability, land and tree cover, drainage status, soil moisture, and burn severity. The modeling approach developed here is well suited for studying these relationships because it allows for the identification of trace gas contributions from individual fires. More specifically, the use of PWRF-STILT in future work may make it possible to link environmental and weather variables at the time and location of a single wildfire to greenhouse gas mole fraction anomalies observed at a tower. The number of days with strong fire signals was relatively low during the summer of 2013, limiting our ability to investigate these relationships. An important next step in this context is to extend this analysis to the high fire seasons observed in the Canadian Northwest Territories in 2014 and in Alaska in 2015.

2.4.3 Top Down Constraints on Fire Emissions Inventories

In past studies, active fires and FRP have been widely used to distribute fire emissions in space and time [*Ichoku and Kaufman*, 2005; *Wooster et al.*, 2005; *van der Werf et al.*, 2006; *Jordan et al.*, 2008; *Kaiser et al.*, 2009a], and in this study we show that AKFED had a similar performance to these more commonly used methods. The relationship between observed trace gas at the CRV tower and AKFED combined with PWRF-STILT, with a correlation coefficient

of 0.68, provides partial validation for AKFED. The difference and similarities among approaches are evident when the models are combined with PWRF-STILT to predict carbon concentrations at CRV tower (Figure 2.8, Table 2.3). All three approaches captured some of the fine-scale temporal dynamics of the fire signals as observed at the tower, however, on average, the signals were somewhat overestimated. Averaged over the fire season, AKFED had a positive bias of 60%. AKFED exhibits this bias primarily during the first fire period, whereas for the FRP-based model the overestimation appears mostly during the second fire period. The three conceptual approaches show discrete differences in fire emissions both temporally (Figure 2.2) and spatially (Figure 2.1). Although conceptually distinct, the models are not completely independent, which contributed to their fairly similar spatiotemporal dynamics. AKFED leverages MODIS active fire data to assign daily burned area and the FRP and active fire approaches essentially redistribute the total carbon emissions from AKFED in space and time based on the timing and locations of the MODIS active fire detections. Daily variability in AKFED is primarily driven by variations in burned area with a smaller influence of differences in carbon consumption. Likewise the number of active fires and burned area are highly correlated [*Giglio et al.*, 2003], highlighting another shared characteristic of the different emissions time series.

2.5 Conclusions

By combining a high-resolution fire emissions inventory with a regional atmospheric model, we estimated fire contributions to trace gas variability measured at a tower in interior Alaska. Our modeling system enabled us to isolate the contribution of individual fires to daily variations in trace gas mole fractions and was uniquely constrained by region-specific emission

factors and injection height information. We found moderate levels of correlation between observed and modeled CO, CH_4, and CO_2 concentrations from boreal fires. Differences between modeled and observed mole fractions can be explained by underlying uncertainties in the emissions inventory, transport modeling system, and our assumptions regarding the use of fixed emission factor and plume injection parameterizations. VPD and temperature variables had a similar level of correlation with daily fire time series as more complex Canadian forest fire weather indexes, including FWI. We found emission factors that were above average relative to the mean of previous studies. Further study of high-resolution CO, CH_4, and CO_2 tower measurements during a high fire year using this method could provide opportunities to estimate boreal forest fire emission ratios. Our analysis demonstrates the feasibility of combining high-resolution fire emissions and atmospheric transport models to study relationships between meteorology and emissions. Further work building on this approach may further reduce uncertainties of fire-climate feedbacks in the boreal forest.

Acknowledgements

The research described in this paper was performed for the Carbon in Arctic Reservoirs Vulnerability Experiment (CARVE), an Earth Ventures (EV-S1) investigation, under contract with the National Aeronautics and Space Administration. E.B.W. thanks the US National Science Foundation for a Graduate Research Fellowship (NSF#2013172241). Computing resources for this work were provided by the NASA High-End Computing (HEC) Program through the NASA Advanced Supercomputing (NAS) Division at Ames Research Center.

Chapter 3

Evidence for a larger contribution of smoldering combustion to boreal forest fire emission factors from tower observations in Alaska

Adapted from:

Wiggins, E.B., Sweeney C., Miller J.B., Andrews A., Miller C.E., Randerson J.T. (2018), Evidence for a larger contribution of smoldering combustion to boreal forest fire emission factors from tower observations in Alaska. *Journal of Geophysical Research: Atmospheres*, in prep.

3.1 Introduction

Boreal forest fires influence the carbon balance and climate in the Northern Hemisphere through a variety of pathways. Boreal forest fires initiate succession, regulate patterns of carbon accumulation, and directly release carbon to the atmosphere [*Johnson*, 1996]. One of the largest reservoirs of global terrestrial carbon resides in organic soils underlying boreal forests [*Apps et al.*, 1993; *McGuire et al.*, 2010], and fires in the boreal forest can consume significant amounts of aboveground and belowground biomass [*Harden et al.*, 2000; *French et al.*, 2004]. Many boreal forest fires are stand replacing and high energy, with enough convective power to inject smoke into the upper troposphere and lower stratosphere where it can be transported across the northern hemisphere [*Forster et al.*, 2001; *Turquety et al.*, 2007].

Emissions from boreal fires can significantly influence global and regional atmospheric particulate and trace gas concentrations [*Wotawa et al.*, 2001; *Kasischke et al.*, 2005]. Boreal forest fires have contributed a substantial amount of carbon-based trace gasses to the atmosphere

over the last 50 years [*French et al.*, 2002]. Roughly 95% of carbon emissions from fires are released as CO_2, CO, and CH_4 [*Urbanski*, 2014]. Large-scale variations in burned area, fire severity, and depth of burn govern overall fire emissions. Annual burned area in the boreal forest has been increasing over the past few decades in response to rising temperatures [*Gillett et al.*, 2004; *Kasischke and Turetsky*, 2006; *Veraverbeke et al.*, 2017]. Future climate models project amplification of warming at high latitudes that will likely increase fire activity and thus emissions in response to favorable hot and dry fire weather conditions [*Flannigan et al.*, 2001; *de Groot et al.*, 2013; *Young et al.*, 2017].

Environmental conditions at the time of combustion, including daily weather, vegetation, and terrain modify the composition and magnitude of emissions [*Ryan*, 2002; *Wiggins et al.*, 2016] by influencing combustion efficiency [*Boby et al.*, 2010] and fire spread rates [*Sedano and Randerson*, 2014]. The combustion characteristics of a fire, specifically the relative contributions of smoldering and flaming combustion, considerably impact the chemical composition of emissions [*Ward and Radke*, 1993; *Yokelson et al.*, 1997; *Akagi et al.*, 2011; *Urbanski*, 2014]. Flaming combustion is more efficient at oxidizing organic matter directly to CO_2 gas than smoldering combustion, and as a consequence, smoldering combustion produces more CO, CH_4, and organic carbon aerosol [*Ward and Radke*, 1993; *Urbanski et al.*, 2008]. Smoldering combustion can be defined as combustion with a modified combustion efficiency less than 0.9 [*Urbanski*, 2014].

Flaming combustion requires the presence of organic material that burns efficiently in a high oxygen environment [*Ottmar*, 2001], and often occurs in boreal forests when fires consume dry aboveground fuels, including vegetation components with low moisture content, litter, and fine woody debris [*French et al.*, 2004]. Smoldering is a dominant combustion phase for

burning of belowground biomass and larger coarse woody debris. Residual smoldering combustion in boreal forests can continue to occur for weeks after a flaming fire front has passed through, especially in areas with carbon rich organic soils [*Bertschi et al.*, 2003].

Given the likelihood of enhanced boreal forest fire emissions in the future, it is imperative to be able to accurately quantify emissions of important trace gases including CO, CH_4, and CO_2 that affect the climate by altering the radiative balance of the planet [*Kasischke et al.*, 2005], and atmospheric chemistry by means of influencing tropospheric concentrations of hydroxyl radical [*Levine and Cofer*, 2000]. Relative proportions of CO, CH_4, and CO_2 emitted from boreal fires provide clues about what phase of combustion is responsible for emissions [*Ward and Radke*, 1993].

The most widely used approach to quantify specific trace gas emissions from fires involves quantifying the amount of dominant vegetation burned by a fire and multiplying that amount by a scalar called an emission factor that relates the amount of a certain gas produced per kilogram of biomass consumed [*Seiler and Crutzen*, 1980]. Emission factor calculations require knowledge of the excess mixing ratios of a trace gas or particulate species of interest, the carbon budget of a fire, and the carbon content of the biomass combusted [*Akagi et al.,* 2011]. Emission factors are most commonly estimated by multiplying an emission ratio by the carbon content of the total biomass consumed [*Andreae and Merlet*, 2001]. An emission ratio represents the amount of a gas or particle emitted relative to a reference species and can be estimated by calculating the slope of trace gas or particulate enhancements above background relative to that of a co-emitted reference species, usually CO_2 or CO. The slope of a best-fit linear regression, or the emission ratio, can then be multiplied by the carbon content of the biomass consumed by the

fire to convert the molar ratio into grams of species emitted per kilogram of biomass burned [*Yokelson et al.*, 1997; *Akagi et al.*, 2011].

The emission factor is often parameterized as a static scalar [*Akagi et al.*, 2011] although in reality it is dynamic and responds to environmental conditions that influence the amount smoldering and flaming combustion and likely simultaneously regulates combustion completeness [*French et al.*, 2002]. To account for this, some studies assign different emission factors for a given percentage of flaming or smoldering combustion that was estimated to have occurred in aboveground and belowground fuels [*Cahoon et al.*, 1994; *French et al.*, 2002; *Kasischke and Bruhwiler*, 2002]. Other studies have used more complex models to estimate carbon trace-gas emissions using emission factors that evolve depending on the spatial distribution of biomass in different vegetation types and the temporal behavior of fire based on fuel moisture conditions [*Amiro et al.*, 2001].

There are a limited number of in-situ previous studies that have measured emission factors from boreal forest fires by flying aircraft nearby plumes and collecting flasks of air to be measured in a laboratory at a later time or measuring the trace gas and/or particulate concentrations in-situ using gas-sensor equipment mounted in the aircraft [*Cofer et al.*, 1989; *Cofer et al.*, 1990; *Radke et al.*, 1991; *Nance et al.*, 1993; *Cofer et al.*, 1998; *Goode et al.*, 2000; *Simpson et al.*, 2011]. Limitations associated with this method of sampling include the inability to capture variability in emission factors stemming from changes in environmental conditions and afternoon-biased measurements with a short temporal and spatial range. An alternative approach to measuring in-situ emission factors involves using a tower equipped with a cavity ring-down spectrometer that continuously measures trace gas concentrations located in an area

downwind of fires. This has been done in a previous boreal forest fire study during a moderate fire season in Alaska [*Wiggins et al.*, 2016].

In this study we used trace gas observations of CO, CH_4, and CO_2 from the CARVE (CRV) tower located in interior Alaska to derive time-weighted emission factors from boreal forest fires that burned during the anomalously high fire season of 2015. 2015 was the second largest fire season in terms of burned area since records began in 1940 with over 5 million acres burned [*Hayasaka et al.*, 2016; *Partain et al.*, 2016]. An unseasonably warm spring and earlier snowmelt allowed fuels to dry early in the season [*Partain et al.*, 2016]. In mid-June, thunderstorms caused an unprecedented lightning event during which over 65,000 strikes in Alaska caused 270 individual fire ignitions on anomalously dry fuel beds over the course of a week [*Hayasaka et al.*, 2016; *Veraverbeke et al.*, 2017]. Fires continued to burn under favorable weather conditions until mid-July, when cool, damp weather minimized fire growth for the rest of the summer fire season.

The CRV tower captured an integrated signal of trace gas emissions from fires across interior Alaska during the 2015 fire season. We coupled a fire emissions inventory, the Alaska Fire Emissions Database (AKFED) [*Veraverbeke et al.*, 2015] with an atmospheric transport model, the Polar Weather Research and Forecasting Stochastic Time Integrated Lagrangian Transport (PWRF-STILT) model [*Henderson et al.*, 2015], to quantify the spatial and temporal variability of individual fires and their influence on CO, CH_4, and CO_2 at the CRV tower. Our tower based approach allows for an integration of emission factors through the day-night fire cycle and suggest the smoldering phase of boreal fires may have a higher contribution to emissions than previously estimated.

3.2 Methods

3.2.1 CARVE (CRV) Tower Observations

Atmospheric CO, CH_4, and CO_2 mole fractions were measured at the CRV tower in Fox, Alaska (64.986°N, 147.598°W) during the summer of 2015 using a cavity ring-down spectrometer (CRDS, Picarro models 2401 and 2401m) [*Karion et al.*, 2016]. The location of the tower was ideally located to sample boreal forest fires in interior Alaska (Figure 3.1). We used observations from air drawn from the top intake height at a height of 32m from the tower base because this level had the highest measurement density and the smallest sensitivity to local ecosystem fluxes near the tower [*Karion et al.*, 2016]. All raw 30 s average measurements were calibrated according to *Chen et al.* [2013] and *Rella et al.* [2013].

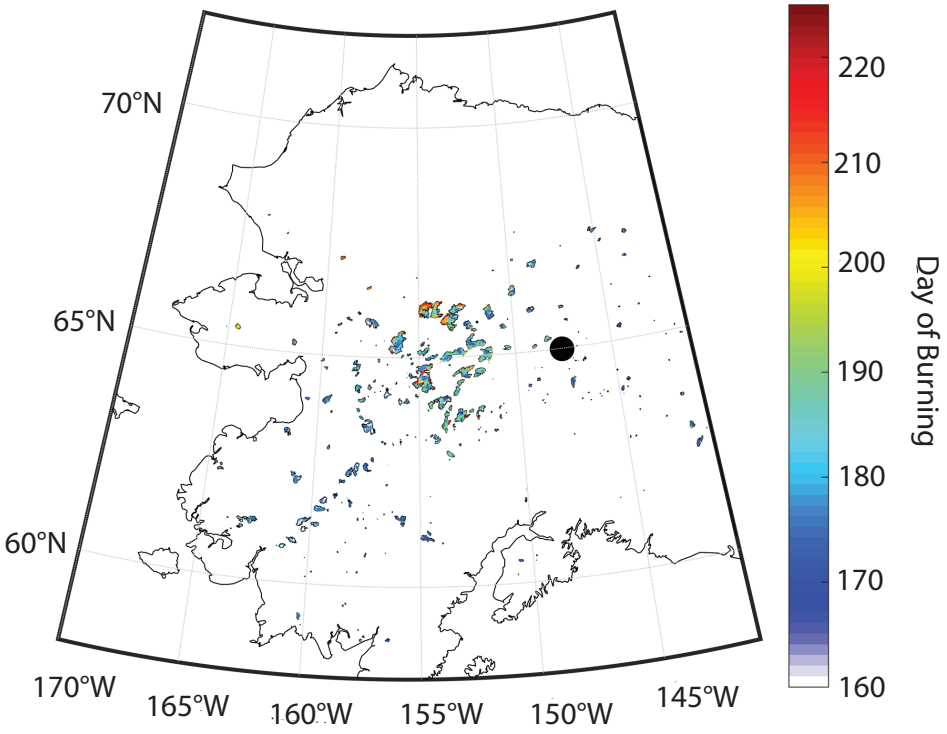

Figure 3.1 Fire Perimeters in Alaska during 2015 with colors representing the day of burning. The location of the CRV tower is denoted with a black circle.

3.2.2 Emission Factors and Modified Combustion Efficiency

We isolated periods when fire had a dominant influence on trace gas variability observed at CRV tower to calculate emission factors. This was achieved by first removing all data when the mole fraction of CO was less than 0.5 ppm. Second, we defined a 240-point (2 hour interval) discrete moving windows to extract CO, CH_4, and CO_2 mole fractions and calculate correlation coefficients between all three. Only periods with highly significant correlations between CO:CO_2 and CH_4:CO_2 ($r^2 > 0.80$) were retained, because covariance among co-emitted species represent almost all carbon emissions from fires [*Urbanski*, 2014].

We calculated background mole fractions of CO and CH_4 by taking an average of observations prior to any major fire activity in interior Alaska (DOY 170 – 172.5). We modeled hourly CO_2 background concentrations to account for the influence of net ecosystem exchange (NEE) using a Bayesian approach multi-variable linear regression model trained on CRV tower observations during 2012, a year with little to no fire influence on trace gas variability. The variables used in the CO_2 model include hourly observations of temperature, vapor pressure deficit, precipitation, day of year, latent heat flux, and hourly CO_2 observations from Barrow, AK (Figure 3.2). Meteorological variables were acquired from the National Climatic Data Center Automated Weather Observing System for Fairbanks International Airport (http://www7.ncdc.noaa.gov/CDO/cdopoemain.cmd). This location was chosen due to its proximity to the CRV tower. We obtained 3-hourly latent heat flux from the NOAH2.7.1 GLDAS/NOAH experiment 001 for version 2 of the Global Land Data Assimilation System (GLDAS-2) [*Rodell et al.*, 2015]. Hourly in-situ CO_2 observations from a clean air site in Barrow, AK were attained from the Earth System Research Laboratory Global Monitoring Division [*Thoning et al.*, 2007].

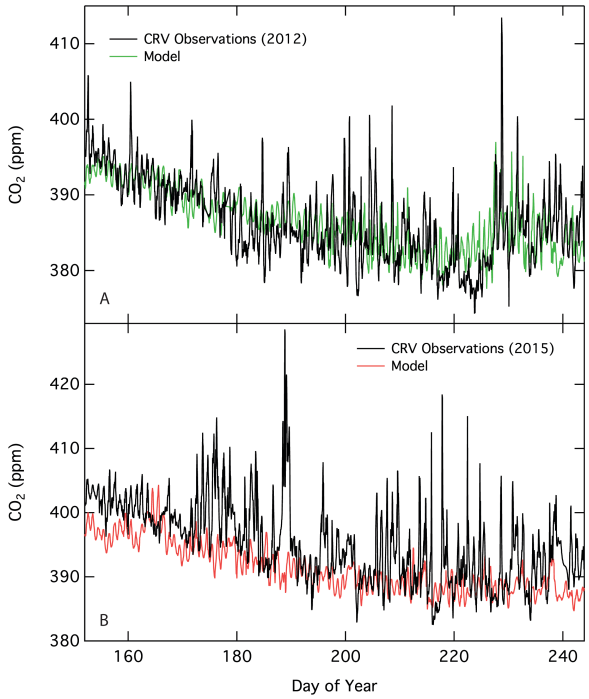

Figure 3.2 Panel A: 2012 CO_2 observations from CRV tower (black) during a low fire year versus modeled CO_2 (green). Panel B: 2015 CO_2 observations from CRV tower (black) versus modeled CO_2 (red).

We estimated emission ratios by calculating the slope from a type II linear regression of CO and CH_4 excess mixing ratios (ΔCO and ΔCH_4) relative to CO_2 (ΔCO_2). Excess mixing ratios refer to observations of trace gas mole fractions with background values subtracted. Emission factors were calculated by multiplying the emission ratio by a scalar to convert the molar ratio into grams of CO or CH_4 emitted per kilogram of biomass burned with the assumption that 450 g C is emitted per kilogram of biomass burned [*Yokelson et al.*, 1997; *Akagi et al.*, 2011].

We calculated modified combustion efficiency (MCE) for each emission factor period. Modified combustion efficiency is defined as the excess mixing ratio of CO divided by the total excess mixing ratio of CO and CO_2 [*Ward and Radke*, 1993]. MCE was used to separate events into three categories: smoldering, mixed, or flaming. These categories reflect the dominant phase of combustion from fires that contributed to trace gas anomalies at the CRV tower during the

summer of 2015. Any period with an MCE less than 0.9 was considered to consist of mostly smoldering combustion, periods with an MCE of 0.9 – 0.91 were classified as consisting of a mixture of smoldering and flaming combustion, and any period with an MCE greater than 0.92 was classified as flaming [*Urbanski*, 2014].

3.2.4 Transport Modeling

We coupled a fire emission model, the Alaskan Fire Emissions Database (AKFED) [*Veraverbeke et al.*, 2015] with an atmospheric transport model, the Polar Weather Research and Forecasting Stochastic Time Integrated Lagrangian Transport model (PWRF-STILT) [*Henderson et al.*, 2015] to estimate fire contribution to trace gas variability from CRV tower observations following *Wiggins et al.* [2016]. AKFED models carbon consumption with a temporal resolution of 1 day and a spatial resolution of 450 m. We regridded AKFED to the same spatial resolution as the atmospheric transport model (0.5°) for the model coupling. To account for diurnal variability in emissions, here we imposed a diurnal cycle on daily emissions following *Kaiser et al.* [2009b], where the diurnal cycle is the sum of a constant and a Gaussian function that peaks in early afternoon with 90% of emissions occurring during the day and 10% at night.

The influence functions or "footprints" (ppm per μmol/m^2/s) from the atmospheric transport model quantify upwind surface fluxes that are observed at the CRV tower at a given time. The footprints are on a 0.5° latitude-longitude grid with a temporal resolution of 1 h during hours 0600 to 1800 (day) local time and 3 h during hours 1800 to 0600 (night). Footprint timing and magnitude for each time period associated with an emission factor period was analyzed. This approach allowed us to confirm CRV tower observations represent an integration of emissions from multiple fires and capture variability in emissions across the diurnal fire cycle.

We used the combined model to determine individual fire contributions to CO anomalies at CRV tower and the contribution of day and night fire emissions to CO variability at the CRV tower. This was achieved by calculating the total CO contribution from each individual 0.5° grid cell from the AKFED×PWRF-STILT combined model and utilizing the fire perimeters from the Alaska Large Fire Database (data provided by Bureau of Land Management (BLM) Alaska Fire Service, on behalf of the Alaska Wildland Fire Coordinating Group (AWFCG) and Alaska Interagency Coordination Center (AICC)) to identify the location of individual fires. We determined an individual fires contribution to CO at the CRV tower by setting all emissions in AKFED for a particular grid cell to zero and rerunning the model coupling with PWRF-STILT. The difference between the original model and the updated coupling is equal to an individual fire's contribution to CO at the CRV tower.

3.3 Results

3.3.1 Emission Factors and Modified Combustion Efficiency

Synchronized enhancements of CO, CH_4, and CO_2 well above background concentrations were prominent in CRV tower observations from DOY 173 – 196 (Figure 3.3). We identified 23 individual events that span about 2 hours each to calculate emission factors from the elevated trace gas observations (Figure 3.4; Figure 3.5; Table 3.1). CO emission factors ranged from 93 to 267 g CO per kg biomass combusted, and CH_4 emission factors ranged from 2.67 to 10.9 g CH_4 per kg biomass combusted. MCE ranged from 0.83 to 0.93. The mean CO emission factor was 144 ± 70.4 g CO per kg biomass combusted, the mean CH_4 emission factor was 5.80 ± 2.92 g CH_4 per kg biomass combusted, and the mean MCE was 0.88. We identified a strong linear relationship between the CH_4 emission factor and MCE (Figure 3.6).

Each event was used to calculate emission factors was classified as a smoldering, mixed, or flaming emissions event using the MCE. We discovered 13 smoldering events, 7 mixed events, and 3 flaming events throughout the fire season (Figure 3.7; Table 3.2). Smoldering events had a mean CO emission factor of 174 ± 39 g CO per kg biomass combusted, a mean CH_4 emission factor of 7.07 ± 1.49 g CH_4 per kg biomass combusted, and a mean MCE of 0.86 ± 0.027. Mixed events consisting of both smoldering and flaming combustion had a mean CO emission factor of 110 ± 6.0 g CO per kg biomass combusted, a mean CH_4 emission factor of 4.59 ± 0.92 g CH_4 per kg biomass combusted, and a mean MCE of 0.90 ± 0.004. Flaming events had a mean CO emission factor of 90.1 ± 6.6 g CO per kg biomass combusted, a mean CH_4 emission factor of 3.11 ± 0.47 g CH_4 per kg biomass combusted, and a mean MCE of 0.92 ± 0.005.

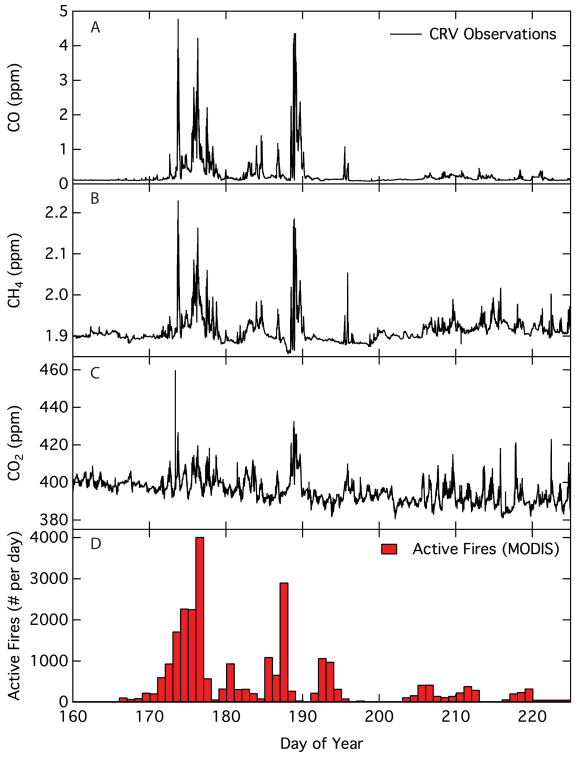

Figure 3.3 CRV tower observations of CO (panel A), CH_4 (panel B), CO_2 (panel C), and active fire counts from MODIS.

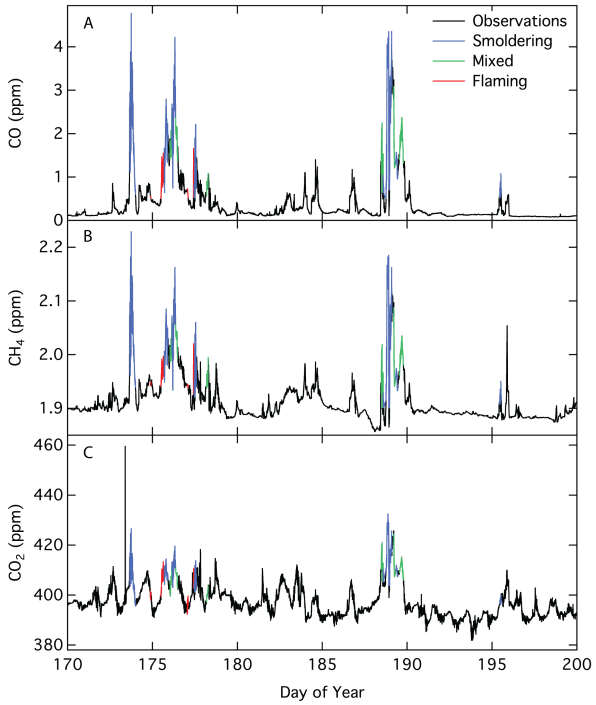

Figure 3.4 CRV tower observations of CO (panel A), CH_4 (panel B), and CO_2 (panel C) with periods used to calculate emission factors highlighted to denote the dominant phase of combustion - smoldering (blue), mixed (green), and flaming (red).

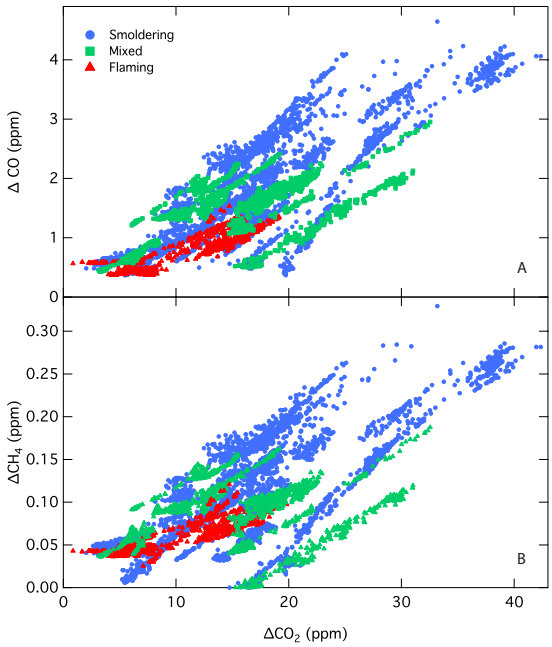

Figure 3.5 Panel A: Excess mixing ratios of CO (ΔCO) versus CO_2 (ΔCO_2) used to calculate emission factors. Red triangles denote excess mixing ratios taken from flaming fire signals in CRV observations, green squares show mixed fire signals, and blue circles show smoldering. Panel B: Excess mixing ratios of CH_4 (ΔCH_4) versus CO_2 (ΔCO_2) used to calculate emission factors.

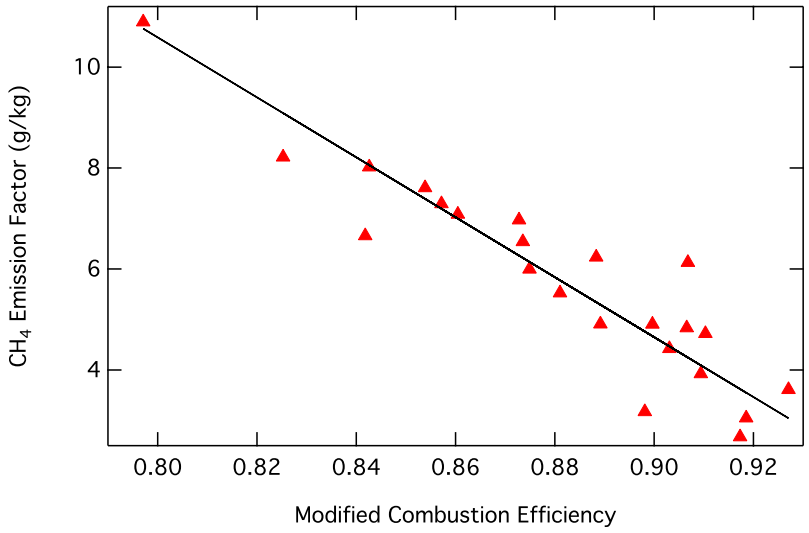

Figure 3.6 Relationship between CH_4 emission factors and corresponding modified combustion efficiency (MCE).

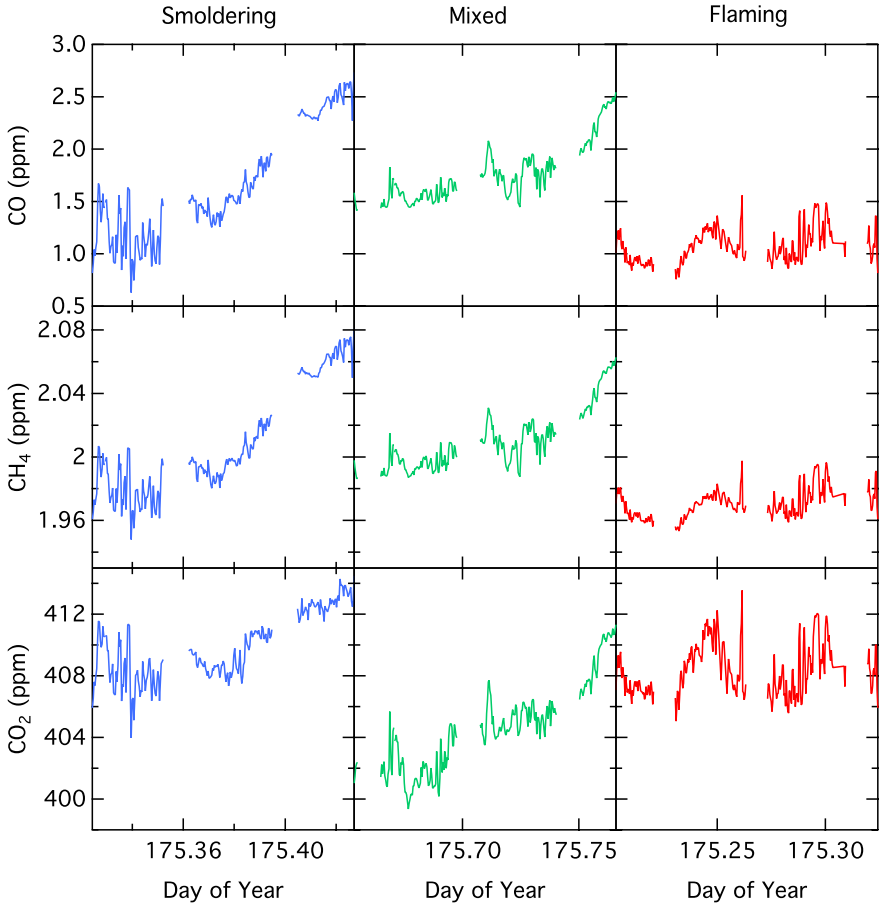

Figure 3.7 Examples of raw trace gas observations used to calculate emission factors for smoldering (blue), mixed (green), and flaming (red) dominated combustion.

Table 3.1 Events of elevated trace gas concentrations at the CRV tower due to fire emissions and their related emission ratios, emission factors (g per kg biomass combusted), and modified combustion efficiency (MCE). Dominant flaming combustion is denoted with an (F), mixed (M), and smoldering (S). Correlation is the r^2 value.

	Time of Event	CO/CO_2 Mole Ratio	CO Emission Factor	CH_4/CO_2 Mole Ratio	CH_4 Emission Factor	MCE	Correlation CO/CO_2	Correlation CH_4/CO_2
Event 1 (S)	173.29 – 173.41	0.125±0.0167	180±3.9	0.008 ±0.001	7.61±0.16	0.85	0.94	0.95
Event 2 (S)	173.41 – 173.51	0.156±0.0129	150±3.4	0.011±9e-4	6±0.14	0.87	0.94	0.94
Event 3 (S)	173.51 - 173.63	0.137±0.0231	131±2.9	0.011±0.002	4.91±0.12	0.89	0.94	0.93
Event 4 (F)	174.50 - 175.20	0.076±0.0143	95±2.3	0.007±0.001	2.67±0.06	0.92	0.93	0.94
Event 5 (F)	175.20 - 175.32	0.063±0.0040	93±1.8	0.005±2.5e-4	3.05±0.08	0.92	0.96	0.92
Event 6 (S)	175.32 - 175.43	0.081±0.0179	222±3.6	0.006±0.001	8.22±0.13	0.83	0.97	0.97
Event 7 (S)	175.43 - 175.54	0.107±0.0103	170±5.9	0.007±7.9e-4	7.08±0.26	0.86	0.86	0.84
Event 8 (M)	175.65 - 175.77	0.128±0.0104	113±2.3	0.009±6.7e-4	4.42±0.09	0.90	0.95	0.95
Event 9 (S)	175.77 - 175.88	0.100±0.0225	196±7.1	0.006±0.002	8.02±0.30	0.84	0.84	0.84
Event 10 (S)	175.88 - 175.99	0.149±0.0066	197±3.7	0.010±3.6e-4	6.66±0.13	0.84	0.96	0.96
Event 11 (M)	175.99 - 176.11	0.154±0.0149	105±2.7	0.011±0.001	3.92±0.09	0.91	0.92	0.94
Event 12 (F)	176.67 - 177.08	0.099±0.0591	83±3.0	0.008±0.004	3.61±0.12	0.93	0.84	0.86
Event 13 (S)	177.08 - 177.21	0.093±0.0097	132±1.2	0.007±0.001	6.23±0.06	0.89	0.99	0.99
Event 14 (M)	177.81 - 177.91	0.113±0.0091	108±2.2	0.010±0.001	6.13±0.25	0.91	0.95	0.81
Event 15 (M)	188.10 - 188.22	0.052±0.0125	117±0.9	0.002±0.001	4.91±0.04	0.90	0.99	0.99
Event 16 (S)	188.22 - 188.46	0.057±0.0287	175±1.6	0.003±0.002	7.29±0.05	0.86	0.99	0.99
Event 17 (S)	188.46 - 188.62	0.089±0.0208	153±1.1	0.005±0.002	6.97±0.04	0.87	0.99	0.99
Event 18 (S)	188.62 - 188.73	0.102±0.0097	267±8.8	0.006±7.4e-4	10.9±0.35	0.80	0.87	0.88
Event 19 (M)	188.84 - 188.95	0.074±0.0051	108±0.8	0.003±7.9e-9	4.83±0.03	0.91	0.99	0.99
Event 20 (S)	188.95 - 189.07	0.073±0.0065	142±3.2	0.003±5.6e-4	5.53±0.13	0.88	0.94	0.94
Event 21 (M)	189.17 - 189.29	0.093±0.0042	103±2.9	0.005±3.6e-4	4.72±0.11	0.91	0.90	0.94
Event 22 (M)	189.29 - 189.41	0.091±0.0053	119±3.0	0.006±2.9e-4	3.17±0.10	0.90	0.92	0.88
Event 23 (S)	195.06 - 195.17	0.082±0.0096	152±1.9	0.003±0.001	6.54±0.09	0.87	0.98	0.98
Mean		0.099±0.0300	144±70.4	0.007±0.003	5.80±2.92	0.88		

Table 3.2 Comparison of CO and CH_4 emission factors partitioned into smoldering, mixed, and flaming combustion. Emission factor units are g of CO or CH_4 per kg of biomass combusted.

	CO Emission Factor	CH_4 Emission Factor
Smoldering (n = 13)	174 ± 39	7.07 ± 1.49
Mixed (n = 7)	110 ± 6.0	4.59 ± 0.92
Flaming (n = 3)	90.1 ± 6.6	3.11 ± 0.47

3.3.2 The Influence of Fires on Trace Gas Variability at the CRV Tower

The model simulations combining AKFED fire emissions with PWRF-STILT provided confirmation that the elevated trace gas signals at the CRV tower were caused by boreal forest fire emissions (Figure 3.8). The AKFED model had a Pearson's correlation coefficient of 0.61 with observed daily mean CO and had a low bias of approximately 7%. The footprints associated with each emission factor event also were used to determine how much of the signal was coming from burning on previous days and the fraction of emissions emitted during day and night periods. We found that 99% of the fire emissions that influenced CRV tower trace gas concentrations occurred within 3 days of the emission factor event at the CRV tower, with 76%

occurring within the first 24 hours, 22% during the next 24 hours, and 2% occurring three days prior to the event (Figure 3.9). Overall, 64% of the fire emissions that impacted the tower occurred during the day (0900 to 1800 local time) and 36% occurred at night (1900 – 0600 local time).

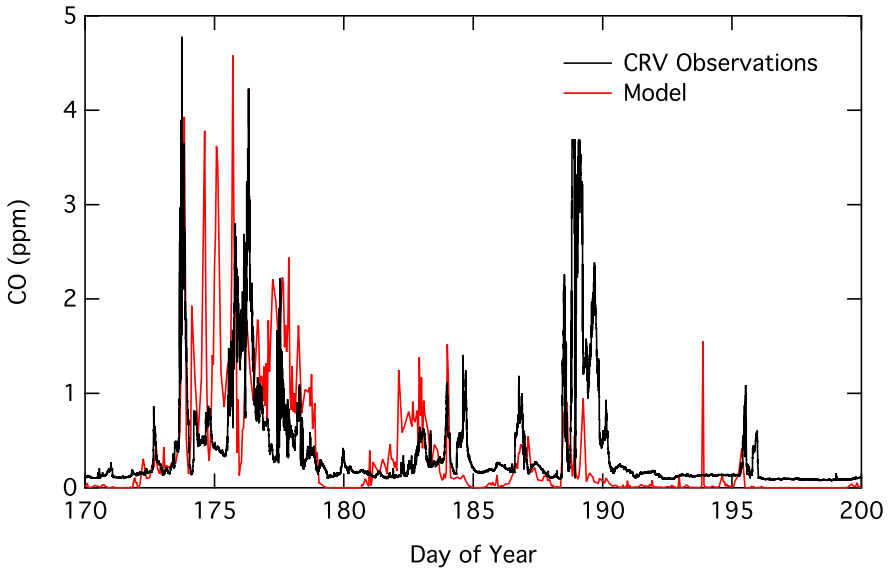

Figure 3.8 CRV observations of CO (black) compared to modeled CO anomaly due to fires (red).

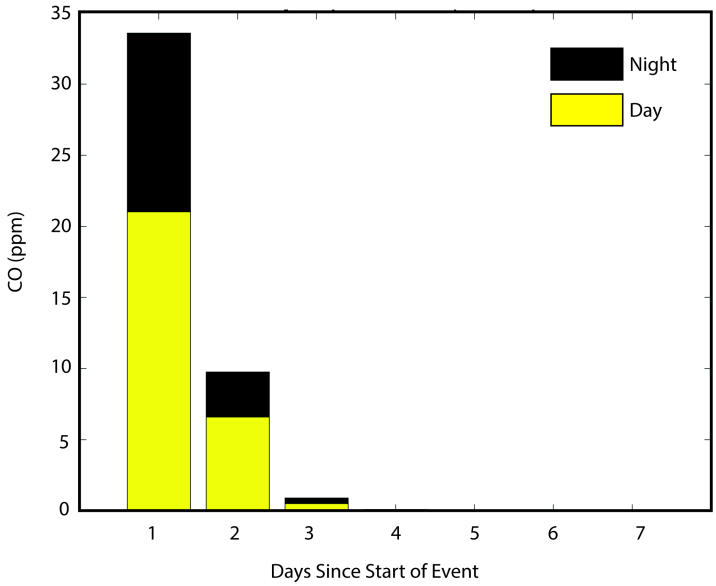

Figure 3.9 Temporal distribution of CO anomaly at the CRV tower caused by fires, calculated by multiplying footprints from PWRF-STILT with fire emissions from AKFED. Only times when emission ratios were calculated are used in the analysis.

We identified 31 individual fires that contributed to at least 1% of the CO mole fraction time series at CRV tower (Figure 3.10-11; Table 1.1). On average, these fires were 958 ± 29 km away from CRV tower. The total CO emitted from these fires accounts for 75% of the total CO mole fraction signal during DOY 160 – 200. The remaining CO signal originated from many smaller fires that were across interior Alaska. The Tozitna and Jackson fires together were responsible for the greatest percentage of the total CO anomaly at CRV tower, and were considered together for this study because of the 0.5° grid size necessary for model coupling. These two fires contributed 17.3 ppm of CO or 9% of the total CO anomaly. The fires that significantly contributed to the CO anomaly at CRV tower were not the closest fires to the tower or the largest fires of the 2015 fire season in terms of burned area.

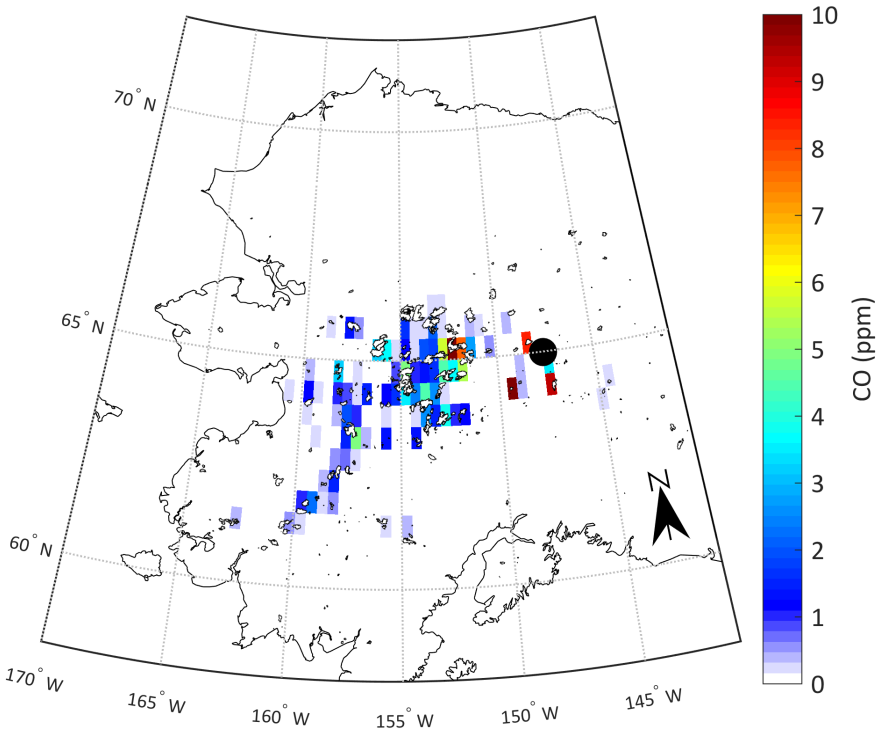

Figure 3.10 Total individual fire contributions to CO anomaly at CRV tower determined by convolving footprints from PWRF-STILT with fire emissions from AKFED. The location of CRV tower is shown as a black dot. Fire perimeters are shown as black outlines.

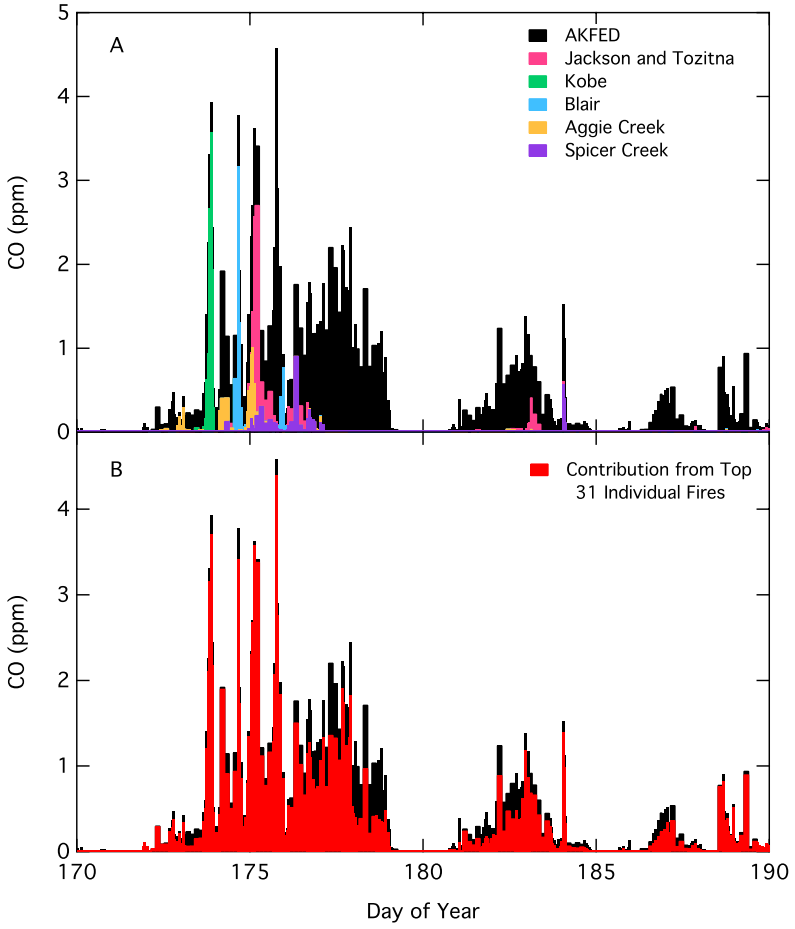

Figure 3.11 Panel A: Top 5 individual fire contributions to the CO anomaly at CRV tower. Black shows original AKFEDxPWRF-STILT model, red depicts contributions from the Jackson and Tozitna fires (grouped together due to both fires being in one 0.5° grid cell), green from Kobe fire, blue from Blair fire, gold from Aggie Creek fire, and purple from Spicer Creek fire. Panel B: Total CO anomaly from all fires that contributed to at least 1% of the modeled CO anomaly at CRV tower (red) compared to the original model (black).

3.4 Discussion

3.4.1 Emission Factors Derived from Tower-Based Observations

Emission factors provide a straightforward way to convert fire emissions into discrete species, such as CO, CH_4, and CO_2. This technique is commonly used to model emissions of select species and or to compare model results with in-situ or remotely sensed observations. The most frequently used approach to measure emission factors involves flying an aircraft through or near an active fire plume and collecting flasks of air for later analysis or measuring

concentrations in-flight using gas-sensor instruments [*Goode et al.*, 2000; *Simpson et al.*, 2011]. Flight safety protocol often prohibits flying too close to the active fire and requires all sampling to occur when smoke plumes are visible. As a result, emission factors derived from this style of sampling have mostly sampled plumes when the fire is more likely to be active and in a flaming combustion stage. Usually, only a few individual fires can be thoroughly sampled in an aircraft campaign.

There are limited previous studies on boreal forest fire emission factors, and almost all derived emission factors were determined from aircraft sampling (Table 1) [*Cofer et al.*, 1989; *Cofer et al.*, 1990; *Radke et al.*, 1991; *Nance et al.*, 1993; *Cofer et al.*, 1998; *Goode et al.*, 2000; *Simpson et al.*, 2011; *Wiggins et al.,* 2016]. In total, all previous studies combined sampled 18 individual active fires and derived emission factors that were likely biased towards flaming fires that occurred in the afternoon, as a product of the sampling strategy. A compilation of all previous studies yields CO emission factors that are significantly lower than the mean from this study and CH_4 emission factors that are in agreement with this study.

We found 31 individual fires scattered across the entire range of interior Alaska directly and significantly impacted trace gas observations at CRV tower. These fires each contributed to between 1% and 9% of the total CO signal observed at the CRV tower, with all 31 fires combined explaining three quarters of the total fire signal. The remaining fire signal not explained by the top 31 fires can be explained by smaller contributions from other fires in interior Alaska. The CRV tower observations instead represent an integrated signal from 31 fires out of the 334 that burned in 2015. Our modeling study confirms that the entire day/night fire cycle was captured by anomalous trace gas observations at CRV tower that was used to calculate emission factors. *Wiggins et al.* [2016] used a similar tower-based approach to estimate boreal

forest emission factors during a moderate fire year, and they found CO and CH_4 emission factors that were higher than the compiled mean from previous studies. We found a strong linear relationship between CH_4 emission factors and MCE that has also been found in previous studies [*Van Leeuwen and Van Der Werf*, 2011; *Yokelson et al.*, 2013; *Urbanski*, 2014].

Although Table 3.3 appears to suggest CO emission factors from boreal forest fires are increasing over time, it is more likely that studies using the tower approach are better suited to sample a more thorough representation of all the phases of combustion that can occur in boreal forest fires. The tower approach is not limited by the time or scale of sampling, unlike aircraft measurement techniques. Aircraft based emission factors are biased towards flaming fires, because most measurements are acquired during the afternoon when active fire plumes are visible. A total of 5520 30s trace gas observations from the CRV tower were used to calculate emission factors, significantly expanding the existing database of in-situ measurements used to calculate emission factors. The emission factors derived from this study provide a more robust estimate of the mean, and indicate that the smoldering phase and nighttime emissions of boreal fires have likely been underestimated in previous studies. The improved emission factors from this study can be used in future modeling efforts to convert carbon emissions to CO and CH_4 trace gas emissions from boreal forest fires more accurately.

3.4.2 Relative Contributions of Smoldering and Flaming Combustion

Following ignition, boreal forest fires generally begin as stand replacing crown fires followed by smoldering combustion in organic soil layers and coarse woody debris behind the fire front that can continue for weeks after ignition [*Bertschi et al.*, 2003]. This residual smoldering combustion could substantially contribute to trace gas emissions, but is difficult to detect and quantify because of low radiative power associated with this phase of combustion. In

the early afternoon when the atmospheric boundary layer is elevated, conditions favor the development and spread of fires. Because most in-situ aircraft measurements used to derive emission factors are collected in the afternoon, they are biased towards products of flaming combustion. Two previous studies sampled separate fires with smoldering, mixed, and flaming dominated combustion [*Cofer et al.*, 1989; *Cofer et al.*, 1998]. Our CO emission factors were significantly higher than their estimations for flaming, mixed, and smoldering fires. The CH_4 emission factors from flaming fires in this study are nearly identical to what has been found in these two studies, and our CH_4 emission factors from smoldering and mixed combustion phase fires is within a standard deviation of estimates from the previous studies.

The majority (13/23) of the emission factor events we sampled indicate smoldering was the dominant phase of combustion. Only 3 of the 23 emission factor events were classified as consisting of mostly flaming combustion. Smoldering, mixed, and flaming emission factor events were measured at CRV tower during all hours of the day, and our modeling analysis confirms that we sampled emissions that occurred across the day/night fire cycle (Figure 3.9). The elevated trace gas mole fractions observed at CRV tower represent an integration of these different combustion phases across both time and space.

The relative contributions of emissions from flaming and smoldering is uncertain for boreal forest fires, but previous studies have assumed 80% of aboveground carbon is consumed in flaming combustion, 20% is consumed in smoldering combustion, and vice versa for belowground carbon [*French et al.*, 2002; *Kasischke and Bruhwiler*, 2002]. Our results suggest that the smoldering phase of combustion contributes to more carbon emissions than has been previously estimated. As a result, it is likely that estimates of CO emissions from boreal forest fires have been underestimated. It is beyond the scope of this study to determine if more

smoldering occurred in aboveground and/or belowground combustion or if the relative proportions of combustion in above and belowground fuels are skewed more towards belowground combustion. The anomalous fire season of 2015 was exacerbated by rising temperatures, and could be considered representative of future fire seasons in the boreal forest. In the future, it is possible that overall trace gas emissions from boreal forest fires will increase with corresponding CO emissions that could be considerably higher than previously estimated.

3.5 Conclusions

Our tower-based approach to calculate emission factors is a new technique that significantly improves our understanding of trace gas emissions from boreal forest fires. Unlike traditional approaches using aircraft observation, our method represents an integration of trace gas emissions across the day and night burning cycles and varying environmental conditions that are both known to considerably influence the composition of fire emissions. We discovered 31 individual fires across interior Alaska significantly influenced trace gas variability at CRV tower from which our emission factors were derived from. This is comparable to the number of individual fires that have been sampled to calculate boreal fire emission factors in all previous studies combined. Our results suggest the smoldering phase of boreal forest fires contributes to more trace gas emissions than previously believed. Total CO emissions from boreal forest fires may have been previously underestimated. The tower-based emission factor method introduced in this study can be applied to other biomes and potentially expand in-situ emission factor observations in regions of interest.

Acknowledgements

E.B.W. thanks the U.S. National Science Foundation for a Graduate Research Fellowship (NSF 2013172241). The CRV tower observations used in our analysis are archived at the U.S. Oak Ridge National Laboratory Distributed Active Archive Center for Biogeochemical Dynamics (insert DOI). The trace gas observations, fire emissions time series, and WRF-STILT model were created through funding support from NASA's CARVE project. JTR acknowledges additional NASA support from CMS, IDS, and SMAP programs.

Chapter 4

Smoke radiocarbon measurements from Indonesian fires provide evidence for burning of millennia-aged peat

Adapted from:

Wiggins, E.B., Czimczik, C.I., Santos, G.M., Chen, Y., Xu, X., Holden, S.R., Randerson, J.T., Harvey, C.F., Kai, F., Liya, Y. (2018). Smoke radiocarbon measurements from Indonesian fires provide evidence for burning of millennia-aged peat. *Proceedings of the National Academy of Sciences*. In review.

4.1 Introduction

During 2015, Indonesia experienced an exceptionally intense September-October fire season fueled by El Niño-induced drought. Emissions from the fires were substantial, increasing CO_2 and CH_4 greenhouse gases in the global atmosphere. Greenhouse gas emissions estimates derived from both land surface and atmospheric remote sensing observations indicate that the fires emitted between 0.89 and 1.5 Pg CO_2-eq [*Field et al.*, 2016; *Huijnen et al.*, 2016; *Heymann et al.*, 2017; *Liu et al.*, 2017; *Lohberger et al.*, 2017]– the largest regional source since the strong 1997-1998 El Niño [*Page et al.*, 2002; *Heil et al.*, 2007; *Field et al.*, 2016; *Huijnen et al.*, 2016], and equivalent to about 20% of the 1 ppm positive CO_2 anomaly observed at Mauna Loa during 2015 [*Betts et al.*, 2016]. Prevailing winds transported aerosols from the Indonesian fires to population centers across the Maritime Continent, reducing air quality in many cities and affecting the health of over 40 million people [*Koplitz et al.*, 2016] Widespread burning from escaped fires across Sumatra, Kalimantan, and West Papua degraded critical habitat for endangered plant and animal species, including orangutans and Sumatran tigers [*Posa et al.*,

2011]. Considered together, the climate, human health, and ecosystem damages of the Indonesian fires were substantial and widely distributed among stakeholders and regional communities [*The World Bank*, 2016; *Chisholm et al.*, 2016; *Tacconi*, 2016]. This contrasts with the benefits accrued to the agricultural sector from land clearing and peatland drainage. Lowering the water table increases agricultural yield by drying near-surface peat but also makes peatlands flammable. The costs and benefits of these land use practices operate on different spatial and temporal scales, making it difficult to design effective policy and management solutions [*Tacconi*, 2016].

The extreme 2015 fire season was a part of a broader set of climate-human-ecosystem interactions across the Maritime Continent that have been evolving over a period of decades from rapid changes in land use [*Field et al.*, 2009]. These interactions are unique because of the widespread distribution of tropical peatlands in low elevation areas that have been intensively deforested, drained, and further modified to support agricultural production, rendering them vulnerable to anthropogenic fire. Loss of forest cover in peatlands has been extensive over the past several decades, declining by 71% across Peninsular Malaysia, Sumatra, and Borneo between 1990 and 2015 [*Miettinen et al.*, 2016] Peatland soils store between 28 and 57 Pg C in Indonesia alone, and far exceed aboveground carbon stocks [*Page et al.*, 2011; *Warren et al.*, 2017]. The vulnerability of peat to fire increases considerably with canal construction used for timber extraction and plantation development [*Konecny et al.*, 2016; *Page and Hooijer*, 2016], with drainage efforts undertaken by both large-scale industrial operators and smallholder farmers [*Miettinen et al.*, 2017b]. Tropical peat becomes flammable when the water table declines, allowing for drying of surface layers [*Usup et al.*, 2004]. Upon ignition, peat fires can persist for long periods at relatively low temperatures and oxygen levels [*Page et al.*, 2002; *Huang et al.*,

2016]. As a consequence of smoldering combustion, peat fires emit three or more times the amount of fine particulate matter released by deforestation fires per kg of fuel consumed [*Akagi et al.*, 2011; *Stockwell et al.*, 2016; *Jayarathne et al.*, 2018; *Wooster et al.*, 2018] Belowground burning can also make it difficult to accurately detect and quantify emissions using optical and thermal remote sensing techniques because of smaller post-fire surface reflectance changes, shielding of the surface by regional smoke plumes and haze, and smaller thermal radiance anomalies [*Lohberger et al.*, 2017]. Burning in deep layers of accumulated peat modifies regional greenhouse gas budgets and indicates that these ecosystems no longer operate as a slow, sustained carbon sink in the global carbon cycle [*Dommain et al.*, 2014; *Turetsky et al.*, 2015].

Although peatland burning is well established as an important source of fire emissions during drought events in Indonesia, uncertainties remain with respect to contributions from different ecosystem and land use activities. *Page et al.* [2002] estimated that between 0.81 and 2.57 Gt C, or 79-84% of total C emissions, were released from fires in drained peatlands across Indonesia during the 1997-1998 El Niño. For more recent El Niño events– and with the availability of higher quality satellite observations– non-peatland fires have been identified as an important emissions source, *Marlier et al.* [2015] for example, estimated that 38% of carbon emissions from forest concessions on Sumatra originated from non-peatland ecosystem types during the 2006 El Niño. Using high-resolution synthetic aperture radar data from the Sentinel 1B satellite, *Lohberger et al.* [2017] estimated that emissions from peat accounted for only 33% to 45% of carbon emissions released by fires during the 2015 El Niño on Sumatra, Borneo and Papau New Guinea. The relatively small fraction of peat emissions in this study originates from the application of lower fuel consumption rates in degraded peatlands [*Konecny et al.*, 2016] and near-complete combustion of aboveground biomass from primary and secondary forests. The

Lohberger et al. [2017] budget contrasts with other satellite remote sensing analyses that provide evidence for a more prominent role of peat soils as a source for emissions and fire activity during the 2015 fire season [*Huijnen et al.*, 2016; *Miettinen et al.*, 2017a; *Van Der Werf et al.*, 2017] The differences in these emissions estimates highlight the need to develop independent constraints on the attribution of emissions among different land cover types and among above- and belowground carbon pools.

Radiocarbon (^{14}C) measurements of carbonaceous aerosols may have the potential to provide independent information about the contribution of peat burning to regional fire emissions budgets, complementing approaches derived from satellite remote sensing and in-situ field measurements. The isotopic constraint comes from a unique ^{14}C labeling of terrestrial biomass that has occurred over the past 60 years as a consequence of aboveground nuclear weapons testing [*Levin and Hesshaimer*, 2000] The uptake and flow of this "bomb"-derived ^{14}C through plant, litter, and soil organic matter pools enables the diagnosis of carbon turnover times on timescales of years to decades for ecosystem [*Trumbore*, 2000] and aerosol samples [*Mouteva et al.*, 2015]. For soil organic matter and other biomass formed prior to the bomb-era, radioactive decay of ^{14}C provides additional information about carbon ages over timescales of centuries to millennia [*Page et al.*, 2004] In the context of tracing the origin of smoke from Indonesian fires, carbonaceous aerosol originating from the combustion of aboveground biomass– as expected for emissions from deforestation fires or agricultural waste burning in plantations– should be bomb-labeled. Using isotope definitions from *Stuiver and Polach* [1977] this means the $D^{14}C$ should be above the contemporary level observed for atmospheric CO_2 (about 25±3‰ in 2015). In contrast, carbonaceous aerosol from older peat should have a negative $D^{14}C$, reflecting the longer-term cumulative effects of radioactive decay in organic carbon layers deposited over a period of

centuries or millennia [*Supiandi and Furukawa*, 1986; *Maloney and McCormac*, 1995; *Page et al.*, 1999; *Page et al.*, 2004; *Wüst et al.*, 2008; *Gandois et al.*, 2014; *Biagioni et al.*, 2015; *Cobb et al.*, 2017].

Here we report radiocarbon measurements of carbonaceous aerosols from Singapore during 2014 and 2015 fire seasons, along with carbon concentration observations. We use additional measurements from background (low-fire) periods to remove the influence of urban emissions, and isolate the carbon isotopic composition of aerosols originating from fires. We use the isotope and aerosol concentration information to estimate the mean age of the combusted organic material and to distinguish among deforestation, agricultural waste burning, and peat sources. Satellite active fire observations and simulations from the Goddard Earth Observing System Chemical Transport Model (GEOS-Chem) provided a means to identify the contribution of emissions from key source sectors and regions to our aerosol observations.

4.2 Methods

4.2.1 Aerosol Collection and Analysis

We collected weekly air samples of particulate matter with an aerodynamic diameter less than or equal to 2.5 μm ($PM_{2.5}$) at the National University of Singapore (1° 17′ 56.65″N, 103° 46′ 16.62″E). Our sampling program spanned the September-October fire seasons of 2014 and 2015 when $PM_{2.5}$ was elevated in Singapore as compared to other background (low fire) periods. We defined the fire season for the purpose of this analysis as 1 September – 31 October, including any samples that were initiated during this period.

Weekly samples were collected using a light-scattering photometer (ADR1500, Thermo Scientific) on circular 37 mm diameter quartz microfiber filters (Pallflex Membrane) over

intervals of 7 to 18 days with a flow rate of 0.0912 m^3 air per hour. Additional daily samples were collected with a custom-built sharp-cut cyclone (URG) on circular 47 mm diameter quartz microfiber filters (Pallflex Membrane). All $PM_{2.5}$ samples were analyzed for their radiocarbon and total carbon (TC) content at the W. M. Keck Carbon Cycle Accelerator Mass Spectrometry Facility at UC Irvine (Table 4.1)

A total of 20 weekly samples were obtained: 4 samples during the 2014 fire season coinciding with haze (12 Sep to 7 Nov), 11 during the 2015 low-fire urban background period (23 Jan to 23 Jun), and 5 during the 2015 fire season (5 Sep to 16 Oct). In addition to the weekly samples described above, in-situ daily aerosol samples were collected at the National University of Singapore over a period of 20.5 to 24.5 hours at a flow rate of 1.002 m^3 air per hour. A total of 15 daily samples were taken: 12 during the 2015 fire season (7 Sep 7 to 2 Oct) and 3 during the 2016 fire season (2 Aug to 9 Sep) when above average precipitation associated with La Niña inhibited fire emissions [*Van Der Werf et al.*, 2017] (Figure 4.1).

A 2.5 cm diameter punch was removed from the center of each filter. For radiocarbon and TC analysis, the remaining area (0.82 cm^2 for weekly (37 mm) and 8.3 cm^2 for daily (47 mm) samples) was combusted in a vacuum sealed, pre-combusted 9 mm OD quartz tube with CuO at 900°C for 3 hours. To estimate an uncertainty for the TC measurements, we used a Monte Carlo approach taking into account uncertainties in the flow rate of the light-scattering photometer, uncertainties in the area and loading of the aerosol filters, and the accuracy of the pressure transducer used to measure the partial pressure of CO_2.

The sample-CO_2 was then purified and quantified on a vacuum line, reduced to graphite via zinc [*Xu et al.*, 2007] or hydrogen reduction [*Santos et al.*, 2004] and analyzed alongside standards and blanks for its radiocarbon content using accelerator mass spectrometry (NEC

0.5MV 1.5SDH-21) [*Beverly et al.*, 2010]. We reported the data using $\Delta^{14}C$ notation (‰) [*Stuiver and Polach*, 1977], and corrected for carbon introduced during sample collection and laboratory processing based on TC and $\Delta^{14}C$ measurements of the standards and blanks. We used the standards and blanks to also create 1 standard deviation estimate of the $\Delta^{14}C$ uncertainty for each sample in Table 4.1. For these samples, we were not near the detection limit for samples with low ^{14}C mass on the Keck AMS, with the largest individual sample uncertainty estimated to be ± 9.3‰.

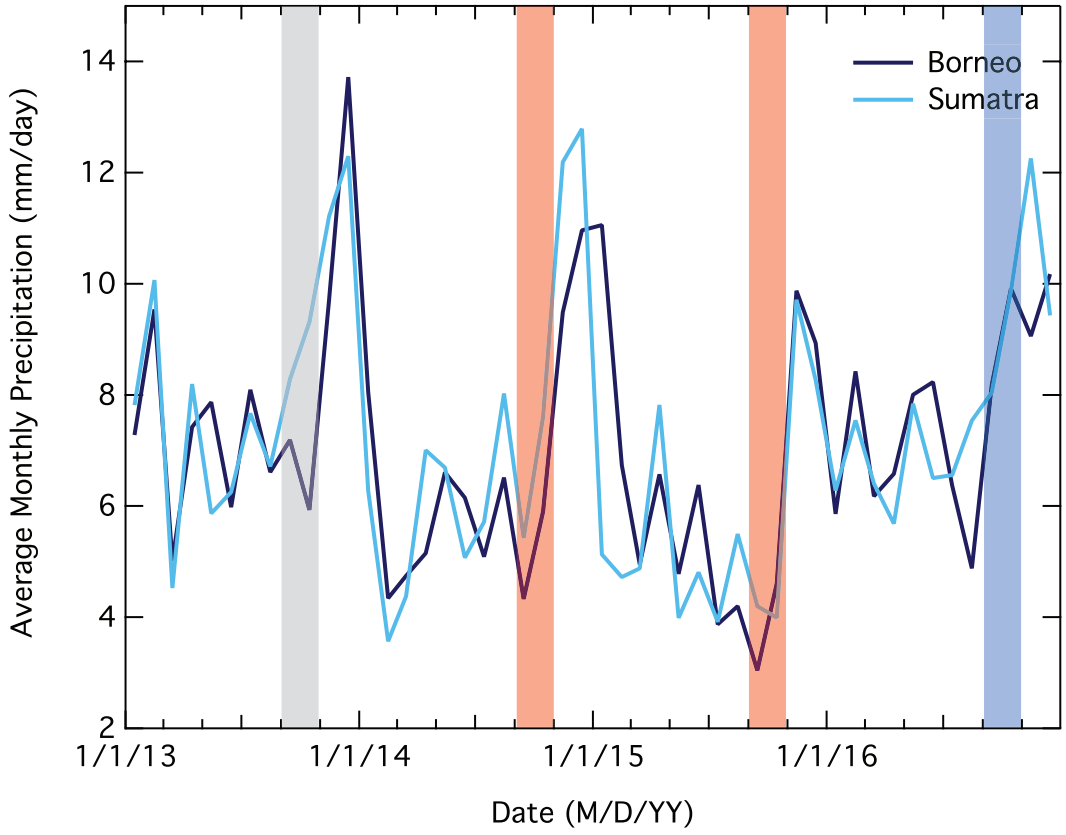

Figure 4.1 Monthly area-averaged and bias-corrected surface precipitation from MERRA-2 reanalysis product for Borneo and Sumatra from January 2013 – December 2016. Shading highlights trends in precipitation during the September-October fire season during ENSO-neutral (gray), El Niño (red), and La Niña (blue).

Table 4.1 Appendix of aerosol observations. *Indicates correction using offset calculated between vacuum line yield and EA/IRMS measurements.

Sample Period	DOY	TC (μg C/m^3)	TC Δ^{14}C (‰)
2014 Fall Fire Season Weekly Samples			
9/12/14 – 9/26/14	255 - 269	28.97 ± 1.21	-298.4 ± 1.7
9/26/14 – 10/9/14	269 - 282	25.03 ± 1.08	-264.6 ± 2.2
10/9/14 – 10/23/14	282 - 296	34.67 ± 1.43	-297.8 ± 2.4
10/23/14 – 11/7/14	296 - 311	23.82 ± 1.02	-423.4 ± 1.7
2015 Urban Background Weekly Samples			
1/23/15 – 2/3/15	23 - 34	10.03 ± 0.67	-468.3 ± 6.8
2/3/15 – 2/13/15	34 - 44	8.16 ± 0.68	-425.7 ± 7.7
2/13/15 – 2/23/15	44 - 54	7.97 ± 0.65	-583.4 ± 9.3
2/24/15 – 3/5/15	55 - 64	12.40 ± 0.83	-651.0 ± 7.6
3/5/15 – 3/20/15	64 - 79	12.44 ± 0.62	-549.5 ± 4.0
3/20/15 – 4/7/15	79 - 97	13.48 ± 0.62	-532.2 ± 3.5
4/7/15 – 4/22/15	97 - 112	10.81 ± 0.57	-625.6 ± 5.0
4/22/15 – 5/5/15	112 - 125	15.07 ± 0.80	-642.4 ± 5.1
5/5/15 – 5/22/15	125 - 142	9.53 ± 0.50	-670.7 ± 5.2
5/22/15 – 6/2/15	142 - 153	9.83 ± 0.66	-623.8 ± 7.3
6/11/15 – 6/23/15	162 - 174	11.26 ± 0.66	-583.5 ± 5.8
2015 Fall Fire Season Weekly Samples			
9/5/15 – 9/16/15	248 - 259	54.38 ± 2.17	-127.2 ± 1.2
9/16/15 – 9/23/15	259 - 266	46.57 ± 1.99	-183.5 ± 1.6
9/23/15 – 9/30/15	266 - 273	111.29 ± 4.37	-59.8 ± 1.2
9/30/15 – 10/7/15	273 - 280	83.99 ± 3.35	-108.7 ± 1.2
10/7/15 – 10/16/15	280 - 289	40.84 ± 1.70	-199.8 ± 1.9
2015 Fall Fire Season Daily Samples			
9/7/15 – 9/8/15	250 - 251	21.94 ± 0.86*	-106.9 ± 1.2
9/9/15 – 9/10/15	252 - 253	30.48 ± 1.20*	-160.4 ± 1.1
9/10/15 – 9/11/15	253 - 254	50.80 ± 1.98*	-65.8 ± 1.2
9/12/15 – 9/13/15	255 - 256	36.92 ± 1.45*	-57.0 ± 1.2
9/14/15 – 9/15/15	257 - 258	41.86 ± 1.63*	-114.9 ± 1.1
9/16/15 – 9/17/15	259 - 260	13.58 ± 0.56*	-225.7 ± 1.1
9/18/15 – 9/19/15	261 - 262	40.17 ± 1.57*	-102.5 ±1.1
9/21/15 – 9/22/15	264 - 265	23.78 ± 0.95*	-137.3 ±1.1
9/23/15 – 9/24/15	266 - 267	81.18 ± 3.19*	-26.5 ± 1.3
9/25/15 – 9/26/15	268 - 269	21.68 ± 0.86*	-90.6 ± 1.3
9/27/15 – 9/28/15	270 - 271	46.22 ± 1.80*	-43.4 ± 1.2
10/1/15 – 10/2/15	274 - 275	23.23 ± 0.92*	-178.6 ± 1.1
2016 Urban Background Daily Samples			
8/2/16 – 8/3/16	214 - 215	6.4 ± 0.24	-596.4 ± 3.7
8/15/16 – 8/16/16	227 - 228	5.0 ± 0.20	-548.9 ± 4.4
9/8/16 – 9/9/16	251 - 252	5.6 ± 0.22	-578.6 ± 4.4

4.2.2 Quantifying fire contributions to TC aerosol

We used two different approaches to separate fire and background components of the TC aerosol samples. First, we used a Keeling Plot to compute the y-axis intercept (the fire end member) from a regression of $\Delta^{14}C$ versus the reciprocal of aerosol concentration. We constructed the regression using all of the weekly aerosol samples during 2014 and 2015. The Keeling Plot approach follows the rules of isotope mass conservation as denoted in the following equations:

$$\Delta^{14}C_a = C_{bg}(\Delta^{14}C_{bg} - \Delta^{14}C_f) * 1/C_a + \Delta^{14}C_f \quad (4.1)$$

where the subscript "a" denotes the mean $\Delta^{14}C$ and total carbon concentration (C; μg/m^3) of the aerosol sample, subscript "bg" denotes background concentrations with no fire influence, and subscript "f" denotes aerosols emitted by fires. We estimated the slope and intercept of this regression using a Model II regression that accounted for errors in both the concentration and isotope measurements using the gmregress routine in Matlab acquired from the MathWorks file exchange online site and written by Antonio Trujillo-Ortiz.

Second, we removed the contribution of non-fire aerosol using isotope mass balance with the concentration and radiocarbon content of individual samples collected during a separate background period when regional fire emissions across the Maritime Continent were low using the following equation:

$$\Delta^{14}C_f = \frac{(\Delta^{14}C_{fs} * C_{fs} - \Delta^{14}C_{bp} * C_{bp})}{(C_{fs} - C_{bp})} \quad (4.2)$$

We refer to this method as an isotope mass balance approach, where a subscript f denotes the $\Delta^{14}C$ and total carbon concentration (C; $\mu g/m^3$) of the fire-emitted component of an aerosol sample, subscript "fs" denotes a sample collected during the fire season, and subscript "bp" denotes a sample collected during a background period. Table 4.1 denotes the individual samples occurring during fire season and background periods. A distribution in which each fire season sample was paired with each possible background sample using equation 4.2 is shown in Figure 4.7A.

4.2.3 Radiocarbon box model

We used a simple steady state one-box model with the observed atmospheric history of $\Delta^{14}C$ [*Hua et al.*, 2013; *Reimer et al.*, 2013] to estimate the turnover time of the combusted carbon that formed the fire-emitted carbonaceous aerosol. We averaged the $\Delta^{14}C$ time series for northern and southern tropical regions from *Hua et al.* [2013] to create a mean time series of atmospheric composition for our equatorial study region for the years from 1950 to 2009. We used observations from Barrow, Alaska (Xiaomei Xu, unpublished) to extend the time series from 2009 through 2015, after adjusting this time series with the mean difference (7.2 ± 2.4‰) observed between the *Hua et al.* [2013] time series and the Barrow time series during a period of overlap between 2003 and 2009.

This simple-box model provides additional evidence that the majority of the fire-emitted carbonaceous aerosols originated from peatland fires. For a user-specified turnover time of the organic carbon reservoir in the terrestrial biosphere, the model simulated the isotopic composition of the carbon from 10 kya before the present to the year 2015, balancing radiocarbon inputs in net primary production (derived from the observed atmospheric $\Delta^{14}C$ time

series) with decomposition losses and radioactive decay. The model also simultaneously tracked flows of ^{12}C, with the same decomposition rate constants but without radioactive decay.

We adjusted the turnover time in the box model until it matched the $\Delta^{14}C$ of the fire-emitted aerosol that we obtained from our Keeling Plot analysis using equation 4.1. This required a mean turnover time of over 800 ± 420 years because the $\Delta^{14}C$ of fire-derived aerosols (-76 ± 51‰) was considerably below the contemporary atmospheric level (25 ± 3‰). We also developed counterfactual end members for the expected $\Delta^{14}C$ of agricultural waste burning and deforestation carbon emissions using the following approach. For agricultural waste burning, we estimated that economic lifetime of a wood pulp or an oil palm plantation in Indonesia is approximately 15 years [*Tan et al.*, 2013]. Assuming that the trees accumulate carbon at similar rate over this interval, and that the coarse woody debris from the oil palm trees is then aggregated and burned, we assigned a turnover time of 7.5 ± 4 years to represent the mean lifetime of carbon atoms from this source. The turnover time for deforestation was calculated as an upper limit using a mean turnover time of non-agricultural forests of 55 ± 28 years [*Whitmore*, 1984; *Yoneda et al.*, 1990; *Kurokawa et al.*, 2003].

4.2.4 GEOS-Chem Modeling

To quantify the spatial and temporal variability of active fires on Borneo and Sumatra, we used active fire/thermal anomaly detections from the Moderate Resolution Imaging Spectroradiometer (MODIS) on NASA's Aqua and Terra satellites [*Giglio et al.*, 2003] These observations had a 1.1 km nadir resolution and were processed at the University of Maryland (Collection 5.1; MCD14ML).

We used the GEOS-Chem global 3-D Chemical Transport Model (version 10-01, www.geos-chem.org) to simulate the atmospheric transport of aerosols emitted by fires and other

sources. The model was forced with archived GEOS-FP meteorological fields for 2014-2015, which had a temporal resolution of 6 hours (3-hour for surface variables and mixing depths), a horizontal resolution degraded to 2° (latitude) × 2.5° (longitude), and 72 vertical layers between the surface and 0.01 hPa. We performed aerosol-only simulations using monthly mean OH, NO_3, O_3 and total nitrate concentrations archived from a previous full-chemistry simulation. Inputs of aerosol emissions to the model included anthropogenic, biofuel, landscape fire, and natural sources [*Park et al.*, 2004] and were managed by the Harvard-NASA Emissions Component (HEMCO) [*Keller et al.*, 2014]. GEOS-Chem used GFED4s emissions [*Van Der Werf et al.*, 2017], which were separated into different chemical species within the model using emission factors for 6 different fire types, including peat fires and deforestation fires, with the emission factors derived mostly from *Akagi et al.* [2011]. Four sets of fire emissions from GFED4s were used in this study. A FULL simulation included all GFED4s emissions, and in three other simulations GFED4s emissions were sequentially turned off over Borneo, Sumatra, and all other source regions.

4.2.5 Peat radiocarbon measurements

We compiled peat radiocarbon measurements from cores collected in Sumatra and Borneo by previous studies [*Anderson and Muller*, 1975; *Silvius et al.*, 1984; *Supiandi and Furukawa*, 1986; *Diemont and Supardi*, 1987; *Shibata et al.*, 1997; *Page et al.*, 1999; *Page et al.*, 2004; *Yulianto et al.*, 2004; *Wüst et al.*, 2008; *Dommain et al.*, 2014; *Gandois et al.*, 2014; *Biagioni et al.*, 2015] (Figure 4.2). In an effort to best represent the wide range of peat radiocarbon, we included cores collected from both pristine and degraded peatlands and from a range of coastal and inland peat. We also included cores taken from a variety of locations on peat domes (center, edge, etc.), because the age of the peat varies as a function of its distance to the

center of the peat dome [*Page et al.*, 2004]. To estimate a mean $\Delta^{14}C$ for the top meter, we assumed any radiocarbon measurements reported as modern (and thus without a $\Delta^{14}C$) had a radiocarbon signature similar to the present-day atmosphere (25‰).

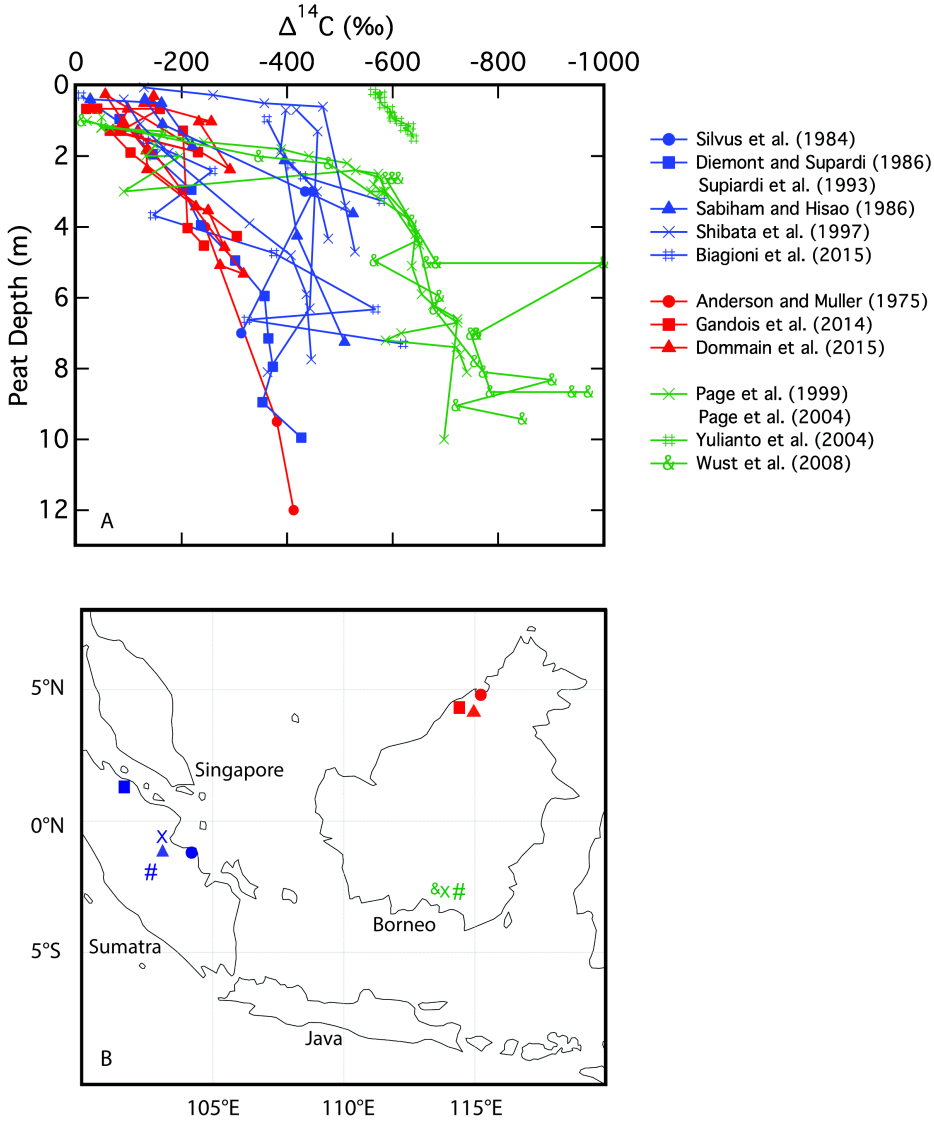

Figure 4.2 (A) Radiocarbon ($\Delta^{14}C$) versus depth for peat cores collected and analyzed in previous studies across Borneo and Sumatra. These data represent both a subset of studies from a larger compilation of radiocarbon dates (29) that reported $\Delta^{14}C$ as well as recently reported $\Delta^{14}C$ values from Northern Borneo. Blue represents coastal peat cores collected in Sumatra, red represents coastal peat cores collected in Borneo, and green represents inland peat cores collected in Kalimantan. (B) Location of peat core collection corresponding to the observations shown in panel A.

4.2.6 Peatland fire contributions to carbonaceous aerosol

In a Monte Carlo analysis, we combined estimates of the mean and standard deviation uncertainty range of the $\Delta^{14}C$ of top meter of peat (-109 ± 73‰) with model estimates of the mean and $\Delta^{14}C$ of a deforestation end member (114 ± 26‰) and the observed mean and uncertainty of the fire-aerosol end member derived from the Keeling Plot (-76 ± 51‰) to estimate the fraction of carbonaceous aerosol that originated from peat. In this analysis we made the assumption that the deforestation end member could not be less than the contemporary atmospheric composition. From this analysis, we obtained an estimate of peat contribution to carbonaceous aerosol as 85 ± 21%.

4.3 Results

During September and October of 2015, the highest densities of satellite detections of active fires were observed in South Sumatra and in the Central Kalimantan province on Borneo (Figure 4.3). During this period, weekly carbonaceous aerosol samples in Singapore had a mean concentration of 67.4 ± 29.6 μg C m^{-3}, approximately 6 times higher than urban background levels measured between January and July (Figure 4.4A; Table 4.1; see section 4.2 Methods for the definition of the urban background). The mean $\Delta^{14}C$ of these samples was -136 ± 57‰, which was considerably elevated compared to the mean of the urban background (-578 ± 78‰) (Figure 4.4B). Intervals with elevated carbonaceous aerosols in Singapore were synchronized with high numbers of satellite active fire detections on Borneo and Sumatra (Figure 4.4C). Atmospheric model simulations with GEOS-Chem indicated fires accounted for more than 80% of the total $PM_{2.5}$ observed in Singapore during September and October of 2015. Sumatra was the most important source region, accounting for 73% of the total $PM_{2.5}$ derived from fires. Within

Sumatra, emissions from the Global Fire Emissions Database version 4s (GFED4s) [*Van Der Werf et al.*, 2017] were highest in southern coastal provinces (e.g., Figure 4.3), where there was considerable burning in degraded peatland forests and escaped fires in industrial pulpwood plantation [*Miettinen et al.*, 2017a] Borneo accounted for another 18% of the fire aerosol reaching Singapore (Figure 4.4D; Table 4.2).

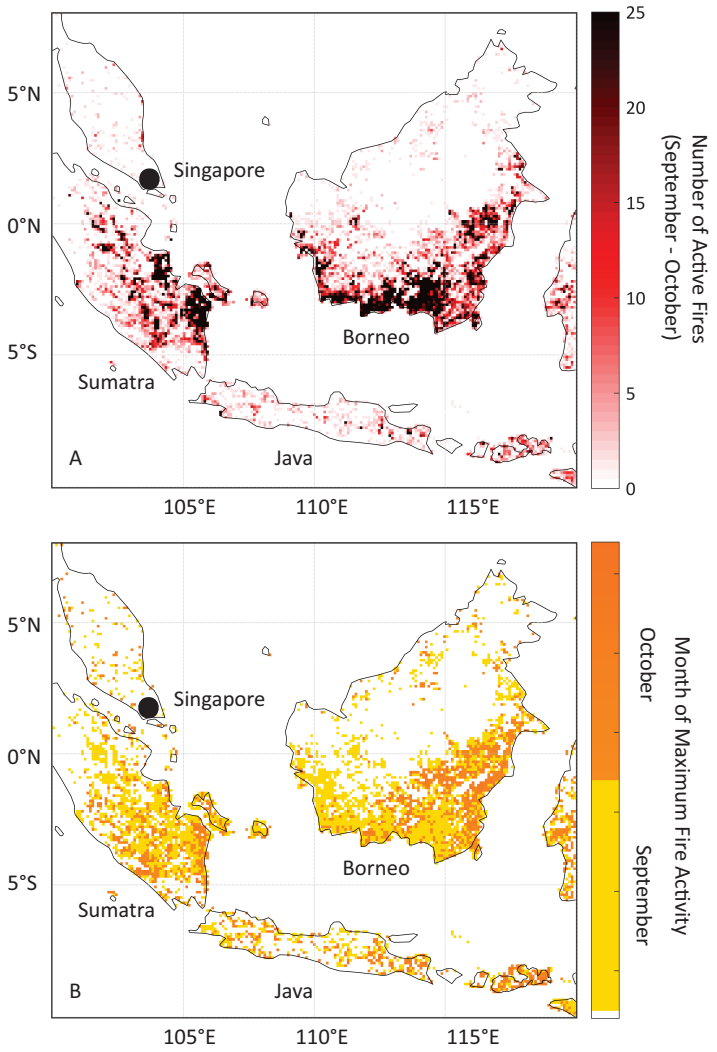

Figure 4.3 Location (A) and timing (B) of satellite-detected active fires during the 2015 September-October fire season across the Maritime Continent. The satellite detections of active fires were from the Moderate Resolution Imaging Spectroradiometer (MODIS) MCD14ML product that combines fire detections from NASA's Aqua and Terra satellites. The units of panel A are number of fire detections per 0.1° grid cell. The month with the maximum number of fire detections in each grid cell is shown in panel B.

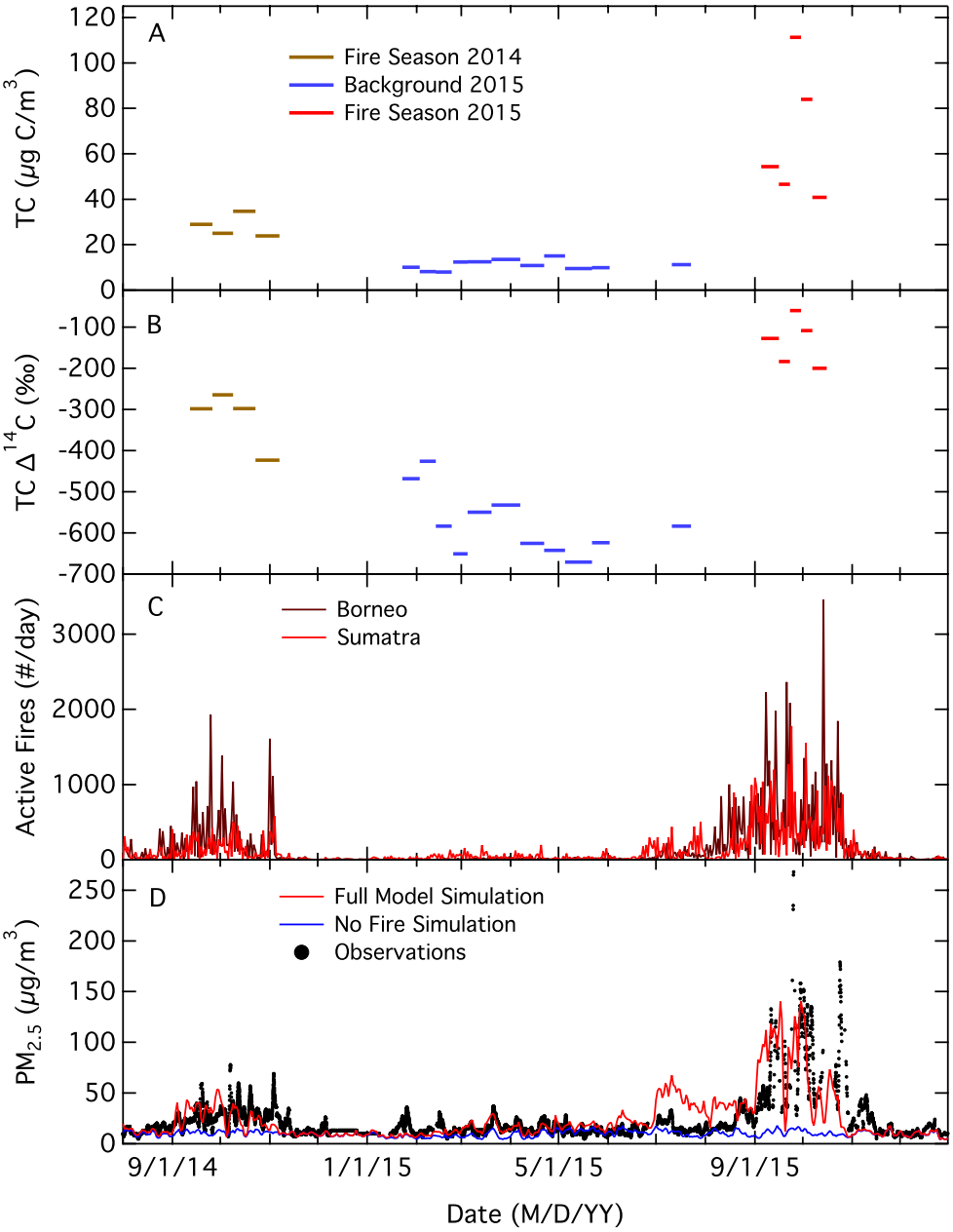

Figure 4.4 Time series of aerosol composition and fire activity during the 2014 and 2015 fire seasons. (A) Total carbon concentration of aerosol samples collected in Singapore during 2014 and 2015. Samples collected during the 2014 fire season are shown in brown, those collected during a low-fire urban background interval during the first half of 2015 are shown in blue, and those collected during the 2015 fire season are shown in red. (B) The radiocarbon content ($\Delta^{14}C$; with units of per mil (‰)) of the carbonaceous aerosol shown in panel A. (C) The number of satellite active fire detections on the islands of Borneo (dark red) and Sumatra (red). (D) $PM_{2.5}$ estimates from the GEOS-Chem atmospheric model with all sources (FULL) and a model simulation in which fire emissions were excluded (NO FIRE). Daily average $PM_{2.5}$ observations from Singapore are shown in panel D with black circles and one standard deviation error bars. The observations represent the mean of daily $PM_{2.5}$ collected from a site at the National University of Singapore (NUS).

Table 4.2 The contribution of fires to $PM_{2.5}$ in Singapore estimated using the GEOS-CHEM model. The all sources column indicates the model simulated average daily concentration of $PM_{2.5}$ during the selected period of time from all sources. The fire contribution column shows the percentage of $PM_{2.5}$ originating from biomass burning from any region. The Borneo and Sumatra columns denote the percentage of $PM_{2.5}$ originating from fires on each of these islands.

Period	$PM_{2.5}$ from all sources ($\mu g/m^3$)	Total Fire Contribution (%)	Sumatra Fires (%)	Borneo Fires (%)	Other Fires (%)
Sep – Oct 2014	16.9	60.0	39.2	15.6	5.2
Sep – Oct 2015	56.9	84.2	61.3	15.0	7.9
Background period (Jan – Jul 2015)	5.5	36.9	15.3	<1.0	21.6

During the previous fire season in 2014, a weaker El Niño [*Hu and Fedorov*, 2016] (Figure 4.1) triggered a similar, but smaller change in aerosol concentration and isotopic composition. Carbonaceous aerosol samples during September and October of 2014 had a mean concentration of 28.1 ± 4.9 μg C m^{-3}, more than 2.5 times higher than measurements from the subsequent background period. The $\Delta^{14}C$ of these samples (-321 ± 70‰) also was elevated compared to the urban background but by a lesser degree as compared to isotopic changes observed during the 2015 fire season. Satellite observations from 2014 showed much lower levels of burning across most of Sumatra and many coastal areas of southern Borneo (Figure 4.5), while the atmospheric modeling simulations indicated Borneo fire emissions were a proportionally larger component of the total fire signal observed in Singapore during this period (Table 4.2). Together, the aerosol observations, satellite measurements, and atmospheric model simulations indicated that fire emissions played a smaller, but important role in modifying $PM_{2.5}$ in Singapore during September and October of 2014.

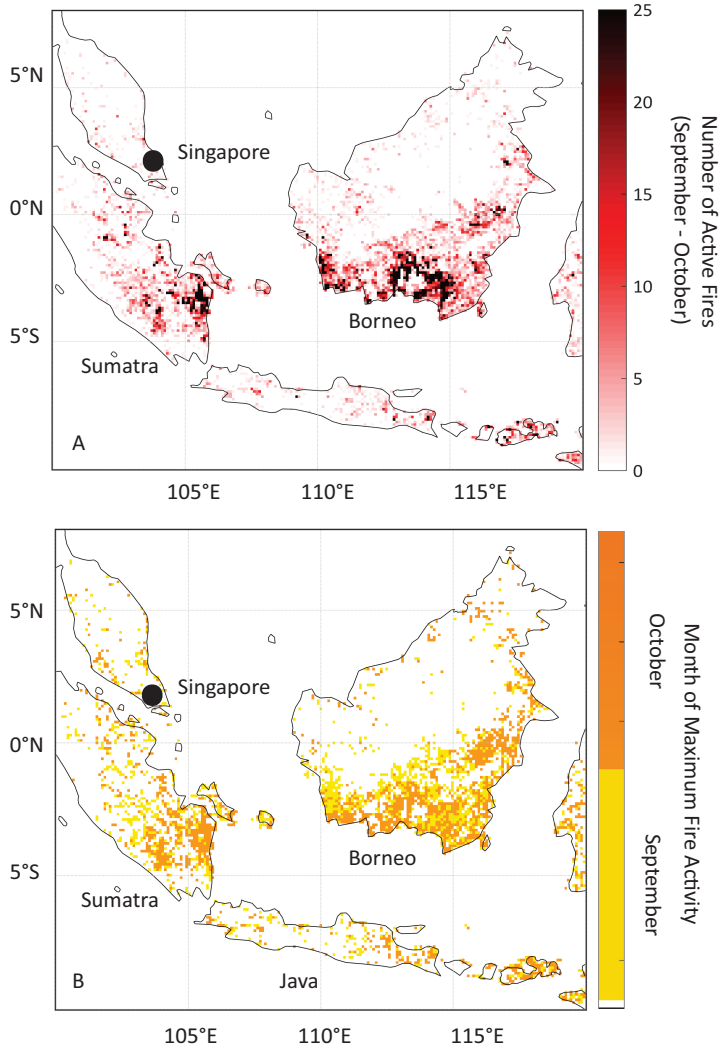

Figure 4.5 Location (A) and timing (B) of satellite-detected active fires during the 2014 September-October fire season across the Maritime Continent. The methodology for constructing the figure is identical to Fig. 1 in the main text. Note that the color bar scale in panel A is the same as Fig 1A.

We estimated the $\Delta^{14}C$ of fire-emitted carbonaceous aerosol using a Keeling Plot approach [*Pataki et al.*, 2003; *Mouteva et al.*, 2015] to separate urban background contributions from our weekly observations collected during the 2014 and 2015 fire seasons (Figure 4.6A). From this approach, we estimated that fire-emitted carbonaceous aerosols during 2014 and 2015 had a mean $\Delta^{14}C$ of –76 ± 51‰ (Figure 4.6A). This estimate was similar to the mean derived from isotope mass balance (Figure 4.7A). The relatively large uncertainty estimate likely originated from temporal variation in the location and source of fire emissions during the two

fire seasons as well as variability in the samples used to estimate the concentration and isotopic composition of the urban background.

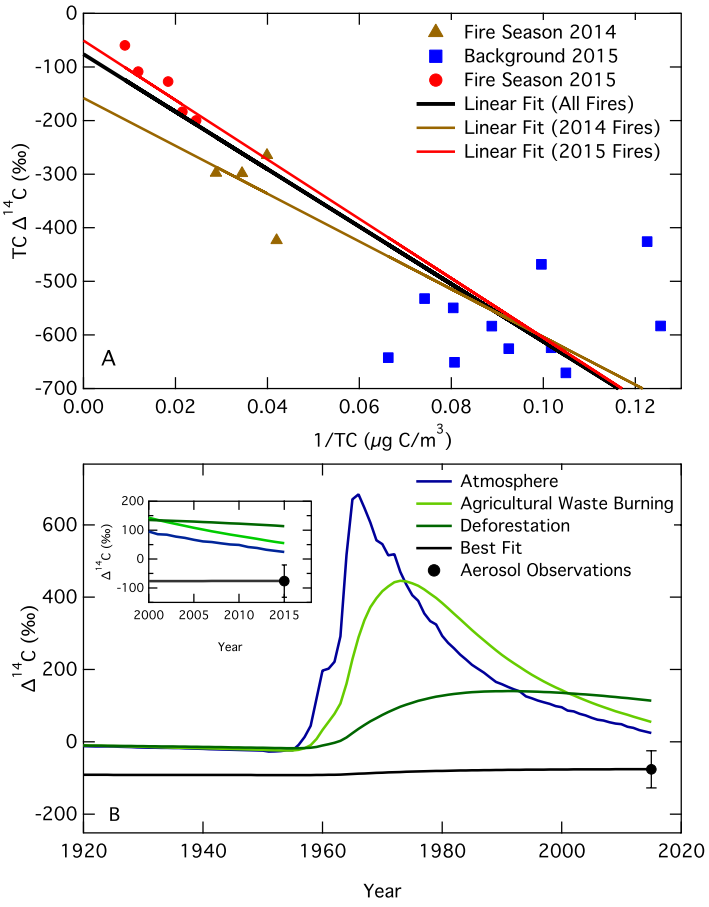

Figure 4.6 (A) A Keeling Plot showing radiocarbon content ($\Delta^{14}C$) versus the reciprocal of aerosol total carbon concentration. A best-fit line derived from a Model II regression, taking into account uncertainty in both $\Delta^{14}C$ and concentration, is shown in black for all of the fire season data from 2014 and 2015. The y intercept for this regression is -76 ± 51 ‰, and represents the isotopic composition of the fire-emitted aerosol. Brown and red lines denote the best fit lines for the 2014 and 2015 fire seasons, respectively. Panel B shows the radiocarbon content ($\Delta^{14}C$) of atmospheric CO_2 (blue line) and model estimates of agricultural waste burning emissions (light green line) and deforestation (dark green line). A source with a turnover time of 800 ± 420 years (black line) was required to match the observed $\Delta^{14}C$ of the fire-emitted aerosols (black circle). The error bar on the fire-emitted aerosol in Panel B denotes one standard deviation and was derived from the All fire regression line shown in panel A.

Using Keeling Plots to separate the $\Delta^{14}C$ of the fire-emitted carbonaceous aerosol for the different years, we found that the 2014 fire season had a more negative $\Delta^{14}C$ (-158 ± 87‰) than the 2015 fire season (-51 ± 69‰). The $\Delta^{14}C$ estimate of fire aerosol from 2014 was more uncertain because of the smaller positive concentration anomalies during the fire season, making

it more difficult to separate the fire aerosol component from the background. An independent set of 11 daily aerosol filters collected during the 2015 fire season (and obtained using a separate sampling protocol) also had a more positive isotopic value of the fire end member that was within the uncertainty range of the estimate derived from the 2015 weekly samples.

Our estimate of the mean $\Delta^{14}C$ of the fire-emitted carbonaceous aerosol during the 2014 and 2015 fire seasons was significantly lower than atmospheric levels (–76 ± 51‰ versus 25 ± 3‰; $p < 0.01$ using a Student's t-test on the data shown in Figure 4.7A and 4.7B). Given the elevated $\Delta^{14}C$ of atmospheric CO_2 over the past 60 years from nuclear weapons testing [*Hua et al.*, 2013] the negative $\Delta^{14}C$ of the fire aerosol provided evidence that most of the combusted organic matter was fixed during photosynthesis before the 20th century. Using a simple carbon cycle model to fit the $\Delta^{14}C$ aerosol observations, we estimated that the turnover time of the combusted carbon was 800 ± 420 years.

To help interpret the aerosol observations, we also used the carbon cycle model to estimate the $\Delta^{14}C$ of fire aerosols if they originated solely from agricultural waste burning or deforestation (Figure 4.7C; Figure 4.7D). For agricultural waste burning in plantations with an estimated turnover time of 7.5 ± 4 years [*Ismail and Mamat*, 2002; *Tan et al.*, 2013] the expected $\Delta^{14}C$ in 2015 would have been 52 ± 17‰ (Figure 4.7C). Similarly, for combustion of forest biomass stocks with an estimated turnover time of 55 ± 28 years [*Yoneda et al.*, 1990; *Kurokawa et al.*, 2003] the expected $\Delta^{14}C$ in 2015 would have been 114 ± 26‰ (Figure 4.7D). For reference, the $\Delta^{14}C$ of tropical atmospheric CO_2 in 2015 was approximately 25 ± 3‰ (Figures 4.6B; Figure 4.7B). The significant difference in the simulated $\Delta^{14}C$ distributions for the two aboveground biomass burning sources compared to the aerosols observations shown in Figure 4.7A provided independent confirmation that deforestation and agricultural waste burning were

unlikely to be important contributors to the carbonaceous aerosol we measured in Singapore (Figure 4.7).

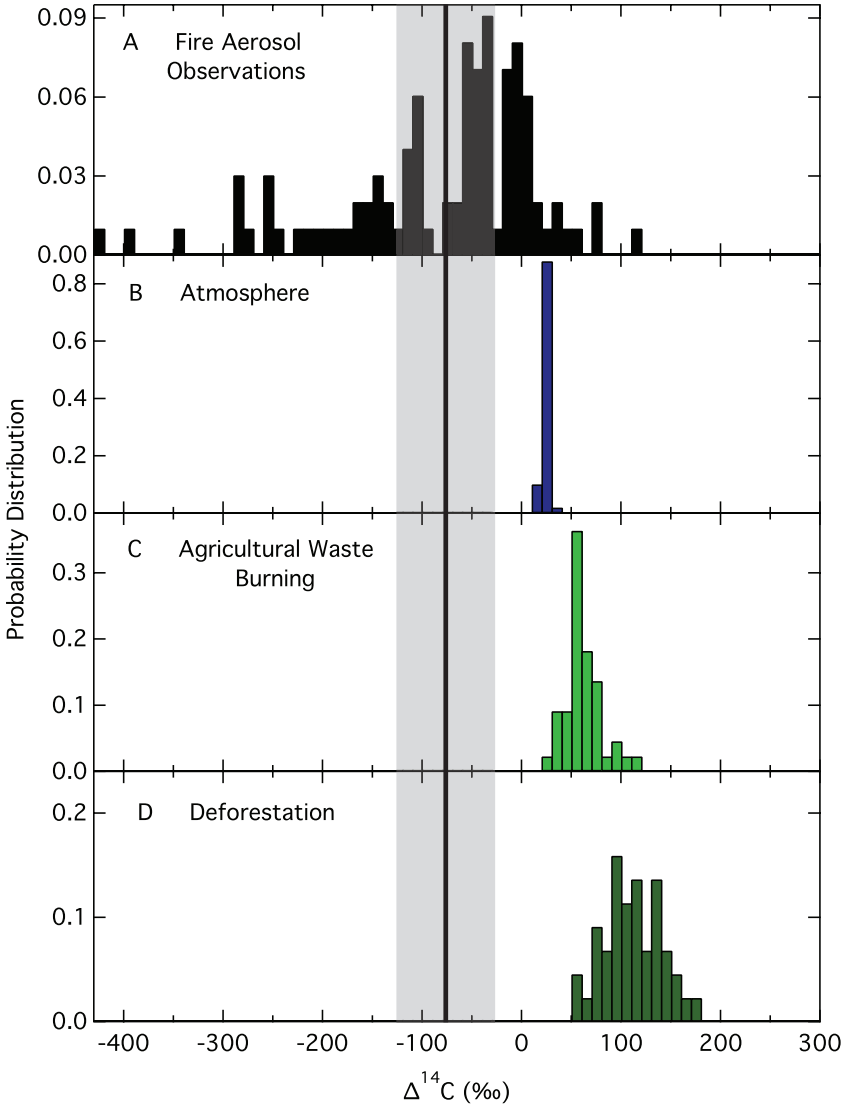

Figure 4.7 (A) Histogram of the radiocarbon content ($\Delta^{14}C$) of fire-derived carbonaceous aerosols using a mass balance approach using all of the aerosol observations from 2014 and 2015. (B) Histogram of $\Delta^{14}C$ value of the 2014-2015 atmosphere using a Monte-Carlo approach with a mean of 25 ± 3 ‰. (C) Histogram of $\Delta^{14}C$ values of agricultural waste burning using a Monte-Carlo approach with a mean of 55 ± 21‰ corresponding to a carbon pool with a turnover time of 7.5 ± 4 years. (D) Histogram of $\Delta^{14}C$ values of deforestation related fires using a Monte-Carlo approach with a mean of 114 ± 26‰ corresponding to a carbon pool with a turnover time of 55 ± 28 years. The vertical black line and gray shaded area represents the mean and standard deviation of the fire-derived carbonaceous aerosol derived from the Keeling Plot approach.

4.4 Discussion

The $\Delta^{14}C$ of the fire-emitted carbonaceous aerosol, along with previous work documenting the $\Delta^{14}C$ of organic soil profiles in peatlands [*Anderson and Muller*, 1975; *Supiandi and Furukawa*, 1986; *Diemont and Supardi*, 1987; *Page et al.*, 1999; *Page et al.*, 2004; *Yulianto et al.*, 2004; *Wüst et al.*, 2008; *Dommain et al.*, 2011; *Gandois et al.*, 2014; *Biagioni et al.*, 2015; *Cobb et al.*, 2017], indicated that most of the fire aerosol we measured in Singapore originated from burning of peat. Specifically, the mean turnover time of combusted carbon (800 ± 420 years) allowed for only a small fraction of the aerosol to originate from decadal-scale vegetation pools [*Yoneda et al.*, 1990; *Kurokawa et al.*, 2003] or surface organic soil layers enriched in ^{14}C atoms from aboveground nuclear weapons testing. A larger fraction of aerosol emissions from aboveground vegetation would have pushed the $\Delta^{14}C$ of fire-emitted aerosols above atmospheric levels (Figure 4.6; Figure 4.7).

Uncertainties in our turnover time estimate were consistent with the combustion of peat from a variety of sources and with a broad spectrum of ages. Key processes that likely influenced the $\Delta^{14}C$ of the fire aerosol were 1) the amount of burning in degraded peatlands [*Konecny et al.*, 2016] since prior burns and peat oxidation would strip away the acrotelm and bomb-labeled carbon in surface layers, 2) spatial and temporal variations in the depth of the water table that influence the depth of burn [*Konecny et al.*, 2016], 3) the magnitude and spatial pattern of peat oxidation [*Miettinen et al.*, 2017b], 4) burning location on peat domes relative to the centripetal pattern of decreasing peat age towards the dome center [*Biagioni et al.*, 2015], and 5) regional variations in the age structure (and thus $\Delta^{14}C$) of peat profiles [*Dommain et al.*, 2011]. Together, these processes were likely important drivers of the large variability in our estimates of fire-aerosol $\Delta^{14}C$ (Figure 4.7A). Because age profiles in peat usually increase monotonically with

depth (Figure 4.2), to generate smoke with a mean turnover time of 800 ± 420 years, a substantial amount of burning had to originate from peat layers that were older than one thousand years.

Aerosol $\Delta^{14}C$ measurements may provide quantitative constraints on the composition of sources contributing to total carbon emissions from fires when these observations are combined with emission factors and peat $\Delta^{14}C$ profiles. For example, if we assume that peat emissions originated from the top meter of the profile [*Konecny et al.*, 2016] with a mean $\Delta^{14}C$ of -109‰ (Figure 4.2) and that deforestation fires had a mean $\Delta^{14}C$ of 114‰ (Figure 4.7D), then about 85 ± 21% of fire aerosol emissions originated from peat, based on a Monte Carlo analysis. This estimate is somewhat higher than the 61-72% estimate of the peat contribution to the fire aerosol load we obtained by combining the fire emissions budget from *Lohberger et al.* [2017] with recent OC emission factors [*Jayarathne et al.*, 2018; *Wooster et al.*, 2018] (Table 4.3). We note that uncertainties remain considerable with respect to appropriate regional-scale estimates of emission factors and estimates of isotopic composition of combusted peat, and that both the *Lohberger et al.* [2017] and GFED4s (Figure 4.8; Table 4.4) estimates of the peat fraction of carbon emissions are within the range of the observational uncertainty. Nevertheless, the aerosol radiocarbon measurements presented here provide a new and independent constraint on source attribution that complements remote sensing observations and highlights the critical importance of burning in peatland soils as a driver of El Niño smoke clouds.

Table 4.3 Organic carbon (OC) emission factors for peatland fires and deforestation related fires used to convert total fire carbon (C) emissions originating from peatland or deforestation fires to total fire OC emissions originating from peatland or deforestation fires.

	Peat	Deforestation	Source
Total Fire C Emissions (%)	33-45	55-67	Lohberger et al. (2017)
Carbon Content of Fuel (%)	59.5[a,b]	50[b]	Dommain et al. (2011) [a] Wooster et al. (2018)[b] Van der Werf et al. (2010)[c]
OC Emission Factor (g/kg)	16 ± 6.8 [a,b]	4.95 ± 3.11[c,d]	Jayaranthne et al. (2017)[a] Wooster et al. (2018)[b] Andreae and Merlot (2001)[c] Akagi et al. (2011)[d]
Total Fire OC Emissions (%)	61-72	28-39	Derived from above quantities

Table 4.4 Carbon and organic carbon aerosol emissions from the Global Fire Emissions Database version 4.1s for the islands of Borneo and Sumatra.

C Emissions (Tg/yr)	
2014	187
2015	326
OC Aerosol Emissions (Tg/yr)	
2014	1.8
2015	3.2
Source Composition (%)	
2014	
Peat	58
Deforestation	39
Agricultural Waste Burning / Other	3
2015	
Peat	65
Deforestation	32
Agricultural Waste Burning / Other	3

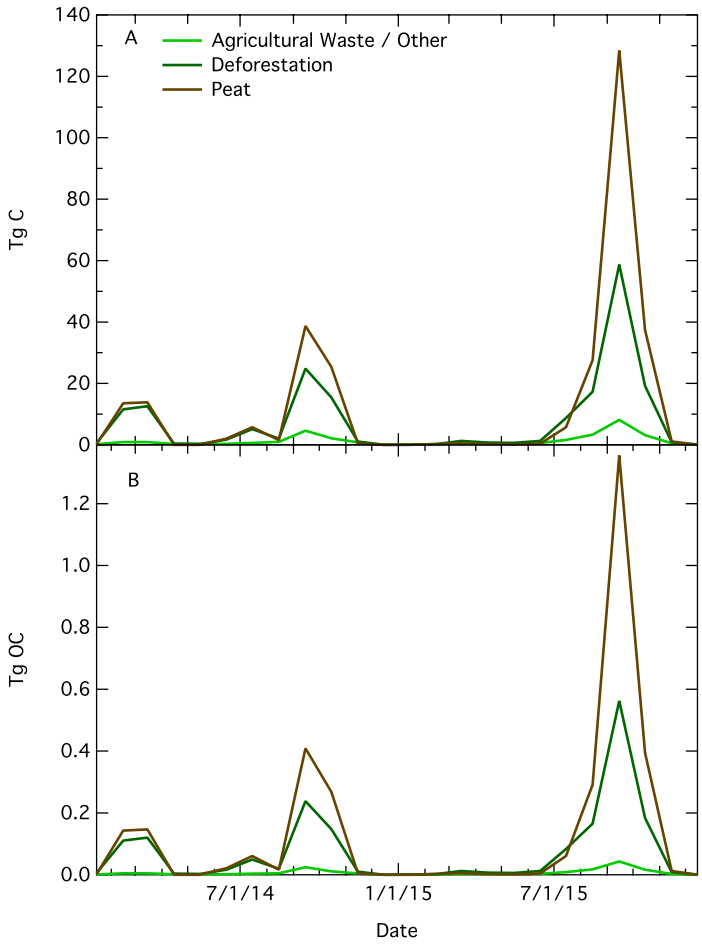

Figure 4.8 Panel A: carbon emissions from agricultural waste burning (light green), deforestation related fires (dark green), and peatlands (brown) in Borneo and Sumatra from GFED4s. Panel B: organic carbon emissions from all agricultural waste burning, deforestation, and peatlands.

Our measurements suggest that systematic regional monitoring of $\Delta^{14}C$ in aerosols and trace gases (CO and CH_4) during future El Niño events may provide insight about the success of mitigation policy. Policies that are successful in limiting peatland fires [*Murdiyarso et al.*, 2010; *Chisholm et al.*, 2016] should simultaneously lower organic carbon aerosol concentrations and raise the $\Delta^{14}C$ of these aerosols. Emission factors of CO, CH_4, and organic carbon aerosols should also decline [*Stockwell et al.*, 2016; *Jayarathne et al.*, 2018; *Wooster et al.*, 2018] highlighting the additional benefits for air quality and the added value accrued from simultaneously measuring CO_2 and other trace gas anomalies at remote sites near vulnerable

regions [*Huijnen et al.*, 2016]. Without improvements in land management and peatland conservation, we hypothesize that the $\Delta^{14}C$ of regional fire emissions during future El Niño events will decrease over the next several decades as lowering water tables expose peat layers formed earlier in the Holocene to decomposition and combustion.

The $\Delta^{14}C$ of fire-emitted aerosol during the 2014 fire season was more negative than during the 2015 fire season, suggesting different land areas with older peat layers were subject to combustion. If fires were confined to the same areas each year, the reverse would have occurred: the $\Delta^{14}C$ in 2014 would have been more positive because peat deposits are age stratified and shallower peat, higher in $\Delta^{14}C$, would have burned off first. One possible explanation for the year-to-year difference in $\Delta^{14}C$ relates to the strength of El Niño. El Nino-induced drought was weaker in 2014 (Figure 4.2). As a consequence, more burning in peatlands in 2014 may have been confined to areas near canal networks and regions that had previously undergone some degradation of surface layers and aboveground biomass pools [*Yulianto et al.*, 2004; *van der Werf et al.*, 2008b]. Analysis of aircraft light detection and ranging observations from Central Kalimantan shows that peatland fires burn more frequently (and thus deeper) in better drained areas near the banks of canals [*Konecny et al.*, 2016] As a result, combusted organic material in 2014 may have originated from deeper and older peat layers (relative to the original surface prior to disturbance) that were depleted in ^{14}C. In contrast, during the very strong El Niño in 2015, a lower regional water table may have increased the vulnerability of more pristine areas that had intact aboveground and surface peat carbon pools with stronger labeling from bomb radiocarbon. Burning from these areas with high $\Delta^{14}C$ may have more than offset emissions of lower $\Delta^{14}C$ aerosols originating from burning near canals and other areas where previous land use had degraded surface peat layers.

The lower $\Delta^{14}C$ of fire aerosols in 2014 may also be tied to shifts in emissions contributions from Sumatra and Borneo. In 2014 Borneo had a higher proportion of total active fire detections (Figure 4.4C) and contributed to a higher percentage of the fire $PM_{2.5}$ observed in Singapore (Table 4.1). In some areas of Central Kalimantan peat slowed or stopped accumulating in the mid-to-late Holocene [*Dommain et al.*, 2011], yielding older peat layers near the surface (Figure 4.3). Burning appeared more concentrated these areas (Figure 4.5), including areas previously degraded from canal building and fires [*Yulianto et al.*, 2004], and thus may have generated smoke with more negative $\Delta^{14}C$. A more quantitative separation of smoke ages from different islands may be possible in future work, but will require a regional network of aerosol sampling, use of a higher resolution atmospheric model, and a spatially-explicit model of peat ages and recent surface losses.

4.5 Conclusions

Here we report some of the first regionally integrated estimates of the radiocarbon content of smoke originating from Indonesian fires during moderate and extreme El Niño events. Our results indicated that the dominant source of carbonaceous aerosols during the 2014 and 2015 fire seasons was Holocene peat from Sumatra and Borneo, and that the mean turnover time of a simple carbon cycle model fit to the observations was 800 ± 420 years. Our measurements confirm in a novel way that Indonesian fires are predominantly releasing CO_2 to the atmosphere that has been out of contact with the atmosphere for centuries and millennia, and thus represent a net perturbation to the global carbon budget. The observations call into question recent fire budgets that suggest a significant amount of emissions originate from aboveground biomass pools or non-peatland land cover types. Systematic long-term monitoring of radiocarbon content

of fire aerosols in the future may be useful for evaluating the effectiveness of mitigation policies designed to protect existing peatland areas, particularly at an integrated province-to-country spatial scale. Together with other recent work, our study highlights the critical dual importance of reducing tropical peatland fires for air quality and climate change mitigation.

Acknowledgements

We thank Shiguo Jia for assistance with field sampling. This work was supported by the US National Science Foundation with a graduate fellowship to E.B. Wiggins (NSF 2013172241), the Gordon and Betty Moore Foundation (GBMF#3269), NASA's Carbon Monitoring System (CMS), Soil Moisture Active Passive (SMAP), and Interdisciplinary Science (IDS) research programs, the National Research Foundation Singapore through the Singapore-MIT Alliance for Research and Technology's Center for Environmental Sensing and Modeling interdisciplinary research program, a grant from Singapore National Environmental Agency to L.E. Yu (R-706-000-043-490), and a U.S. NOAA Climate and Global Change Fellowship to S.R. Holden.

Chapter 5

Conclusions

5.1 Summary of Results

In my dissertation research my goal was to improve our understanding and characterization of fire emissions from ecosystems vulnerable to climate and land use change. Within this topic I addressed a diverse set of research questions covering a wide range of spatial and temporal scales. My research consisted of laboratory measurements, in-situ and remote sensing observations, data analysis, atmospheric transport modeling, and fieldwork. I focused on fire emissions from vulnerable forest and peatland ecosystems in the boreal region of North America and in tropical Asia. My work contributes to our understanding the composition and transport of fire emissions and fire-weather feedbacks.

In Chapter 2 I studied the influence of daily weather on boreal fire activity and fire contributions to regional trace gas variability. Fire behavior and thus the amount and chemical composition of boreal fire emissions are highly sensitive to ambient and antecedent weather conditions [*Johnson*, 1996]. Most boreal fire management agencies rely heavily on fire weather indices, such as the Canadian Forest Fire Weather Index System, to predict fire danger in the near and more distant future [*Lee et al.*, 2002]. Studies forecasting future fire danger on regional to global scales using climate models also tend to employ fire weather indices as a metric of fire danger [*Flannigan et al.*, 2000; *Wotton*, 2009]. Fire weather indices are calculated using empirical formulas based on past and present meteorological conditions [*Van Wagner and Pickett*, 1985]. However, in my study I found two basic meteorological variables, temperature and vapor pressure deficit, are more highly correlated with active fire counts, burned area, fire radiative power, and fire emissions than commonly used fire weather indices. The fire weather

indices from the Canadian Forest Fire Danger Rating System were developed many decades ago when fire observations were limited. Revisiting the formulas from the original calculations and optimizing them using more recent observations from the past few decades could potentially improve the performance of fire weather indices. My study suggests fire managers and fire forecast modelers should consider using temperature and vapor pressure deficit as predictors of fire behavior together with the more complex fire weather indices.

Relationships between meteorology and fire emissions are complex and dynamic. Meteorology can influence fire behavior and emissions on time-scales of seconds to days [*Moritz et al.*, 2012]. Although fire-weather interactions have been extensively studied in the North American boreal forest, there is a need to improve fire emissions models using information regarding how weather influences the composition and magnitude of fire emissions at a daily or higher resolution. In chapter 2 I also tested the feasibility of combining high-resolution fire emissions with an atmospheric transport model to understand the influence of fire on regional trace gas variability. My modeling technique allowed me to isolate individual fire contributions to daily variability in trace gas concentrations and was constrained by region-specific emission factors and injection height information. I found moderate but significant levels of correlation between observed and modeled CO, CH_4, and CO_2 concentrations. The differences between modeled and observed atmospheric trace gas concentrations can be explained by uncertainties in my use of a static emission factor, the fire emissions inventory, and atmospheric transport. This approach could be used in future studies to improve understanding of fire emissions and weather feedbacks in the boreal forest.

Another key element needed to quantify the impacts of fires on atmospheric composition is the emission factor. Emission factors are scalars used to convert the amount of biomass

consumed in a fire into emissions of a specific trace gas or particulate species [*Akagi et al.*, 2011]. The ability to model exactly what is emitted from a fire, under different environmental conditions, is important for understanding fire impacts on weather, climate, atmospheric chemistry, and human health. Unfortunately, there is large uncertainty in emission factors for boreal forest fire emissions due to a highly limited number of in-situ measurements. In all previous studies combined, only 15 individual fire plumes have been sampled to calculate emission factors. The limited number of previous emission factor studies in addition to potential biases stemming from the sampling strategy employed by previous studies creates a high level of uncertainty for emission factors from this biome.

In chapter 3 I used a novel approach to calculate emission factors from high-resolution tower based trace gas measurements as opposed to the traditional method of flying an aircraft through an active fire plume and collecting flasks of air to be measured in a laboratory at a later time. My approach allowed me to sample emissions from at least 31 individual fires during a single fire season. I expanded my methodology from chapter 2 to confirm the tower-based observations captured signals from fire emissions occurring throughout the day-night fire-cycle and integrated emissions from multiple fires under varying environmental conditions. I discovered a CO emission factor of 144 ± 70 g CO per kg of biomass combusted. This is much higher than the mean from previous studies of 127 ± 45 g CO per kg of biomass combusted [*Akagi et al.*, 2011] and more variable. The mean modified combustion efficiency (MCE) from my study was significantly lower than the mean from previous studies. The higher CO emission factor and lower MCE indicates that smoldering combustion in boreal forest fires has been previously underestimated. The higher contribution from smoldering combustion that I discovered results in more emissions of less-oxidized trace gas and particulate species, including

CO, CH_4, and organic carbonaceous aerosols. This is important because it means the fire science and atmospheric chemistry communities may have underestimated the effect of boreal fires on atmospheric composition and human health. I focused my study on a high fire year in Alaska (2015) that could be considered representative of future fire years under a warming climate in the boreal forest.

My work implies that future boreal fire emissions could be much richer in CO, CH_4, and organic carbonaceous aerosols than has been previously estimated. An increase in fire CO emissions indicates fires play a larger role in consuming important atmospheric oxidants, including the hydroxyl radical [*Wotawa et al.*, 2001]. CH_4 is a powerful greenhouse gas that influences the radiative balance of the atmosphere. More CH_4 production means fires may play a larger role in regulating interannual variability and long-term trends in the atmospheric CH_4 budget [*Bousquet et al.*, 2006]. Carbonaceous aerosols found in fine particulate fire emissions can impact cloud microphysical properties [*Tosca et al.*, 2011; *Chen et al.*, 2018], the Earth's radiative balance, and human health [*Pöschl*, 2005]. Carbonaceous aerosols make up around 70% of $PM_{2.5}$ emitted by fires [*Lighty et al.*, 2000; *Jayarathne et al.*, 2018]. Worldwide, exposure to fine particulate matter from biomass burning causes adverse health impacts on respiratory and cardiovascular systems that can ultimately result in mortality [*Johnston et al.*, 2012]. More organic aerosol means that these fires are likely having a larger effect on human health.

On the other side of the world forests and peatlands in Indonesia are becoming increasingly vulnerable to fire. During 2015 a massive month-long regional haze episode caused by fire emissions in Indonesia adversely affected millions of people and caused an estimated 100,000 excess deaths from exposure to $PM_{2.5}$ [*Koplitz et al.*, 2016]. In this region, degraded peatlands collocated with agricultural waste burning and deforestation related fires are the

dominant sources of fire emissions [*Field et al.*, 2009; *Marlier et al.*, 2015]. El Niño causes regional drought and contributes to increased fire activity from agriculture, deforestation, and peatland fires [*Field et al.*, 2016]. However, the original source of the deadly $PM_{2.5}$ is unclear, because of difficulties in detecting smoldering combustion using remote-sensing techniques.

I utilized the radiocarbon signature of carbonaceous aerosols collected down-wind from the Indonesian fires to determine the biomass burning source of the emissions and better quantify total organic carbon aerosol emissions from fires. Based on the radiocarbon content of the carbonaceous aerosols, I determined approximately 85% of all $PM_{2.5}$ emissions originated from the burning of degraded peatlands. Fire managers and policy makers can use my methodology to test the effectiveness of peatland protections put in place to mitigate future haze episodes. In theory, if peatland protection litigation is successful, the radiocarbon content of fire-emitted carbonaceous aerosols should become more positive. My work highlights the importance of protecting Indonesian peatlands to reduce adverse human health and climate impacts from fire emissions.

5.2 Future directions

The North American boreal forest is currently experiencing rapid climate change. Although this forest has been a slow but stable carbon sink during the Holocene [*Lynch et al.*, 2004], and an important contributor to the contemporary terrestrial carbon sink [*Myneni et al.*, 2001; *Goodale et al.*, 2002; *Pan et al.*, 2011], numerous studies predict widespread temperature changes could lead to extreme fire danger and activity by the end of this century [*Bonan*, 2008; *Balshi et al.*, 2009; *Turetsky et al.*, 2011; *de Groot et al.*, 2013]. The tropical peatlands of Indonesia are experiencing a similar situation for a different reason. Anthropogenic land-use

change has severely degraded the majority of natural peatlands in Indonesia, making them highly susceptible to fire [*Page et al.*, 2009]. Both of these vulnerable regions contain substantial terrestrial stores of carbon that is released to the atmosphere during a fire. A shift in the fire regimes in these ecosystems can result in excessive carbon emissions that contribute to the long-term buildup of atmospheric greenhouse gases. Despite the importance of fires concerning climate change and human health consequences, our ability to characterize fire emissions still requires further investigation. This includes additional in-situ field measurements, satellite based observations, model development and optimization, and analysis. I highlight important needs and next steps for each of these in the following sections.

5.2.1 Observational Datasets

My dissertation research emphasizes the need for additional observational datasets on boreal forest and tropical peatland fires, both for understanding and modeling present and future fire emissions. Our understanding of the relationship between environmental conditions and combustion completeness could be greatly improved with studies that relate the composition of fire emissions to fire dynamics. Field campaigns aimed at obtaining emission factors from numerous fires across the landscape and during both daytime and nighttime should be conducted and related to ambient and antecedent weather conditions. An ideal sampling strategy would involve measuring trace gas and/or particulate concentrations at a high spatial and temporal resolution alongside measurements of environmental conditions at the same high resolution.

For example, this could be accomplished using high-resolution tower based trace gas and particulate observations coupled with environmental observations or by using wireless sensor networks. Wireless sensor networks generally consist of nodes, sensors, and modules that can collect real-time meteorological information such as temperature, humidity, and wind speed

along with atmospheric trace gas and particulate concentrations [*Yan et al.*, 2016]. Disposable wireless sensors could also be deployed from aircraft near and within large fires. Empirical equations that define relationships between environmental conditions and combustion completeness could be developed from these types of observational datasets and used to improve our understanding of fire emissions under various environmental conditions.

Remotely sensed fire-related observations are improving in quality and magnitude with current and upcoming satellite missions from NASA and other similar agencies. The data from these efforts could help relate the composition of fire emissions to fire behavior and environmental conditions at a regional to global scale. For example, active fire detections from the new Visible Infrared Imaging Radiometer Suite (VIIRS) sensor have a higher spatial and temporal resolution than traditional active fire detections from the aging MODIS sensor and should be used in future studies [*Schroeder et al.,* 2014]. The upcoming ECOsystem Spaceborne Thermal Radiometer Experiment on Space Station (ECOSTRESS) will measure the temperature of vegetation and utilize those observations to quantify drought stress [*Schimel et al.,* 2015]. An improved understanding of plant responses to drought could help advance our understanding of fire behavior and emissions in certain ecosystems vulnerable to drought. Similarly, the Global Ecosystem Dynamics Investigation (GEDI) Lidar will provide high-resolution detail about the structure of forests in the mid-latitudes and tropics [*Patterson and Healey*, 2015]. GEDI and other similar Lidar instruments can help improve our understanding of fuel structure and likely improve emission estimates from fires.

There is a need to advance satellite-based observations of smoldering fires to improve emission estimates of CO, CH_4, and $PM_{2.5}$. It is currently difficult to detect smoldering fires using traditional remote sensing techniques due to their low radiative power. However, our

results suggest the smoldering combustion contribution is higher than previously estimated in the boreal forest and possibly in Indonesian peatlands. Landsat 8's short wave infrared sensor and long wave infrared sensor are capable of detecting flaming combustion during the day and smoldering combustion at nighttime [*Elvidge et al.*, 2015]. In future studies, Landsat 8's long wave infrared sensor data should be used alongside traditional approaches when possible to include smoldering nighttime fire emissions.

The strong relationship between environmental conditions, fire behavior, and fire emissions highlighted by my research could be better quantified with remote-sensing observations that cover variability in these metrics over the entire day-night fire cycle. Agencies such as NASA should also consider launching a geostationary satellite with a high spatial and temporal resolution to cover the full diurnal cycle of an active fire. Fire activity increases during the day and decreases during the night [*Kaiser et al.*, 2009a], but we do not have a good understanding of nighttime fire emissions because of the lack of satellite based observations.

Remote sensing is an invaluable tool for understanding the landscape source of fire emissions. However, in regions where the origin of fire emissions is unclear from traditional remote-sensing techniques, the isotopic signature of emissions can be used to quantify different landscape –source contributions. Relating the isotopic composition of fire emissions to their landscape source requires knowledge of both the isotopic signature of the observations and the landscape source of emissions [*Pataki et al.*, 2003; *Schuur et al.*, 2003; *Mouteva et al.*, 2015]. Unfortunately, there are a limited number of previous studies that have measured the isotopic composition, specifically the radiocarbon content, of peat cores. There is a need for more radiocarbon-dated peat cores from the boreal forest and Indonesian peatlands. Ideally, the peat core would be sampled at a high resolution near the surface of the peat in order to more easily

translate fire-emitted aerosol radiocarbon signatures to depth of burn in peatlands. Higher resolution radiocarbon and emission factor sampling near and around peat areas during future El Niño events could also help to identify whether conservation efforts were helping to reduce vulnerability of deeper peats.

5.2.2 Models and Analyses

The most common approach for estimating emissions from fires involves combining information on burned area, fuel loading, fraction of fuel consumed, and emission factors (Equation 1.1) [*Seiler and Crutzen*, 1980]. Each of these parameters has their own unique limitations, biases, and uncertainty. Improving any of the parameters will increase accuracy in emission estimates. In the context of this dissertation research, it is important to recognize emission factors are dynamic and respond to environmental conditions. Further work should aim to implement dynamic emission factors in models by using meteorological variability to constrain combustion completeness. Fire emissions inventories would greatly benefit from this methodology applied at a high spatial and temporal resolution.

The research from this dissertation highlights the need to tease apart smoldering and flaming combustion contributions from fires. Future studies could address this issue by using region-specific and independent emission factors for smoldering and flaming fires to model emissions. The results from these studies could be compared to trace gas or particulate matter observational datasets to verify emission factors and constrain contributions from smoldering or flaming combustion.

More smoldering in boreal forest fires could imply burn severity is increasing. Although smoldering combustion consumes organic material at a lower magnitude per unit time than flaming combustion, residual smoldering combustion can continue for days, weeks, or even

months after a flaming fire front has passed through a forest. There is a need to connect relationships between residual, persistent smoldering combustion in the organic soil layers underlying spruce-dominated boreal forests and burn severity. If an increase in smoldering implies greater burn severity, there could be a shift in the dominant tree species of certain boreal ecosystem from spruce to deciduous [*Johnstone and Chapin,* 2006; *Johnstone et al.,* 2008]. Spruce forests support the development of thick organic soil layers that can store carbon for hundreds to thousands of years while deciduous dominated forests do not [*Johnstone and Chapin,* 2006]. However, fires emit less carbon overall from burning in deciduous dominant forests versus spruce dominant forests with thicker organic soil layers [*Johnstone et al.,* 2008]. There is a need to determine the relationships between the magnitude of smoldering combustion and burn severity in order to model future carbon storage and fire regimes in the boreal forest, with major implications for both climate and human health.

My results from chapter 4 highlight the importance of continuing to monitor the radiocarbon content of fire-derived aerosols in Indonesia. Steps are being taken by local government and international conservation groups to protect the peatlands in this region from deforestation, conversion to agricultural plantations, and fire [*Posa et al.,* 2011]. If these protections are successful, the radiocarbon content of fire-emitted aerosols in Indonesia should become more enriched (more positive) as a result of less fire emissions from peatlands. This methodology can be used to mitigate future haze events through successful peatland protection, and likely reduce the high rates of mortality in Indonesia associated with exposure to excessive $PM_{2.5}$ emissions from the burning of carbon rich peatlands. Ensuring the peatlands are protected from future fires will also help preserve the terrestrial carbon stores in Indonesia and reduce the positive feedback loop between carbon emissions from peatlands and climate change.

References

Abatzoglou, J. T., and C. A. Kolden (2011), Relative importance of weather and climate on wildfire growth in interior Alaska, *International Journal of Wildland Fire*, *20*(4), 479-486.

Abood, S. A., J. S. H. Lee, Z. Burivalova, J. Garcia‐Ulloa, and L. P. Koh (2015), Relative contributions of the logging, fiber, oil palm, and mining industries to forest loss in Indonesia, *Conservation Letters*, *8*(1), 58-67.

Akagi, S., R. J. Yokelson, C. Wiedinmyer, M. Alvarado, J. Reid, T. Karl, J. Crounse, and P. Wennberg (2011), Emission factors for open and domestic biomass burning for use in atmospheric models, *Atmospheric Chemistry and Physics*, *11*(9), 4039-4072.

Alexander, M. E. (1982), Calculating and interpreting forest fire intensities, *Canadian Journal of Botany*, *60*(4), 349-357.

Amiro, B., J. Todd, B. Wotton, K. Logan, M. Flannigan, B. Stocks, J. Mason, D. Martell, and K. G. Hirsch (2001), Direct carbon emissions from Canadian forest fires, 1959-1999, *Canadian Journal of Forest Research*, *31*(3), 512-525.

Amiro, B., A. Orchansky, A. Barr, T. Black, S. Chambers, F. Chapin Iii, M. Goulden, M. Litvak, H. Liu, and J. McCaughey (2006), The effect of post-fire stand age on the boreal forest energy balance, *Agricultural and Forest Meteorology*, *140*(1-4), 41-50.

Andela, N., D. Morton, L. Giglio, Y. Chen, G. van der Werf, P. Kasibhatla, R. DeFries, G. Collatz, S. Hantson, and S. Kloster (2017), A human-driven decline in global burned area, *Science*, *356*(6345), 1356-1362.

Anderson, J., and J. Muller (1975), Palynological study of a Holocene peat and a Miocene coal deposit from NW Borneo, *Review of Palaeobotany and Palynology*, *19*(4), 291-351.

Anderson, K. (2002), A model to predict lightning-caused fire occurrences, *International Journal of Wildland Fire*, *11*(4), 163-172.

Anderson, K., B. Simpson, R. J. Hall, P. Englefield, M. Gartrell, and J. M. Metsaranta (2015), Integrating forest fuels and land cover data for improved estimation of fuel consumption and carbon emissions from boreal fires, *International Journal of Wildland Fire*, *24*(5), 665-679.

Andreae, M. O., and P. Merlet (2001), Emission of trace gases and aerosols from biomass burning, *Global Biogeochemical Cycles*, *15*(4), 955-966.

Anshari, G. Z., M. Afifudin, M. Nuriman, E. Gusmayanti, L. Arianie, R. Susana, R. Nusantara, J. Sugardjito, and A. Rafiastanto (2010), Drainage and land use impacts on changes in selected peat properties and peat degradation in West Kalimantan Province, Indonesia, *Biogeosciences*, *7*(11), 3403 - 3419.

Apps, M., W. Kurz, R. Luxmoore, L. Nilsson, R. Sedjo, R. Schmidt, L. Simpson, and T. Vinson (1993), Boreal forests and tundra, *Water, Air, and Soil Pollution*, *70*(1-4), 39-53.

Balshi, M. S., A. D. McGuire, P. Duffy, M. Flannigan, D. W. Kicklighter, and J. Melillo (2009), Vulnerability of carbon storage in North American boreal forests to wildfires during the 21st century, *Global Change Biology*, *15*(6), 1491-1510.

The World Bank (2016), The Cost of Fire: An Economic Analysis of Indonesia's 2015 Fire Crisis, *(Indonesia Sustainable Landscape Knowledge)*.

Bedia, J., S. Herrera, J. M. Gutiérrez, A. Benali, S. Brands, B. Mota, and J. M. Moreno (2015), Global patterns in the sensitivity of burned area to fire-weather: Implications for climate change, *Agricultural and Forest Meteorology*, *214*, 369-379.

Bergeron, Y., M. Flannigan, S. Gauthier, A. Leduc, and P. Lefort (2004), Past, current and future fire frequency in the Canadian boreal forest: implications for sustainable forest management, *AMBIO: A Journal of the Human Environment*, *33*(6), 356-360.

Beringer, J., L. Hutley, N. Tapper, A. Coutts, A. Kerley, and A. O'grady (2003), Fire impacts on surface heat, moisture and carbon fluxes from a tropical savanna in northern Australia, *International Journal of Wildland Fire*, *12*(4), 333-340.

Bertschi, I., R. J. Yokelson, D. E. Ward, R. E. Babbitt, R. A. Susott, J. G. Goode, and W. M. Hao (2003), Trace gas and particle emissions from fires in large diameter and belowground biomass fuels, *Journal of Geophysical Research: Atmospheres*, *108*(D13), 8472.

Bessie, W., and E. Johnson (1995), The relative importance of fuels and weather on fire behavior in subalpine forests, *Ecology*, *76*(3), 747-762.

Betts, R. A., C. D. Jones, J. R. Knight, R. F. Keeling, and J. J. Kennedy (2016), El Niño and a record CO2 rise, *Nature Climate Change*, *6*(9), 806 - 810.

Beverly, R. K., W. Beaumont, D. Tauz, K. M. Ormsby, K. F. von Reden, G. M. Santos, and J. R. Southon (2010), The Keck Carbon Cycle AMS Laboratory, University of California, Irvine: status report, *Radiocarbon*, *52*(2), 301-309.

Biagioni, S., V. Krashevska, Y. Achnopha, A. Saad, S. Sabiham, and H. Behling (2015), 8000 years of vegetation dynamics and environmental changes of a unique inland peat ecosystem of the Jambi Province in Central Sumatra, Indonesia, *Paleogeography, Paleoclimatology, Paleoecology*, *440*, 813-829.

Boby, L. A., E. A. Schuur, M. C. Mack, D. Verbyla, and J. F. Johnstone (2010), Quantifying fire severity, carbon, and nitrogen emissions in Alaska's boreal forest, *Ecological Applications*, *20*(6), 1633-1647.

Bonan, G. B. (2008), Forests and climate change: forcings, feedbacks, and the climate benefits of forests, *Science*, *320*(5882), 1444-1449.

Bousquet, P., P. Ciais, J. Miller, E. Dlugokencky, D. Hauglustaine, C. Prigent, G. Van der Werf, P. Peylin, E.-G. Brunke, and C. Carouge (2006), Contribution of anthropogenic and natural sources to atmospheric methane variability, *Nature*, *443*(7110), 439-443.

Bowman, D. M., J. K. Balch, P. Artaxo, W. J. Bond, J. M. Carlson, M. A. Cochrane, C. M. D'Antonio, R. S. DeFries, J. C. Doyle, and S. P. Harrison (2009), Fire in the Earth system, *Science*, *324*(5926), 481-484.

Cahoon, D. R., B. J. Stocks, J. S. Levine, W. R. Cofer, and J. M. Pierson (1994), Satellite analysis of the severe 1987 forest fires in northern China and southeastern Siberia, *Journal of Geophysical Research: Atmospheres*, *99*(D9), 18627-18638.

Chang, R. Y.-W., C. E. Miller, S. J. Dinardo, A. Karion, C. Sweeney, B. C. Daube, J. M. Henderson, M. E. Mountain, J. Eluszkiewicz, and J. B. Miller (2014), Methane emissions from

Alaska in 2012 from CARVE airborne observations, *Proceedings of the National Academy of Sciences*, *111*(47), 16694-16699.

Chen, H., A. Karion, C. Rella, J. Winderlich, C. Gerbig, A. Filges, T. Newberger, C. Sweeney, and P. Tans (2013), Accurate measurements of carbon monoxide in humid air using the cavity ring-down spectroscopy (CRDS) technique, *Atmospheric Measurement Techniques*, *6*, 1031-1040.

Chen, J., S. H. Budisulistiorini, T. Miyakawa, Y. Komazaki, and M. Kuwata (2018), Secondary aerosol formation promotes water uptake by organic-rich wildfire haze particles in equatorial Asia, *Atmospheric Chemistry and Physics*, *18*(11), 7781-7798.

Chisholm, R. A., L. S. Wijedasa, and T. Swinfield (2016), The need for long‐term remedies for Indonesia's forest fires, *Conservation Biology*, *30*(1), 5-6.

Cobb, A. R., A. M. Hoyt, L. Gandois, J. Eri, R. Dommain, K. A. Salim, F. M. Kai, N. S. H. Su'ut, and C. F. Harvey (2017), How temporal patterns in rainfall determine the geomorphology and carbon fluxes of tropical peatlands, *Proceedings of the National Academy of Sciences*, *114*(26), E5187-E5196.

Cofer, W., J. Levine, D. Sebacher, E. Winstead, P. Riggan, B. Stocks, J. Brass, V. Ambrosia, and P. Boston (1989), Trace gas emissions from chaparral and boreal forest fires, *Journal of Geophysical Research: Atmospheres*, *94*(D2), 2255-2259.

Cofer, W., J. S. Levine, E. L. Winstead, and B. J. Stocks (1990), Gaseous emissions from Canadian boreal forest fires, *Atmospheric Environment. Part A. General Topics*, *24*(7), 1653-1659.

Cofer, W., E. Winstead, B. Stocks, J. Goldammer, and D. Cahoon (1998), Crown fire emissions of CO_2, CO, H_2, CH_4, and TNMHC from a dense jack pine boreal forest fire, *Geophysical Research Letters*, *25*(21), 3919-3922.

De Groot, W. J. (1998), Interpreting the canadian forest fire weather index (fwi) system, paper presented at Proc. of the Fourth Central Region Fire Weather Committee Scientific and Technical Seminar.

de Groot, W. J., M. D. Flannigan, and A. S. Cantin (2013), Climate change impacts on future boreal fire regimes, *Forest Ecology and Management*, *294*, 35-44.

Diemont, W., and Supardi (1987), Accumulation of organic matter and inorganic constituents in a peat dome in Sumatra, Indonesia, paper presented at International Peat Society Symposium on Tropical Peat and Peatlands for Development, Yogyakarta, Indonesia.

Dommain, R., J. Couwenberg, and H. Joosten (2011), Development and carbon sequestration of tropical peat domes in south-east Asia: links to post-glacial sea-level changes and Holocene climate variability, *Quaternary Science Reviews*, *30*(7-8), 999-1010.

Dommain, R., J. Couwenberg, P. H. Glaser, H. Joosten, and I. N. N. Suryadiputra (2014), Carbon storage and release in Indonesian peatlands since the last deglaciation, *Quaternary Science Reviews*, *97*, 1-32.

Duck, T. J., B. J. Firanski, D. B. Millet, A. H. Goldstein, J. Allan, R. Holzinger, D. R. Worsnop, A. B. White, A. Stohl, and C. S. Dickinson (2007), Transport of forest fire emissions from Alaska and the Yukon Territory to Nova Scotia during summer 2004, *Journal of Geophysical Research: Atmospheres*, *112*(D10), D10S44.

Duffy, P. A., J. E. Walsh, J. M. Graham, D. H. Mann, and T. S. Rupp (2005), Impacts of large‐scale atmospheric‐ocean variability on Alaskan fire season severity, *Ecological Applications*, *15*(4), 1317-1330.

Elvidge, C. D., M. Zhizhin, F.-C. Hsu, K. Baugh, M. R. Khomarudin, Y. Vetrita, P. Sofan, and D. Hilman (2015), Long-wave infrared identification of smoldering peat fires in Indonesia with nighttime Landsat data, *Environmental Research Letters*, *10*(6), 065002.

Field, R. D., G. R. Van Der Werf, and S. S. Shen (2009), Human amplification of drought-induced biomass burning in Indonesia since 1960, *Nature Geoscience*, *2*(3), 185-188.

Field, R. D., G. R. Van Der Werf, T. Fanin, E. J. Fetzer, R. Fuller, H. Jethva, R. Levy, N. J. Livesey, M. Luo, and O. Torres (2016), Indonesian fire activity and smoke pollution in 2015 show persistent nonlinear sensitivity to El Niño-induced drought, *Proceedings of the National Academy of Sciences*, *113*(33), 9204-9209.

Flanner, M. G., C. S. Zender, J. T. Randerson, and P. J. Rasch (2007), Present‐day climate forcing and response from black carbon in snow, *Journal of Geophysical Research: Atmospheres*, *112*(D11), D11202.

Flannigan, M., and J. B. Harrington (1988), A study of the relation of meteorological variables to monthly provincial area burned by wildfire in Canada (1953–80), *Journal of Applied Meteorology*, *27*(4), 441-452.

Flannigan, M., I. Campbell, M. Wotton, C. Carcaillet, P. Richard, and Y. Bergeron (2001), Future fire in Canada's boreal forest: paleoecology results and general circulation model-regional climate model simulations, *Canadian Journal of Forest Research*, *31*(5), 854-864.

Flannigan, M. D., B. J. Stocks, and B. M. Wotton (2000), Climate change and forest fires, *Science of the Total Environment*, *262*(3), 221-229.

Forster, C., U. Wandinger, G. Wotawa, P. James, I. Mattis, D. Althausen, P. Simmonds, S. O'Doherty, S. G. Jennings, and C. Kleefeld (2001), Transport of boreal forest fire emissions from Canada to Europe, *Journal of Geophysical Research: Atmospheres*, *106*(D19), 22887-22906.

Freitas, S., K. Longo, M. S. Dias, R. Chatfield, P. S. Dias, P. Artaxo, M. Andreae, G. Grell, L. Rodrigues, and A. Fazenda (2007), The Coupled Aerosol and Tracer Transport model to the Brazilian developments on the Regional Atmospheric Modeling System (CATT-BRAMS)? Part 1: Model description and evaluation, *Atmospheric Chemistry and Physics Discussions*, *7*(3), 8525-8569.

Freitas, S., K. Longo, M. Silva Dias, R. Chatfield, P. Silva Dias, P. Artaxo, M. Andreae, G. Grell, L. Rodrigues, and A. Fazenda (2009), The coupled aerosol and tracer transport model to the Brazilian developments on the regional atmospheric modeling system (CATT-BRAMS)–Part 1: Model description and evaluation, *Atmospheric Chemistry and Physics*, *9*(8), 2843-2861.

French, N. H., E. S. Kasischke, and D. G. Williams (2002), Variability in the emission of carbon‐based trace gases from wildfire in the Alaskan boreal forest, *Journal of Geophysical Research: Atmospheres*, *107*(D1).

French, N. H., P. Goovaerts, and E. S. Kasischke (2004), Uncertainty in estimating carbon emissions from boreal forest fires, *Journal of Geophysical Research: Atmospheres*, *109*(D14), D14S08.

French, N. H., D. McKenzie, T. Erickson, B. Koziol, M. Billmire, K. A. Endsley, N. K. Yager Scheinerman, L. Jenkins, M. E. Miller, and R. Ottmar (2014), Modeling regional-scale wildland fire emissions with the Wildland Fire Emissions Information System, *Earth Interactions*, *18*(16), 1-26.

Gandois, L., R. Teisserenc, A. Cobb, H. Chieng, L. Lim, A. Kamariah, A. Hoyt, and C. Harvey (2014), Origin, composition, and transformation of dissolved organic matter in tropical peatlands, *Geochimica et Cosmochimica Acta*, *137*, 35-47.

Gauthier, S., P. Bernier, T. Kuuluvainen, A. Shvidenko, and D. Schepaschenko (2015), Boreal forest health and global change, *Science*, *349*(6250), 819-822.

Giglio, L., J. Descloitres, C. O. Justice, and Y. J. Kaufman (2003), An enhanced contextual fire detection algorithm for MODIS, *Remote Sensing of Environment*, *87*(2-3), 273-282.

Gillett, N., A. Weaver, F. Zwiers, and M. Flannigan (2004), Detecting the effect of climate change on Canadian forest fires, *Geophysical Research Letters*, *31*(18), L18211.

Goodale, C. L., M. J. Apps, R. A. Birdsey, C. B. Field, L. S. Heath, R. A. Houghton, J. C. Jenkins, G. H. Kohlmaier, W. Kurz, and S. Liu (2002), Forest carbon sinks in the Northern Hemisphere, *Ecological Applications*, *12*(3), 891-899.

Goode, J. G., R. J. Yokelson, D. E. Ward, R. A. Susott, R. E. Babbitt, M. A. Davies, and W. M. Hao (2000), Measurements of excess O_3, CO_2, CO, CH_4, C_2H_4, C_2H_2, HCN, NO, NH_3, HCOOH, CH_3COOH, HCHO, and CH_3OH in 1997 Alaskan biomass burning plumes by airborne Fourier transform infrared spectroscopy (AFTIR), *Journal of Geophysical Research: Atmospheres*, *105*(D17), 22147-22166.

Grell, G., S. Freitas, M. Stuefer, and J. Fast (2010), Inclusion of biomass burning in WRF-Chem: impact of wildfires on weather forecasts, *Atmospheric Chemistry & Physics Discussions*, *10*(12), 5289.

Harden, J., S. Trumbore, B. Stocks, A. Hirsch, S. Gower, K. O'neill, and E. Kasischke (2000a), The role of fire in the boreal carbon budget, *Global Change Biology*, *6*(S1), 174-184.

Hayasaka, H., H. L. Tanaka, and P. A. Bieniek (2016), Synoptic-scale fire weather conditions in Alaska, *Polar Science*, *10*(3), 217-226.

Heil, A., B. Langmann, and E. Aldrian (2007), Indonesian peat and vegetation fire emissions: Study on factors influencing large-scale smoke haze pollution using a regional atmospheric chemistry model, *Mitigation and Adaptation Strategies for Global Change*, *12*(1), 113-133.

Henderson, J., J. Eluszkiewicz, M. Mountain, T. Nehrkorn, R.-W. Chang, A. Karion, J. Miller, C. Sweeney, N. Steiner, and S. Wofsy (2015), Atmospheric transport simulations in support of the Carbon in Arctic Reservoirs Vulnerability Experiment (CARVE), *Atmospheric Chemistry & Physics*, *15*(8), 4093–4116.

Heymann, J., M. Reuter, M. Buchwitz, O. Schneising, H. Bovensmann, J. Burrows, S. Massart, J. Kaiser, and D. Crisp (2017), CO_2 emission of Indonesian fires in 2015 estimated from

satellite‐derived atmospheric CO_2 concentrations, *Geophysical Research Letters*, *44*(3), 1537-1544.

Hobbie, S. E., J. P. Schimel, S. E. Trumbore, and J. R. Randerson (2000), Controls over carbon storage and turnover in high‐latitude soils, *Global Change Biology*, *6*(S1), 196-210.

Hu, S., and A. V. Fedorov (2016), Exceptionally strong easterly wind burst stalling El Niño of 2014, *Proceedings of the National Academy of Sciences*, *113*(8), 2005-2010.

Hua, Q., M. Barbetti, and A. Z. Rakowski (2013), Atmospheric radiocarbon for the period 1950–2010, *Radiocarbon*, *55*(4), 2059-2072.

Huang, X., F. Restuccia, M. Gramola, and G. Rein (2016), Experimental study of the formation and collapse of an overhang in the lateral spread of smouldering peat fires, *Combustion and Flame*, *168*, 393-402.

Huijnen, V., M. Wooster, J. Kaiser, D. Gaveau, J. Flemming, M. Parrington, A. Inness, D. Murdiyarso, B. Main, and M. van Weele (2016), Fire carbon emissions over maritime southeast Asia in 2015 largest since 1997, *Scientific Reports*, *6*, 26886.

Ichoku, C., and Y. J. Kaufman (2005), A method to derive smoke emission rates from MODIS fire radiative energy measurements, *IEEE transactions on Geoscience and Remote Sensing*, *43*(11), 2636-2649.

Ismail, A., and M. N. Mamat (2002), The optimal age of oil palm replanting, *Oil Palm Industry Economic Journal*, *2*(1), 11-18.

Jaenicke, J., J. Rieley, C. Mott, P. Kimman, and F. Siegert (2008), Determination of the amount of carbon stored in Indonesian peatlands, *Geoderma*, *147*(3-4), 151-158.

Jayarathne, T., C. E. Stockwell, A. A. Gilbert, K. Daugherty, M. A. Cochrane, K. C. Ryan, E. I. Putra, B. H. Saharjo, A. D. Nurhayati, and I. Albar (2018), Chemical characterization of fine particulate matter emitted by peat fires in central Kalimantan, Indonesia, during the 2015 El Niño, *Atmospheric Chemistry & Physics*, *18*(4), 2585-2600.

Johnson, E. A. (1996), *Fire and vegetation dynamics: studies from the North American boreal forest*, Cambridge University Press.

Johnston, F. H., S. B. Henderson, Y. Chen, J. T. Randerson, M. Marlier, R. S. DeFries, P. Kinney, D. M. Bowman, and M. Brauer (2012), Estimated global mortality attributable to smoke from landscape fires, *Environmental Health Perspectives*, *120*(5), 695-701.

Johnstone, J. F., and F. S. Chapin (2006), Effects of soil burn severity on post-fire tree recruitment in boreal forest, *Ecosystems*, *9*(1), 14-31.

Johnstone, J. F., F. Chapin Iii, J. Foote, S. Kemmett, K. Price, and L. Viereck (2004), Decadal observations of tree regeneration following fire in boreal forests, *Canadian Journal of Forest Research*, *34*(2), 267-273.

Jones, P., D. Lister, T. Osborn, C. Harpham, M. Salmon, and C. Morice (2012), Hemispheric and large‐scale land‐surface air temperature variations: An extensive revision and an update to 2010, *Journal of Geophysical Research: Atmospheres*, *117*(D5), D05127.

Jordan, N. S., C. Ichoku, and R. M. Hoff (2008), Estimating smoke emissions over the US Southern Great Plains using MODIS fire radiative power and aerosol observations, *Atmospheric Environment*, *42*(9), 2007-2022.

Kahn, R. A., Y. Chen, D. L. Nelson, F. Y. Leung, Q. Li, D. J. Diner, and J. A. Logan (2008), Wildfire smoke injection heights: Two perspectives from space, *Geophysical Research Letters*, *35*(4), L04809.

Kaiser, J., M. Suttie, J. Flemming, J. J. Morcrette, O. Boucher, and M. Schultz (2009a), Global real‐time fire emission estimates based on space‐borne fire radiative power observations, paper presented at AIP conference proceedings, AIP.

Kaiser, J., J. Flemming, M. Schultz, M. Suttie, and M. Wooster (2009b), The macc global fire assimilation system: First emission products (gfasv0), *ECMWF Technical Memoranda*(596), 1-16.

Karion, A., C. Sweeney, J. B. Miller, A. E. Andrews, R. Commane, S. Dinardo, J. M. Henderson, J. Lindaas, J. C. Lin, and K. A. Luus (2016), Investigating Alaskan methane and carbon dioxide fluxes using measurements from the CARVE tower, *Atmospheric Chemistry and Physics*, *16*(8), 5383-5398.

Kasischke, E. S., and L. P. Bruhwiler (2002), Emissions of carbon dioxide, carbon monoxide, and methane from boreal forest fires in 1998, *Journal of Geophysical Research: Atmospheres*, *107*(D1), 8146.

Kasischke, E. S., and M. R. Turetsky (2006), Recent changes in the fire regime across the North American boreal region—spatial and temporal patterns of burning across Canada and Alaska, *Geophysical Research Letters*, *33*(9), L09703.

Kasischke, E. S., and B. J. Stocks (2012), *Fire, climate change, and carbon cycling in the boreal forest*, Springer Science & Business Media.

Kasischke, E. S., N. Christensen Jr, and B. J. Stocks (1995), Fire, global warming, and the carbon balance of boreal forests, *Ecological Applications*, *5*(2), 437-451.

Kasischke, E. S., E. J. Hyer, P. C. Novelli, L. P. Bruhwiler, N. H. French, A. I. Sukhinin, J. H. Hewson, and B. J. Stocks (2005), Influences of boreal fire emissions on Northern Hemisphere atmospheric carbon and carbon monoxide, *Global Biogeochemical Cycles*, *19*(1), GB1012.

Keller, C. A., M. S. Long, R. M. Yantosca, A. Da Silva, S. Pawson, and D. J. Jacob (2014), HEMCO v1. 0: a versatile, ESMF-compliant component for calculating emissions in atmospheric models, *Geosci. Model Dev.*, *7*, 1409-1417.

Konecny, K., U. Ballhorn, P. Navratil, J. Jubanski, S. E. Page, K. Tansey, A. Hooijer, R. Vernimmen, and F. Siegert (2016), Variable carbon losses from recurrent fires in drained tropical peatlands, *Global Change Biology*, *22*(4), 1469-1480.

Koplitz, S. N., L. J. Mickley, M. E. Marlier, J. J. Buonocore, P. S. Kim, T. Liu, M. P. Sulprizio, R. S. DeFries, D. J. Jacob, and J. Schwartz (2016), Public health impacts of the severe haze in Equatorial Asia in September–October 2015: demonstration of a new framework for informing fire management strategies to reduce downwind smoke exposure, *Environmental Research Letters*, *11*(9), 094023.

Kurokawa, H., T. Yoshida, T. Nakamura, J. Lai, and T. Nakashizuka (2003), The age of tropical rain-forest canopy species, Borneo ironwood (Eusideroxylon zwageri), determined by ^{14}C dating, *Journal of Tropical Ecology*, *19*(1), 1-7.

Langmann, B., B. Duncan, C. Textor, J. Trentmann, and G. R. van der Werf (2009), Vegetation fire emissions and their impact on air pollution and climate, *Atmospheric Environment*, *43*(1), 107-116.

Larkin, N. K., S. M. O'Neill, R. Solomon, S. Raffuse, T. Strand, D. C. Sullivan, C. Krull, M. Rorig, J. Peterson, and S. A. Ferguson (2010), The BlueSky smoke modeling framework, *International Journal of Wildland Fire*, *18*(8), 906-920.

Latham, D. J., and J. A. Schlieter (1989), *Ignition probabilities of wildland fuels based on simulated lightning discharges*, US Department of Agriculture, Forest Service, Intermountain Research Station.

Lavorel, S., M. D. Flannigan, E. F. Lambin, and M. C. Scholes (2007), Vulnerability of land systems to fire: Interactions among humans, climate, the atmosphere, and ecosystems, *Mitigation and Adaptation Strategies for Global Change*, *12*(1), 33-53.

Lawrence, M. G. (2005), The relationship between relative humidity and the dewpoint temperature in moist air: A simple conversion and applications, *Bulletin of the American Meteorological Society*, *86*(2), 225-234.

Lawson, D. E. (1986), Response of permafrost terrain to disturbance: a synthesis of observations from northern Alaska, USA, *Arctic and Alpine Research*, *18*(1), 1-17.

Lee, B., M. Alexander, B. Hawkes, T. Lynham, B. Stocks, and P. Englefield (2002), Information systems in support of wildland fire management decision making in Canada, *Computers and Electronics in Agriculture*, *37*(1-3), 185-198.

Leung, F. Y. T., J. A. Logan, R. Park, E. Hyer, E. Kasischke, D. Streets, and L. Yurganov (2007), Impacts of enhanced biomass burning in the boreal forests in 1998 on tropospheric chemistry and the sensitivity of model results to the injection height of emissions, *Journal of Geophysical Research: Atmospheres*, *112*(D10), D10313.

Levin, I., and V. Hesshaimer (2000), Radiocarbon–a unique tracer of global carbon cycle dynamics, *Radiocarbon*, *42*(1), 69-80.

Levine, J. S., and W. R. Cofer (2000), Boreal forest fire emissions and the chemistry of the atmosphere, in *Fire, climate change, and carbon cycling in the boreal forest*, edited, pp. 31-48, Springer.

Li, F., B. Bond-Lamberty, and S. Levis (2014), Quantifying the role of fire in the Earth system, *Biogeosciences*, *11*(5), 1345 - 1360.

Lighty, J. S., J. M. Veranth, and A. F. Sarofim (2000), Combustion aerosols: factors governing their size and composition and implications to human health, *Journal of the Air & Waste Management Association*, *50*(9), 1565-1618.

Lin, J., C. Gerbig, S. Wofsy, V. Chow, E. Gottlieb, B. Daube, and D. Matross (2007), Designing Lagrangian experiments to measure regional‐scale trace gas fluxes, *Journal of Geophysical Research: Atmospheres*, *112*(D13), D13312.

Liu, J., K. W. Bowman, D. S. Schimel, N. C. Parazoo, Z. Jiang, M. Lee, A. A. Bloom, D. Wunch, C. Frankenberg, and Y. Sun (2017), Contrasting carbon cycle responses of the tropical continents to the 2015–2016 El Niño, *Science*, *358*(6360), eaam5690.

Liu, Y., J. Stanturf, and S. Goodrick (2010), Trends in global wildfire potential in a changing climate, *Forest Ecology and Management*, *259*(4), 685-697.

Lohberger, S., M. Stängel, E. C. Atwood, and F. Siegert (2017), Spatial evaluation of Indonesia's 2015 fire affected area and estimated carbon emissions using Sentinel-1, *Global Change Biology*, *24*(2), 644-654.

Luus, K., and J. Lin (2015), The Polar Vegetation Photosynthesis and Respiration Model: a parsimonious, satellite-data-driven model of high-latitude CO_2 exchange, *Geoscientific Model Development*, *8*, 2655-2674.

Lynch, J. A., J. L. Hollis, and F. S. Hu (2004), Climatic and lands landscape controls of the boreal forest fire regime: Holocene records from Alaska, *Journal of Ecology*, *92*(3), 477-489.

Maloney, B., and F. McCormac (1995), A 30,000-year pollen and radiocarbon record from Highland Sumatra as evidence for climatic change, *Radiocarbon*, *37*(2), 181-190.

Marlier, M. E., R. S. DeFries, P. S. Kim, S. N. Koplitz, D. J. Jacob, L. J. Mickley, and S. S. Myers (2015), Fire emissions and regional air quality impacts from fires in oil palm, timber, and logging concessions in Indonesia, *Environmental Research Letters*, *10*(8), 085005.

Marlier, M. E., R. S. DeFries, A. Voulgarakis, P. L. Kinney, J. T. Randerson, D. T. Shindell, Y. Chen, and G. Faluvegi (2013), El Niño and health risks from landscape fire emissions in southeast Asia, *Nature Climate Change*, *3*(2), 131-136.

Martin, M. V., R. E. Honrath, R. C. Owen, G. Pfister, P. Fialho, and F. Barata (2006), Significant enhancements of nitrogen oxides, black carbon, and ozone in the North Atlantic lower free troposphere resulting from North American boreal wildfires, *Journal of Geophysical Research-Atmospheres*, *111*(D23), D23S60.

McGuire, A. D., R. W. Macdonald, E. A. Schuur, J. W. Harden, P. Kuhry, D. J. Hayes, T. R. Christensen, and M. Heimann (2010), The carbon budget of the northern cryosphere region, *Current Opinion in Environmental Sustainability*, *2*(4), 231-236.

Miettinen, J., C. Shi, and S. C. Liew (2012), Two decades of destruction in Southeast Asia's peat swamp forests, *Frontiers in Ecology and the Environment*, *10*(3), 124-128.

Miettinen, J., C. Shi, and S. C. Liew (2016), Land cover distribution in the peatlands of Peninsular Malaysia, Sumatra and Borneo in 2015 with changes since 1990, *Global Ecology and Conservation*, *6*, 67-78.

Miettinen, J., C. Shi, and S. C. Liew (2017a), Fire distribution in Peninsular Malaysia, Sumatra and Borneo in 2015 with special emphasis on peatland fires, *Environmental Management*, *60*(4), 747-757.

Miettinen, J., A. Hooijer, R. Vernimmen, S. C. Liew, and S. E. Page (2017b), From carbon sink to carbon source: extensive peat oxidation in insular Southeast Asia since 1990, *Environmental Research Letters*, *12*(2), 024014.

Moritz, M. A., M.-A. Parisien, E. Batllori, M. A. Krawchuk, J. Van Dorn, D. J. Ganz, and K. Hayhoe (2012), Climate change and disruptions to global fire activity, *Ecosphere*, *3*(6), 1-22.

Mouteva, G., C. Czimczik, S. Fahrni, E. Wiggins, B. Rogers, S. Veraverbeke, X. Xu, G. Santos, J. Henderson, and C. Miller (2015), Black carbon aerosol dynamics and isotopic composition in Alaska linked with boreal fire emissions and depth of burn in organic soils, *Global Biogeochemical Cycles*, *29*(11), 1977-2000.

Mu, M., J. Randerson, G. Van der Werf, L. Giglio, P. Kasibhatla, D. Morton, G. Collatz, R. DeFries, E. Hyer, and E. Prins (2011), Daily and 3‐hourly variability in global fire emissions and consequences for atmospheric model predictions of carbon monoxide, *Journal of Geophysical Research: Atmospheres*, *116*(D24), D24303.

Murdiyarso, D., K. Hergoualc'h, and L. Verchot (2010), Opportunities for reducing greenhouse gas emissions in tropical peatlands, *Proceedings of the National Academy of Sciences*, *107*(46), 19655-19660.

Myneni, R., J. Dong, C. Tucker, R. Kaufmann, P. Kauppi, J. Liski, L. Zhou, V. Alexeyev, and M. Hughes (2001), A large carbon sink in the woody biomass of northern forests, *Proceedings of the National Academy of Sciences*, *98*(26), 14784-14789.

Nance, J. D., P. V. Hobbs, L. F. Radke, and D. E. Ward (1993), Airborne measurements of gases and particles from an Alaskan wildfire, *Journal of Geophysical Research: Atmospheres*, *98*(D8), 14873-14882.

Nash, C., and E. Johnson (1996), Synoptic climatology of lightning-caused forest fires in subalpine and boreal forests, *Canadian Journal of Forest Research*, *26*(10), 1859-1874.

Nazarenko, L., G. Schmidt, R. Miller, N. Tausnev, M. Kelley, R. Ruedy, G. Russell, I. Aleinov, M. Bauer, and S. Bauer (2015), Future climate change under RCP emission scenarios with GISS ModelE2, *Journal of Advances in Modeling Earth Systems*, *7*(1), 244-267.

Nehrkorn, T., J. Henderson, M. Leidner, M. Mountain, J. Eluszkiewicz, K. McKain, and S. Wofsy (2013), WRF simulations of the urban circulation in the Salt Lake City area for CO2 modeling, *Journal of Applied Meteorology and Climatology*, *52*(2), 323-340.

Nelson, D. L., M. J. Garay, R. A. Kahn, and B. A. Dunst (2013), Stereoscopic height and wind retrievals for aerosol plumes with the MISR INteractive eXplorer (MINX), *Remote Sensing*, *5*(9), 4593-4628.

Ottmar, R. D. (2001), Smoke source characteristics, *Smoke Management Guide for Prescribed and Wildland Fire*, 420-422.

Page, S., J. Rieley, Ø. Shotyk, and D. Weiss (1999), Interdependence of peat and vegetation in a tropical peat swamp forest, *Philosophical Transactions of the Royal Society of London B: Biological Sciences*, *354*(1391), 1885-1897.

Page, S., R. Wűst, D. Weiss, J. Rieley, W. Shotyk, and S. H. Limin (2004), A record of Late Pleistocene and Holocene carbon accumulation and climate change from an equatorial peat bog (Kalimantan, Indonesia): implications for past, present and future carbon dynamics, *Journal of Quaternary Science*, *19*(7), 625-635.

Page, S., A. Hoscilo, A. Langner, K. Tansey, F. Siegert, S. Limin, and J. Rieley (2009), Tropical peatland fires in Southeast Asia, in *Tropical Fire Ecology*, edited, pp. 263-287, Springer.

Page, S. E., and A. Hooijer (2016), In the line of fire: the peatlands of Southeast Asia, *Phil. Trans. R. Soc. B*, *371*(1696), 20150176.

Page, S. E., J. O. Rieley, and C. J. Banks (2011), Global and regional importance of the tropical peatland carbon pool, *Global Change Biology*, *17*(2), 798-818.

Page, S. E., F. Siegert, J. O. Rieley, H.-D. V. Boehm, A. Jaya, and S. Limin (2002), The amount of carbon released from peat and forest fires in Indonesia during 1997, *Nature*, *420*(6911), 61-65.

Page, S. E., R. Wűst, D. Weiss, J. O. Rieley, W. Shotyk, and S. H. Limin (2004), A record of Late Pleistocene and Holocene carbon accumulation and climate change from an equatorial peat bog (Kalimantan, Indonesia): implications for past, present and future carbon dynamics, *Journal of Quaternary Science*, *19*(7), 625-635.

Pan, Y., R. A. Birdsey, J. Fang, R. Houghton, P. E. Kauppi, W. A. Kurz, O. L. Phillips, A. Shvidenko, S. L. Lewis, and J. G. Canadell (2011), A large and persistent carbon sink in the world's forests, *Science*, *333*(6045), 988-993.

Park, R. J., D. J. Jacob, B. D. Field, R. M. Yantosca, and M. Chin (2004), Natural and transboundary pollution influences on sulfate‐nitrate‐ammonium aerosols in the United States: Implications for policy, *Journal of Geophysical Research: Atmospheres*, *109*(D15), D15204.

Partain, J. L., S. Alden, H. Strader, U. S. Bhatt, P. A. Bieniek, B. R. Brettschneider, J. E. Walsh, R. T. Lader, P. Q. Olsson, and T. S. Rupp (2016), An assessment of the role of anthropogenic climate change in the Alaska fire season of 2015, *Bulletin of the American Meteorological Society*, *97*(12), S14-S18.

Pataki, D. E., J. R. Ehleringer, L. Flanagan, D. Yakir, D. R. Bowling, C. Still, N. Buchmann, J. Kaplan, and J. Berry (2003), The application and interpretation of Keeling plots in terrestrial carbon cycle research, *Global Biogeochemical Cycles*, *17*(1), 1022.

Patterson, P.L., S. Healey (2015), Global ecosystem dynamics investigation (GEDI) LiDAR sampling strategy. In: S.M. Stanton, G.A. Christensen, Pushing boundaries: new directions in inventory techniques and applications: Forest Inventory and Analysis (FIA) symposium 2015. 2015 December 8–10; Portland, Oregon. Gen. Tech. Rep. PNW-GTR-931. Portland, OR: U.S. Department of Agriculture, Forest Service, Pacific Northwest Research Station. p. 245

Pavlovic, R., J. Chen, K. Anderson, M. D. Moran, P.-A. Beaulieu, D. Davignon, and S. Cousineau (2016), The FireWork air quality forecast system with near-real-time biomass burning emissions: Recent developments and evaluation of performance for the 2015 North American wildfire season, *Journal of the Air & Waste Management Association*, *66*(9), 819-841.

Pechony, O., and D. Shindell (2009), Fire parameterization on a global scale, *Journal of Geophysical Research: Atmospheres*, *114*(D16), D16115.

Podgorny, I., F. Li, and V. Ramanathan (2003), Large aerosol radiative forcing due to the 1997 Indonesian forest fire, *Geophysical Research Letters*, *30*(1), 1028.

Posa, M. R. C., L. S. Wijedasa, and R. T. Corlett (2011), Biodiversity and conservation of tropical peat swamp forests, *BioScience*, *61*(1), 49-57.

Pöschl, U. (2005), Atmospheric aerosols: composition, transformation, climate and health effects, *Angewandte Chemie International Edition*, *44*(46), 7520-7540.

Preston, C., and M. Schmidt (2006), Black (pyrogenic) carbon: a synthesis of current knowledge and uncertainties with special consideration of boreal regions, *Biogeosciences*, *3*(4), 397-420.

Radke, L. F., D. A. Hegg, P. V. Hobbs, J. D. Nance, J. H. Lyons, K. K. Laursen, R. E. Weiss, P. J. Riggan, and D. E. Ward (1991), Particulate and trace gas emissions from large biomass fire in North America, *Global Biomass Burning: Atmospheric, Climatic, and Biospheric Implications*, 209-224.

Randerson, J. T., H. Liu, M. G. Flanner, S. D. Chambers, Y. Jin, P. G. Hess, G. Pfister, M. Mack, K. Treseder, and L. Welp (2006), The impact of boreal forest fire on climate warming, *Science*, *314*(5802), 1130-1132.

Rapalee, G., S. E. Trumbore, E. A. Davidson, J. W. Harden, and H. Veldhuis (1998), Soil carbon stocks and their rates of accumulation and loss in a boreal forest landscape, *Global Biogeochemical Cycles*, *12*(4), 687-701.

Reichle, R. H., R. D. Koster, G. J. De Lannoy, B. A. Forman, Q. Liu, S. P. Mahanama, and A. Touré (2011), Assessment and enhancement of MERRA land surface hydrology estimates, *Journal of Climate*, *24*(24), 6322-6338.

Reimer, P. J., E. Bard, A. Bayliss, J. W. Beck, P. G. Blackwell, C. B. Ramsey, C. E. Buck, H. Cheng, R. L. Edwards, and M. Friedrich (2013), IntCal13 and Marine13 radiocarbon age calibration curves 0–50,000 years cal BP, *Radiocarbon*, *55*(4), 1869-1887.

Rella, C., H. Chen, A. Andrews, A. Filges, C. Gerbig, J. Hatakka, A. Karion, N. Miles, S. Richardson, and M. Steinbacher (2013), High accuracy measurements of dry mole fractions of carbon dioxide and methane in humid air, *Atmospheric Measurement Techniques*, *6*(3), 837-860.

Rodell, M., H. Beaudoing, and NASA/GSFC/HSL (2015), GLDAS Noah Land Surface Model L4 3 hourly 0.25 x 0.25 degree V2. 0, edited, Goddard Earth Sciences Data and Information Services Center (GES DISC) Greenbelt, MD.

Rogers, B., S. Veraverbeke, G. Azzari, C. Czimczik, S. Holden, G. Mouteva, F. Sedano, K. Treseder, and J. Randerson (2014), Quantifying fire‐wide carbon emissions in interior Alaska using field measurements and Landsat imagery, *Journal of Geophysical Research: Biogeosciences*, *119*(8), 1608-1629.

Rogers, B. M., J. T. Randerson, and G. B. Bonan (2012), High latitude cooling associated with landscape changes from North American boreal forest fires, *Biogeosciences Discuss.*, *9*(9), 12087-12136.

Rogers, B. M., A. J. Soja, M. L. Goulden, and J. T. Randerson (2015), Influence of tree species on continental differences in boreal fires and climate feedbacks, *Nature Geoscience*, *8*(3), 228.

Ryan, K. C. (2002), Dynamic interactions between forest structure and fire behavior in boreal ecosystems, *Silva Fennica*, *36*(1), 13-39.

Santos, G., J. Southon, K. Druffel-Rodriguez, S. Griffin, and M. Mazon (2004), Magnesium perchlorate as an alternative water trap in AMS graphite sample preparation: a report on sample preparation at KCCAMS at the University of California, Irvine, *Radiocarbon*, *46*(01), 165-173.

Schimel, D., R. Pavlick, J.B. Fisher, G.P. Asner, S. Saatchi, P. Townsend, C. Miller, C. Frankenberg, K. Hibbard, and P.Cox (2015), Observing terrestrial ecosystems and the carbon cycle from space, *Global Change Biology 21*(5), 1762-1776.

Schroeder, W., P. Oliva, L. Giglio, and I.A. Csiszar (2014), The New VIIRS 375 m active fire detection data product: Algorithm description and initial assessment, *Remote Sensing of Environment*, *143*, 85-96.

Schultz, M. G., A. Heil, J. J. Hoelzemann, A. Spessa, K. Thonicke, J. G. Goldammer, A. C. Held, J. M. Pereira, and M. van Het Bolscher (2008), Global wildland fire emissions from 1960 to 2000, *Global Biogeochemical Cycles*, *22*(2), GB2002.

Schuur, E. A., S. E. Trumbore, M. C. Mack, and J. W. Harden (2003), Isotopic composition of carbon dioxide from a boreal forest fire: Inferring carbon loss from measurements and modeling, *Global Biogeochemical Cycles*, *17*(1), 1001.

Sedano, F., and J. Randerson (2014), Multi-scale influence of vapor pressure deficit on fire ignition and spread in boreal forest ecosystems, *Biogeosciences*, *11*(14), 3739-3755.

Seiler, W., and P. J. Crutzen (1980), Estimates of gross and net fluxes of carbon between the biosphere and the atmosphere from biomass burning, *Climatic Change*, *2*(3), 207-247.

Shibata, S., E. Kawano, and T. Nakabayashi (1997), Research Center of Radioisotopes at University of Osaka Prefecture Radiocarbon Dates I, *Radiocarbon*, *39*(1), 79-87.

Silvius, M. J., H. Simons, and W. Verheugt (1984), Soils, vegetation, fauna and nature conservation of the Berbak game reserve, Sumatra, Indonesia*Rep.*, RIN.

Simpson, I. J., S. Akagi, B. Barletta, N. Blake, Y. Choi, G. Diskin, A. Fried, H. Fuelberg, S. Meinardi, and F. Rowland (2011), Boreal forest fire emissions in fresh Canadian smoke plumes:

C 1-C 10 volatile organic compounds (VOCs), CO_2, CO, NO_2, NO, HCN and CH_3CN, *Atmospheric Chemistry and Physics*, *11*(13), 6445-6463.

Skamarock, W. C., J. B. Klemp, J. Dudhia, D. O. Gill, D. M. Barker, W. Wang, and J. G. Powers (2005), A description of the advanced research WRF version 2*Rep.*, National Center For Atmospheric Research Boulder Co Mesoscale and Microscale Meteorology Div.

Stocks, B. J., M. A. Fosberg, M. B. Wotton, T. J. Lynham, and K. C. Ryan (2000), Climate change and forest fire activity in North American boreal forests, in *Fire, climate change, and carbon cycling in the boreal forest*, edited, pp. 368-376, Springer.

Stocks, B. J., M. Fosberg, T. Lynham, L. Mearns, B. Wotton, Q. Yang, J. Jin, K. Lawrence, G. Hartley, and J. Mason (1998), Climate change and forest fire potential in Russian and Canadian boreal forests, *Climatic Change*, *38*(1), 1-13.

Stockwell, C. E., T. Jayarathne, M. A. Cochrane, K. C. Ryan, E. I. Putra, B. H. Saharjo, A. D. Nurhayati, I. Albar, D. R. Blake, and I. J. Simpson (2016), Field measurements of trace gases and aerosols emitted by peat fires in Central Kalimantan, Indonesia, during the 2015 El Niño, *Atmospheric Chemistry and Physics*, *16*(18), 11711-11732.

Stuiver, M., and H. A. Polach (1977), Discussion reporting of 14C data, *Radiocarbon*, *19*(03), 355-363.

Sudo, K., and M. Takahashi (2001), Simulation of tropospheric ozone changes during 1997–1998 El Nino: Meteorological impact on tropospheric photochemistry, *Geophysical Research Letters*, *28*(21), 4091-4094.

Supiandi, S., and H. Furukawa (1986), A study of floral composition of peat soil in the lower batang hari river basin of Jambi, Sumatra *The Southeast Asian Studies*, *24*(2), 113-132.

Tacconi, L. (2016), Preventing fires and haze in Southeast Asia, *Nature Climate Change*, *6*(7), 640-643.

Tan, K. P., K. D. Kanniah, and A. P. Cracknell (2013), Use of UK-DMC 2 and ALOS PALSAR for studying the age of oil palm trees in southern peninsular Malaysia, *International Journal of Remote Sensing*, *34*(20), 7424-7446.

Tetens, O. (1930), Uber einige meteorologische Begriffe, *Z. geophys*, *6*, 297-309.

Thoning, K., D. Kitzis, and A. Crotwell (2007), Atmospheric carbon dioxide dry air mole fractions from quasi-continuous measurements at Barrow, Alaska.

Tosca, M., J. Randerson, C. Zender, D. Nelson, D. Diner, and J. Logan (2011), Dynamics of fire plumes and smoke clouds associated with peat and deforestation fires in Indonesia, *Journal of Geophysical Research: Atmospheres*, *116*(D8), D08207.

Trumbore, S. (2000), Age of soil organic matter and soil respiration: radiocarbon constraints on belowground C dynamics, *Ecological Applications*, *10*(2), 399-411.

Trumbore, S. E., and J. Harden (1997), Accumulation and turnover of carbon in organic and mineral soils of the BOREAS northern study area, *Journal of Geophysical Research: Atmospheres*, *102*(D24), 28817-28830.

Turetsky, M. R., B. Benscoter, S. Page, G. Rein, G. R. Van Der Werf, and A. Watts (2015), Global vulnerability of peatlands to fire and carbon loss, *Nature Geoscience*, *8*(1), 11-14.

Turetsky, M. R., E. S. Kane, J. W. Harden, R. D. Ottmar, K. L. Manies, E. Hoy, and E. S. Kasischke (2011), Recent acceleration of biomass burning and carbon losses in Alaskan forests and peatlands, *Nature Geoscience*, *4*(1), 27-31.

Turner, M. G., W. L. Baker, C. J. Peterson, and R. K. Peet (1998), Factors influencing succession: lessons from large, infrequent natural disturbances, *Ecosystems*, *1*(6), 511-523.

Turquety, S., J. A. Logan, D. J. Jacob, R. C. Hudman, F. Y. Leung, C. L. Heald, R. M. Yantosca, S. Wu, L. K. Emmons, and D. P. Edwards (2007), Inventory of boreal fire emissions for North America in 2004: Importance of peat burning and pyroconvective injection, *Journal of Geophysical Research: Atmospheres*, *112*(D12), D12S03.

Urbanski, S. (2014), Wildland fire emissions, carbon, and climate: Emission factors, *Forest Ecology and Management*, *317*, 51-60.

Urbanski, S. P., W. M. Hao, and S. Baker (2008), Chemical composition of wildland fire emissions, *Developments in Environmental Science*, *8*, 79-107.

Usup, A., H. Yoshihiro, H. Takahashi, and H. Hayasaka (2004), Combustion and thermal characteristics of peat fire in tropical peatland in Central Kalimantan, Indonesia, *Tropics*, *14*(1), 1-19.

van Der Werf, G. R., J. T. Randerson, L. Giglio, N. Gobron, and A. Dolman (2008a), Climate controls on the variability of fires in the tropics and subtropics, *Global Biogeochemical Cycles*, *22*(3), GB3028.

van der Werf, G. R., J. T. Randerson, L. Giglio, G. J. Collatz, P. S. Kasibhatla, and A. F. Arellano Jr (2006), Interannual variability in global biomass burning emissions from 1997 to 2004, *Atmospheric Chemistry and Physics*, *6*(11), 3423-3441.

van der Werf, G. R., J. Dempewolf, S. N. Trigg, J. T. Randerson, P. S. Kasibhatla, L. Giglio, D. Murdiyarso, W. Peters, D. Morton, and G. Collatz (2008b), Climate regulation of fire emissions and deforestation in equatorial Asia, *Proceedings of the National Academy of Sciences*, *105*(51), 20350-20355.

van der Werf, G. R., J. T. Randerson, L. Giglio, G. Collatz, M. Mu, P. S. Kasibhatla, D. C. Morton, R. DeFries, Y. v. Jin, and T. T. van Leeuwen (2010), Global fire emissions and the contribution of deforestation, savanna, forest, agricultural, and peat fires (1997–2009), *Atmospheric Chemistry and Physics*, *10*(23), 11707-11735.

van der Werf, G. R., J. T. Randerson, L. Giglio, T. T. Van Leeuwen, Y. Chen, B. M. Rogers, M. Mu, M. J. Van Marle, D. C. Morton, and G. J. Collatz (2017), Global fire emissions estimates during 1997–2016, *Earth System Science Data*, *9*(2), 697-720.

Van Leeuwen, T., and G. Van Der Werf (2011), Spatial and temporal variability in the ratio of trace gases emitted from biomass burning, *Atmospheric Chemistry and Physics*, *11*(8), 3611-3629.

Van Wagner, C., and T. Pickett (1985), *Equations and FORTRAN program for the Canadian forest fire weather index system*.

Veraverbeke, S., B. Rogers, and J. Randerson (2015a), Daily burned area and carbon emissions from boreal fires in Alaska, *Biogeosciences*, *12*(11), 3579-3601.

Veraverbeke, S., B. M. Rogers, M. L. Goulden, R. R. Jandt, C. E. Miller, E. B. Wiggins, and J. T. Randerson (2017), Lightning as a major driver of recent large fire years in North American boreal forests, *Nature Climate Change*, *7*(7), 529-534.

Viereck, L. (1983), The effects of fire in black spruce ecosystemsof Alaska and northern Canada, *The role of fire in northern circumpolar ecosystems NewYork: Wiley. p*, 210-220.

Walker, X. J., J. L. Baltzer, S. G. Cumming, N. J. Day, J. F. Johnstone, B. M. Rogers, K. Solvik, M. R. Turetsky, and M. C. Mack (2018), Soil organic layer combustion in boreal black spruce and jack pine stands of the Northwest Territories, Canada, *International Journal of Wildland Fire*, *27*(2), 125-134.

Ward, D., and L. Radke (1993), Emissions measurements from vegetation fires: A comparative evaluation of methods and results, *Fire in the Environment: The Ecological, Atmospheric and Climatic Importance of Vegetation Fires*, *13*, 53-76.

Warren, M., K. Hergoualc'h, J. B. Kauffman, D. Murdiyarso, and R. Kolka (2017), An appraisal of Indonesia's immense peat carbon stock using national peatland maps: uncertainties and potential losses from conversion, *Carbon Balance and Management*, *12*(1), 12.

Whitmore, T. (1984), *Tropical rain forests of the Far East*, Oxford: Clarendon Press.

Wiedinmyer, C., S. Akagi, R. J. Yokelson, L. Emmons, J. Al-Saadi, J. Orlando, and A. Soja (2011), The Fire INventory from NCAR (FINN): A high resolution global model to estimate the emissions from open burning, *Geoscientific Model Development*, *4*(3), 625.

Wiggins, E., S. Veraverbeke, J. Henderson, A. Karion, J. Miller, J. Lindaas, R. Commane, C. Sweeney, K. Luus, and M. Tosca (2016), The influence of daily meteorology on boreal fire emissions and regional trace gas variability, *Journal of Geophysical Research: Biogeosciences*, *121*(11), 2793-2810.

Wirth, C., E.-D. Schulze, W. Schulze, D. von Stünzner-Karbe, W. Ziegler, I. Miljukova, A. Sogatchev, A. Varlagin, M. Panvyorov, and S. Grigoriev (1999), Above-ground biomass and structure of pristine Siberian Scots pine forests as controlled by competition and fire, *Oecologia*, *121*(1), 66-80.

Wooster, M. J., G. Roberts, G. Perry, and Y. Kaufman (2005), Retrieval of biomass combustion rates and totals from fire radiative power observations: FRP derivation and calibration relationships between biomass consumption and fire radiative energy release, *Journal of Geophysical Research: Atmospheres*, *110*(D24), D24311.

Wooster, M. J., D. L. Gaveau, M. A. Salim, T. Zhang, W. Xu, D. Green, V. Huijnen, D. Murdiyarso, D. Gunawan, and N. Borchard (2018), New Tropical Peatland Gas and Particulate Emissions Factors Indicate 2015 Indonesian Fires Released Far More Particulate Matter (but Less Methane) than Current Inventories Imply, *Remote Sensing*, *10*(4), 495.

Wotawa, G., P. Novelli, M. Trainer, and C. Granier (2001), Interannual variability of summertime CO concentrations in the Northern Hemisphere explained by boreal forest fires in North America and Russia, *Geophysical Research Letters*, *28*(24), 4575-4578.

Wotton, B. M. (2009), Interpreting and using outputs from the Canadian Forest Fire Danger Rating System in research applications, *Environmental and Ecological Statistics*, *16*(2), 107-131.

Wüst, R. A., G. E. Jacobsen, H. von der Gaast, and A. M. Smith (2008), Comparison of radiocarbon ages from different organic fractions in tropical peat cores: insights from Kalimantan, Indonesia, *Radiocarbon*, *50*(3), 359-372.

Xu, X., S. E. Trumbore, S. Zheng, J. R. Southon, K. E. McDuffee, M. Luttgen, and J. C. Liu (2007), Modifying a sealed tube zinc reduction method for preparation of AMS graphite targets: reducing background and attaining high precision, *Nuclear Instruments and Methods in Physics Research Section B: Beam Interactions with Materials and Atoms*, *259*(1), 320-329.

Yan, X., H. Cheng, Y. Zhao, W. Yu, H. Huang, and X. Zheng (2016), Real-Time identification of smoldering and flaming combustion phases in forest using a wireless sensor network-based multi-sensor system and artificial neural network, *Sensors*, *16*(8), 1228.

Yokelson, R. J., R. Susott, D. E. Ward, J. Reardon, and D. W. Griffith (1997), Emissions from smoldering combustion of biomass measured by open‐path Fourier transform infrared spectroscopy, *Journal of Geophysical Research: Atmospheres*, *102*(D15), 18865-18877.

Yokelson, R. J., I. Burling, J. Gilman, C. Warneke, C. Stockwell, J. d. Gouw, S. Akagi, S. Urbanski, P. Veres, and J. Roberts (2013), Coupling field and laboratory measurements to

estimate the emission factors of identified and unidentified trace gases for prescribed fires, *Atmospheric Chemistry and Physics*, *13*(1), 89-116.

Yoneda, T., R. Tamin, and K. Ogino (1990), Dynamics of aboveground big woody organs in a foothill dipterocarp forest, West Sumatra, Indonesia, *Ecological Research*, *5*(1), 111-130.

Young, A. M., P. E. Higuera, P. A. Duffy, and F. S. Hu (2017), Climatic thresholds shape northern high‐latitude fire regimes and imply vulnerability to future climate change, *Ecography*, *40*(5), 606-617.

Yulianto, E., K. Hirakawa, and H. Tsuji (2004), Charcoal and organic geochemical properties as an evidence of Holocene fires in tropical peatland, Central Kalimantan, Indonesia, *Tropics*, *14*(1), 55-63.